Effects of permeability and head steepness of groynes on local flow characteristics

Modelling open channel flow for the features of a flexible groyne

E. van Alderwegen

bam

TU Delft Delft University of Technology

Modelling open channel flow for the features of a flexible groyne

Effects of permeability and head steepness of groynes on local flow characteristics

by

Earvin van Alderwegen

to obtain the degree of Master of Science

at the Delft University of Technology,

to be defended publicly on Monday December 13, 2021 at 14:00 AM.

Student number:	4618521	
Thesis committee:	Dr. ir. A. Blom,	TU Delft, chair
	Dr. ir. E. Mosselman,	TU Delft, supervisor
	Dr. ir. M. Zijlema,	TU Delft
	Ir. B. Reedijk,	BAM Infra, supervisor
External advisor:	Dr. ir. R.J. Labeur,	TU Delft
	Dr. ir. M. Bahrami-Yarahmadi,	Shahid Chamran University of Ahvaz

TU Delft

Preface

Before you lies the master thesis 'Modelling open channel flow for the features of a flexible groyne' which presents a numerical model for groynes with a permeable characteristic and variable head slopes. This thesis describes the research work that was conducted to obtain my Masters degree in Civil engineering at the Delft University of Technology (TU Delft). Over the period from September 2020 to December 2021, I was engaged in researching and writing this thesis as graduate intern at BAM Infraconsult. Therefore, I would like to thank BAM Infra for facilitating this amazing opportunity and providing this research with the necessary supervising and data.

First, I would like to thank my daily supervisor from BAM Infra Bas Reedijk who helped me through the entire process of the research and facilitated me with a great working environment. In addition, I would like to thank my daily supervisor from TU Delft Erik Mosselman who supported me through the research with great amount of feedback and discussions if needed. I would like to thank Marcel Zijlema for his quick commitment for joining the committee and providing me with extra computational resources. Furthermore, I would like to express my grattitude to Astrid Blom for her analytical feedback and great organization skills, in which I truly feel appreciated for. Apart from my supervisors, I would like to express my grattitude to Mohammad Bahrami-Yarahmadi from Shahid Chamran University of Ahvaz who provided me with extensive experimental data sets and information about the subject.

Without the help of my supervisors, this report would not be the same.

At last, I would like to give a special thanks to my father and friends who have helped me during the difficult times and continuous support throughout my education.

I hope that this research will give you some inspiring new insights into the rather unexplored area of extensive modelling in open channel flow coupled with porous flow for a permeable groyne.

Earvin van Alderwegen
Delft, December 2021

Summary

Recent river programmes have shown that an integrated approach is required for improving multiple functions such as safety against flooding, riverine nature rehabilitation and maintaining a navigational water depth. Conventional groynes are typically used to improve functions within the river programme, whose primary function is to maintain navigational water depth. In addition, the groynes are used to protect the bank in the river bend and maintain a desirable cross-section of the channel for flood control.

Groynes partly block the wet cross-section of a river, leading to separation flow downstream of the groyne. Large turbulent structures occur from the separation flow, which is directly related with the bed shear stresses. Consequently, flow around groynes may give rise to the development of significant local scour. The most important processes leading to these local scour are the horseshoe vortex system upstream, vortex shedding at the tip of the groyne and the large turbulent fluctuations in the mixing layer downstream of the groyne. Hence, investigations for improving alternative groyne configurations to decrease the maximum local bed shear stresses are interesting to analyse.

The flexible groyne is considered to be an improvement of the conventional groyne due to the characteristics of the permeability and possibility to increase the steepness of the groyne. Although a fair amount of research has already been carried out on different groyne configurations, little research has been carried out on permeability and head steepness. This research aims to numerically quantify the effects of groyne permeability and head steepness on flow characteristics in an open-channel flow.

The starting point is to apply a suitable software package containing the required implementations for modelling the flow around a porous, head steep-sloped groyne. The most critical implementations include non-hydrostatic effects, adapting the large turbulent structures and implementing the porous zone using a non-linear function. Fluent and OpenFOAM were observed to be capable of implementing the required processes. From a practical perspective, Fluent was chosen for further modelling.

The validation of the numerical model is executed by using three different experimental studies. The turbulence closure model is deduced to a Detached Eddy Simulation model (DES) model and the $k-\omega$ Shear Stress Transport (SST) model. From the literature and the manual, these turbulent closure models adequately capture the separation flow. By using a sensitivity analysis, it is observed that the mean flow velocities is captured more sufficiently by using the DES model. In addition, the PISO algorithm is compared with the SIMPLE algorithm for the pressure-velocity solving method by using sensitivity analysis. It is observed that the PISO algorithm slightly captures the mean flow velocities more sufficiently than the SIMPLE algorithm.

The validation of the experimental studies shows that the numerical model has sufficiently agreement with the mean flow velocities. The numerical model tends to underestimate the mean streamwise velocity slightly. Most of the critical mean flow properties have been observed to be within an RMSE of 30 % and a PBIAS of 25 %. The Reynolds shear stresses are overestimated and shifted further downstream than the experimental data set. Eventually, it is indicated that the model can represent open-channel flow in combination with a porous structure.

Four configurations were identified for the simulations, varying the slopes between 1:1 and 1:3 and impermeable and permeable groynes with 60 % porosity. Porous groynes showed a shift of the re-circulation zone downstream due to the momentum exchange between the flow around the groyne and through the groyne structure. The shift of the re-circulation zone is also affected by the flow that exits the porous groyne, decreases the deflection, and induces the re-circulation zone to shift downstream. Gentle sloped groynes show a shift of the re-circulation zone towards the groyne, which indicates that the deflection of the flow around the groyne is strong. The flow follows the geometry of the groyne more smoothly, and thus increased deflection of the flow around the groyne is present.

The mixing layer is observed near the edge of the re-circulation zone. For porous groynes, the large Reynolds shear stresses are observed in the mixing layer, which is shifted downstream and reduced compared to the impermeable groynes. The decrease of the Reynolds shear stresses is rough 10 %. In addition, porous groynes showed a reduction in the development of large eddies in the mixing layer compared to impermeable groynes. The decrease of the turbulence intensities is due to smaller velocity gradients, reducing the momentum exchange in the mixing layer. For gentle sloped groynes, the opposite is observed. The large Reynolds shear stresses are present close to the groyne, and the significant eddies are mainly observed near the groyne. This is most likely occurring due to the flow that smoothly follows the groyne's geometry. The large Reynolds shear stresses are slightly reduced compared to the steep-sloped groynes, approximately 5 %, which is due to the decrease of the velocity gradient within the mixing layer. The horseshoe vortex system is observed in the steeply sloped groyne simulations, however, the intensity is reduced using porosity. The effect of the horseshoe vortex decreases when momentum exchange is possible with the free flow region and a porous structure.

For a porosity of 60 %, a reduction of roughly 5 % for the peak values of the bed shear stresses were observed compared with the impermeable groyne. In addition, the bed shear stresses are shifted downstream compared to impermeable groynes, due to the appearance of the momentum exchange between the free flow region and the flow through the porous structure. Decreasing the steepness of the slope from 1:1 to 1:3 showed minor decreases of the bed shear stresses.

Comparing the flexible groyne with the conventional groyne, it is observed that the porosity of the flexible groyne reduces the intensity of the re-circulation zone because of the appearance of the momentum exchange between the free flow region and the porous structure. In addition, the deflection is reduced for the main flow for an increase of the porosity. These observations are also shown extensively for the multiple groynes. The simulation for the multiple series of flexible groyne shows a significant difference in the appearance of the re-circulation zone. The re-circulation zone is very much present for the conventional groynes, however not that significant for the flexible groynes. In addition, both the Reynolds shear stresses and bed shear stresses are observed downstream for the flexible groynes compared to the conventional groynes. The peak values are roughly similar.

Porosity decreases the maximum values for the Reynolds shear stresses and slightly decreases the bed shear stresses. Both properties are shifted downstream for an increase in porosity. A decrease in the slope (from 1:1 to 1:3) reduces the maximum values of the Reynolds shear stresses as well. However, this is less remarkable for the bed shear stresses. Most turbulent properties and bed shear stresses are observed more towards the groyne structure. Hence, it is observed that the flexible groyne significantly affect the flow properties and shifts the turbulence and bed shear stresses downstream of the groyne. Therefore, stability failure due to scour near the groyne is less expected to occur.

Contents

1 Introduction

1.1 Background

The biodiversity in the Dutch rivers is increasing, and a more natural landscape is achieved thanks to large-scale measures such as Room for the River, Natura2000 and Water Framework Directive (SSRS, 2020). However, these recent programmes increasingly lead to essential conflicts between safety against flooding and riverine nature rehabilitation with the navigational water depths. Hence, an integrated approach for improving the management of the river within these programmes (Havinga, 2020) is required. Furthermore, rivers are under pressure by climate change, tight budgets of the maintenance and management department for rivers and high demands from the society to respond to current local developments in the area. Therefore, the Self-Supporting River System (SSRS) is called out upon to search for potential, renewable, and affordable measures to manage the river system. One of the main issues in a river system is the difficulties related to the deposition and transport of sediment in rivers. Too much sediment deposition can hinder the navigation channel by reducing water depths, while sediment shortage may result in bank erosion. Building with nature and balancing the river in the long term should be the main focus of this issue. Hence, the optimizations of groynes can be one of the solutions to solve these sedimentation difficulties (Przedwojski et al., 1995).

Groyne structures are placed transverse to the river's flow direction and are commonly used for river training (Przedwojski et al., 1995). Accordingly, the primary purpose of a groyne is maintaining a navigational water depth, the protection of the bank by reducing erosion and maintaining a desirable cross-section of the channel for flood control (Yossef, 2002). Groynes partly block the wet cross-section of a river, leading to a flow pattern that is highly influenced by large turbulent structures (Uijttewaal, 2005). The flow behaviour may lead to various negative processes and consequently develop significant local scours. A negative effect of local scours is the stability failure concerning the groyne structure (Zhang & Nakagawa, 2008). The most important processes leading to these local scours are the horseshoe vortex system upstream, vortex shedding at the tip of the groyne and the large turbulent fluctuations in the mixing layer downstream of the groyne (Ettema & Muste, 2004), (Koken & Constantinescu, 2009) and (Jeon et al., 2018). More precisely, the area around the tip of the groyne and in the mixing layer has the highest bed shear stresses contributing to the erosion of the bottom material (Duan, 2009), consequently resulting in local scour holes.

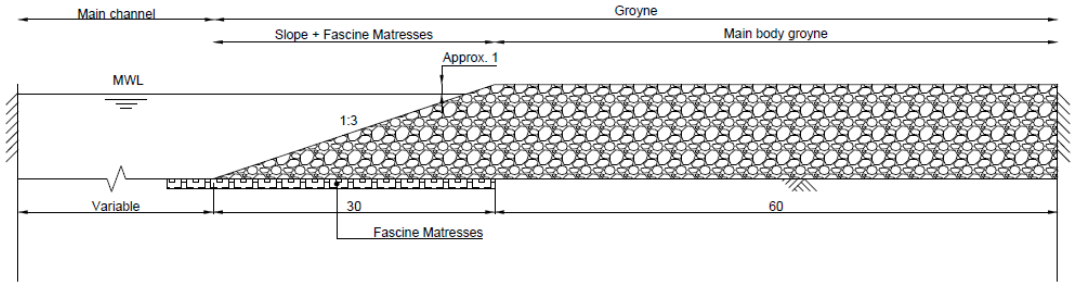

(a) Side view groyne construction

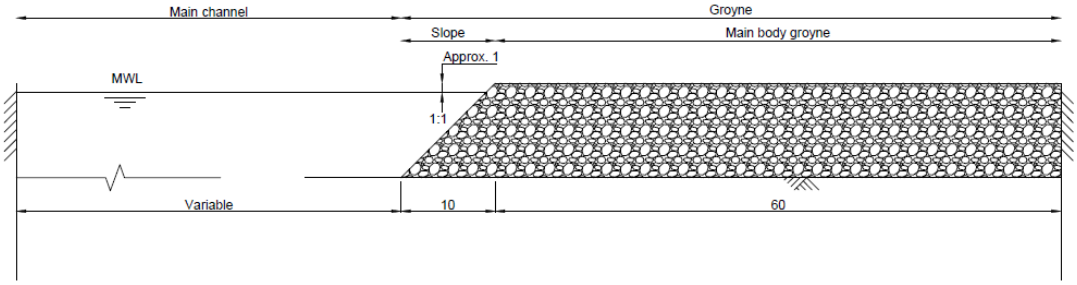

(b) Side view flexible groyne construction

Figure 1.1: Side views of a conventional groyne construction and a flexible groyne construction with standard measures in meters (figure by author)

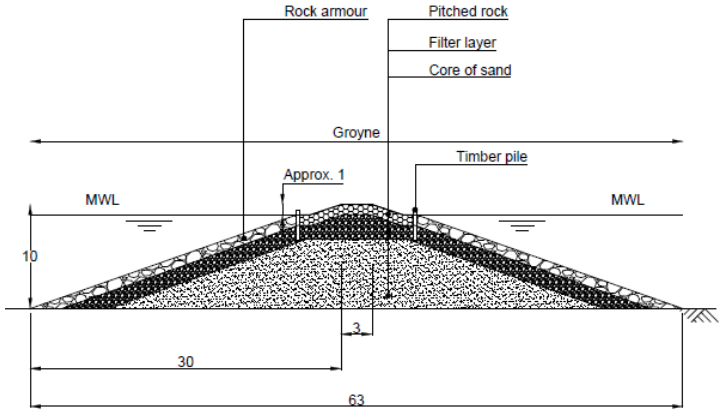

(a) Cross-section conventional groyne construction

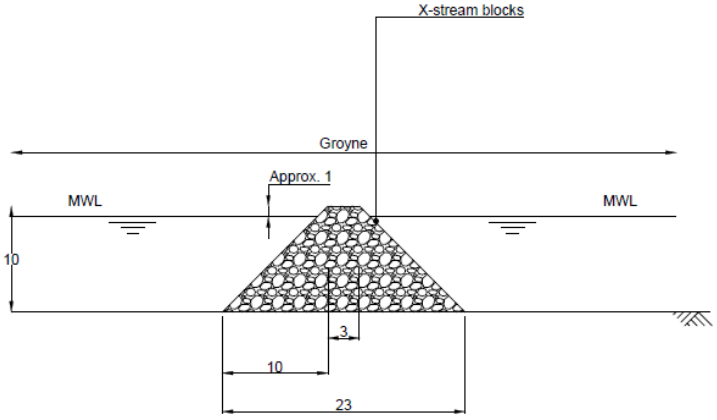

(b) Cross-section flexible groyne construction

Figure 1.2: Cross-section of a conventional groyne construction and a flexible groyne construction with standard measures in meters (figure by author)

Nowadays, conventional groyne structures in the Netherlands are made of a sand core with several layers of different stone sizes on top (Jansen et al., 1979). Besides, fascine mattresses are used to maintain the stability of the groynes by preventing erosion directly around the groynes. A standard type of construction for a groyne is shown in Figure 1.1a and Figure 1.2a. The figures show that the construction work is time-consuming and labour-intensive, due to the amount of material and order of steps in constructing the groyne (Bradbury et al., 2003). Nonetheless, the main problem related to conventional groyne constructions is the development of local scour holes, which could lead to failure of the groyne. Therefore, optimizations of this kind of structures have often been studied.

Groynes made of one material may optimise conventional groyne structures and could benefit in the development of local scours. This idea was conceived in part of the SSRS programme from the executive agency of the Dutch Ministry of Infrastructure and Water Management, in which the so-called flexible groyne is made of only x-stream blocks as shown in Figure 1.1b and Figure 1.2b. This groyne structure essential characteristics are it's permeability and the possible use of steep slopes without bed protection. Besides the benefit of the potential decrease of the local scour holes; also ecological added values to the river can emerge by creating habitat. Additionally, the flexibility of the placement of the structure is also a minor advantage. SSRS would like to develop such solutions. Therefore in 2016, a report about this flexible groyne was written by Wetser (2016). In this document, a design for the pilot project in the IJssel was suggested, and the characteristics of the flexible groyne were investigated using scale models. Nowadays, the pilot project is located near Kampen in the IJssel and is installed with modified lengths compared to conventional groynes. The length of flexible groyne in the outer bend will be extended in the near future, so existing data may be used for further investigation.

Differences in groyne geometry and permeability result in non-uniform behaviour of the flow around the groyne. These alternative designs aim to reduce the velocity gradients. Hence the bed shear stresses around the groyne construction without disrupting the main channel's mean flow velocity. Side slopes reduce adverse pressure gradients in the direction perpendicular to the core of the vortex, and thus turbulent structures may be reduced Uijttewaal (2005), Koken & Constantinescu (2014). The reduction of the bed shear stresses is also observed for reducing the scour hole by using more gentle slopes Melville (1992). However, it appears that the decrease of the local scour with more gentle slopes becomes relatively low after an angle of 1:1. Regarding the permeability of a groyne construction, an increase of the permeability results in a linear decrease of the large turbulent fluctuations and local scour depths Kang et al. (2011b), van der Wal M. (2020). Furthermore, the absence of a bed protection results in a decrease of the local scour depths van der Wal M. (2020) but could lead to failure of the structures' stability.

1.2 The problem

Different investigators have already studied the hydrodynamics and morphology in rivers for various configurations of groynes Kang et al. (2011b), Yeo et al. (2005), Uijttewaal (2005), Ghaldarbandi et al. (2013), Mansoori (2014), Saberi & Galoie (2017), Bahrami Yarahmadi et al. (2020). Similarly, studies have been carried out for groyne configurations in coastal waters Raudkivi (1996), Trampenau et al. (2004), Zhang (2020). Most of these studies supported the known physics and processes by using numerical models and scale models. Although a fair amount of research has already been carried out on different groyne configurations, plenty of research is still missing for detailed groyne configurations and their local effects. In particular, flow around permeable, sloped groynes modelled as porous media, coupled with the free-surface flow, have not been investigated extensively. Consequently, detailed flow characteristics for the flow around and through permeable, sloped groynes is limited Iqbal et al. (2021).

Important aspects of the flow features are large turbulent structures, which is still profoundly investigated. Large turbulent fluctuations around the groyne lead to significant bed shear stresses and develop extensive scour holes Duan (2009). Extensive local scour holes could result in failure of the structure's stability Zhang & Nakagawa (2008). These large turbulent fluctuations are typically present just upstream of the groyne, around the tip of the groyne, and downstream of the head of the groyne construction, in the mixing layer Duan (2009). Therefore, investigating new alternative groyne configurations for decreasing the maximum local bed shear stresses without losing the primary function is worthwhile to study.

1.3 Objective and Research questions

This study focuses on the flow characteristics for various groyne properties based on the flexible groyne. The notable features of the flexible groyne are adapted to the groynes' head slope and permeability. This research aims to numerically quantify the effects of permeability and head steepness of groynes in an open channel flow on the flow characteristics. Consequently, obtaining more insight into the hydrodynamics of the flow around these particular groynes.

The main research question is proposed as:

"What are the effects of permeability and head steepness of groynes on flow characteristics?"

The sub questions assists in creating a satisfactory conclusion for the research. Therefore, five different questions are identified:

- What are the required capabilities of the software package, and what software package satisfies these requirements?
- How capable is the chosen numerical model to represent flow around and through a porous groyne?
- How do permeability and head steepness of groynes affect macro-turbulent structures?
- What are the effects of permeability and head steepness of groynes on bed shear stresses?
- How does the flexible groyne improve the flow characteristics compared to a conventional groyne?

1.4 Research method

Numerical modelling is used for the various groyne configurations to define the data required for analyzing the hydrodynamics around a groyne. Hence, a procedure is established to determine a suitable numerical model that includes essential processes. The first step is to evaluate the literature review about groyne modelling regarding the porous structure. Subsequently, an overview is made of the different processes required in the numerical model. The literature review and previous numerical studies are used to validate the important processes within the numerical model. Lastly, the numerical model is verified for simulating three critical aspects: the large turbulent fluctuations for a rectangular groyne, the coupled system for the porous media with the free surface-flow, and the flow around a triangular groyne. Subsequently, comparing the data of the simulations with the experiments leads to conclusions about the numerical model's performance.

After the numerical model has been verified and validated, the input values and properties are considered for the various groyne configurations. Two specifications are analyzed and validated for the study: the turbulent processes and the bed shear stresses as a function of the permeability and head steepness of the groyne. Additionally, the results are compared to analyze whether the flexible groyne improves instead the conventional groyne. Eventually this research intends to obtain more insight into the effects of permeability and head steepness of the groyne on the hydrodynamics.

1.5 Thesis outline

The thesis consists of a literature review in Chapter 2 in which the theoretical background is provided to determine the required processes for modelling flow around permeable groynes. The software package is identified in Chapter 3 with the required processes. Next, a model is created within the software package, which is validated in Chapter 4. Results of the validated model are shown for multiple simulations in both Chapter 5 and Chapter 6. The results are discussed in Chapter 7. Finally, this research is wrapped up by the conclusion and recommendations.

2 Literature review

In this section, information is given from recent studies about the hydrodynamics and morphology around groyne structures. The focus is on river modelling, in which special attention is paid to the flow patterns and local scour around groyne structures. With the information, further modelling can be executed for developing improved relations for emerged groynes.

2.1 Conventional groyne structures

2.1.1 General

River training is the term for maintaining the desired cross-section and alignment of the river by regulating the river flow. In general, river training works can be divided into multiple objectives such as channel regulation for high and low discharges, discharge regulation, water level regulation and bank and flood protections. However, natural processes and human interference may occur, which causes non-equilibrium outcomes. This affects the stability of the river and may result in negative consequences such as flooding and riverbank erosion. Unfavourable consequences within the river system can be solved by using training structures such as bed fixations and bottom vanes, longitudinal structures and transverse structures. Groynes are typical examples of these transverse structures, which are widely used in the Netherlands (Przedwojski et al., 1995).

The advantages of groynes are stimulating erosion in the navigational part of the river, protecting the outer bank, and flood control by maintaining the desired cross-section. Depending on the situation, considerations are made to optimize the effect of the groynes. The most critical design considerations for groynes are the plan-view shape, the length of the groynes, the spacing between the groynes, orientation to the flow, crest elevation and slope, cross-section, and construction material, and scour (Yossef, 2002).

Conventional groyne structures in the Netherlands are mostly made of multiple layers of stones, a core of sand and placed on a fascine mattress. Also, timber piles are often used in between the transition with the water surface for the different layers of stones (Jansen et al., 1979). The typical length of groynes is dependant on the desired width and depth of the navigation channel, and the spacing between groynes is around 1 to 3 times its length (Uijttewaal, 2005). Slopes vary between 1:1.25 to 1:5 (Yossef, 2002) with a minimum crest width of 1 m, and the height of the crest is chosen close above the yearly averaged water level (Uijttewaal, 2005).

New designs of groynes are still being investigated to improve the functioning and unfavourable consequences such as local scours and large turbulence structures around groynes. In this research, the properties of the flexible groyne are used for a new structure design, which has different characteristics than conventional groyne structures. The flexible groyne uses one particular material called X-stream blocks for the whole construction. By using only X-stream blocks, the groyne becomes slightly permeable, and it is possible to form a steep slope of 1:1 for the groyne. Hence, the flexible groyne can be applied using variations of the head steepness while maintaining the stability of the structure.

Before studying the various properties of the flexible groyne, more insight into the recent studies about the conventional groyne structures is given in the following sections.

2.1.2 Hydrodynamic effects of groynes

Flow patterns around groynes are influenced by the large turbulent structures and the momentum exchange between the groyne field and the main channel flow (Uijttewaal, 2005). The essential flow regions affected by groynes are seen in Figure 2.1 and is more generally indicated as the separation zone upstream of the groyne, the mixing zone and the recirculation zone downstream of the groyne (Paik & Sotiropoulos, 2005).

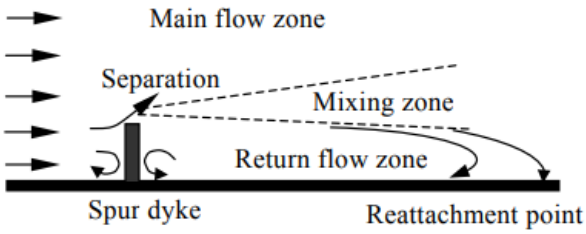

Figure 2.1: Flow characteristics with reattachment point for a groyne construction from Zhang & Nakagawa (2008)

Flow dynamics around groynes

Important experimental studies such as Uijttewaal (2005), Ettema & Muste (2004), Rajaratnam & Nwachukwu (1983), Koken & Constantinescu (2011), Duan (2009), Jeon et al. (2018) and numerical studies such as Paik & Sotiropoulos (2005), Koken & Constantinescu (2008, 2009, 2014) have examined the turbulent and mean flow properties around single groynes and have concluded the relatively complex flow around the groyne. The flow around a single straight groyne includes; the (1) upstream flow as a quasi-periodic recirculation zone due to the adverse pressure gradient (Paik & Sotiropoulos, 2005); (2) The formation of the horseshoe vortex at the base of the groyne in combination with the downwards flow caused by vertical pressure gradients and the interaction with the boundary layer (Koken & Constantinescu, 2009); (3) A development of a recirculation zone due to contraction and expansion (Jeon et al., 2018); (4) A turbulent mixing layer or detached shear layer between the recirculation zone and the main flow (Ettema & Muste, 2004, Koken & Constantinescu, 2009); (5) Vortex shedding at the head of the groyne Paik & Sotiropoulos (2005). The most extensive flow patterns are the horseshoe vortex formation, detached shear layer and vortex shedding at the head of the groyne, producing enormous bed shear stresses and large-scale time-dependent turbulent structures (Duan, 2009).

As already stated, the most extensive flow patterns are indicated in the horseshoe vortex formation, detached shear layer and the vortex shedding. The mean flow, turbulent kinetic energy, and Reynolds shear stresses indicate the turbulent flow field (Duan, 2009). In these areas, it has been concluded that the bed shear stresses, calculated from the Reynolds shear stresses, have been around three times larger than the approached bed shear stresses as seen in Duan (2009). The observed Reynolds shear stresses is comparable to the results of Ariëns (1993), which indicated that the most turbulent fluctuations remain in the mixing layer for the downstream part of the groyne as seen in Figure 2.3. Based on the bed shear stresses and turbulent properties, these areas are significant for studying the flow characteristics around groynes.

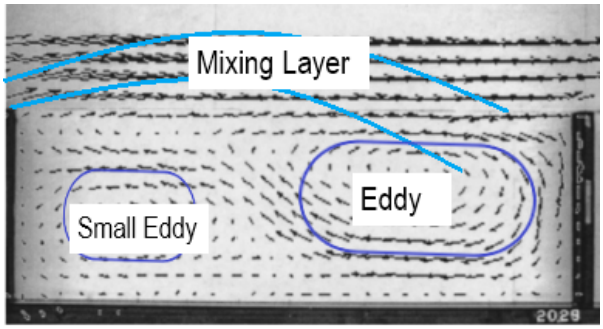

Figure 2.2: Flow field for a series of groynes in a straight channel by using experiments with indicative regions (Uijttewaal et al., 2001)

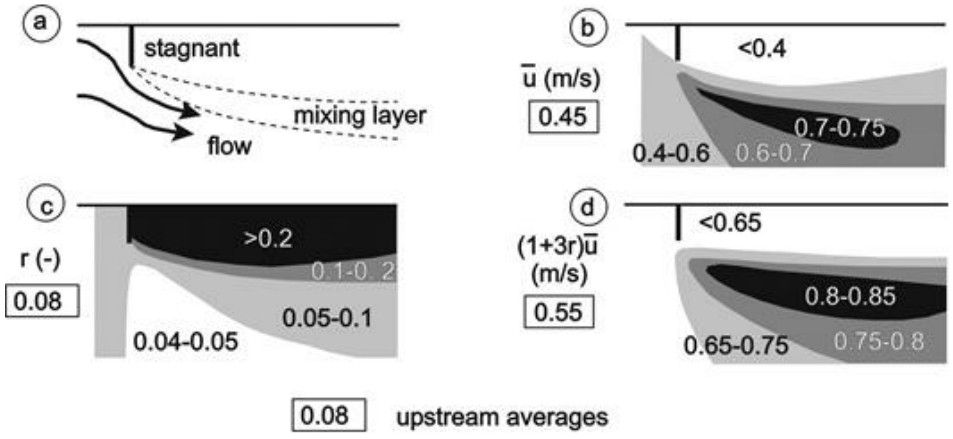

Figure 2.3: Flow characteristics for a horizontal constriction, figure from Ariëns (1993)

Hydrodynamics for multiple groynes

Multiple groynes lead to different flow behaviour compared to flow around single groynes. Numerous experimental investigations observe various notable behaviour of the flow as shown in Uijttewaal et al. (2001), Weitbrecht et al. (2008), Yossef & de Vriend (2011), which is also observed by numerical investigations examined in Zhang et al. (2005). The main difference between a series of groynes and a single groyne is the flow effects of downstream groynes and the development of the groyne field. Downstream groynes have relatively minor flow behaviour than the first groyne. Besides, multiple eddies are observed within the groyne field (recirculation zone) (Uijttewaal et al., 2001, Yossef & de Vriend, 2011). These eddies are noticeable in Figure 2.2, in which a large, primary eddy and a small eddy in counter-rotation are visible in the downstream part of the groyne field. The exchange of momentum drives the whole recirculation zone through the detached shear layer, mainly observed as large-scale time-dependent turbulence structures (Yossef & de Vriend, 2011). In particular, a series of groynes with explicit groyne fields results in different flow characteristics for the flow around the groynes and is observed when modelling a series of groynes.

Hydrodynamics in river bends

Large flow velocities near groynes typically occur in the main channel and mixing layer, whereas, in the groyne field, the flow velocities are small. Generally, groynes are used in bending parts of a river, in which the large flow velocities are present in the outer side of the river bend due to the combination of secondary flow effects and downstream velocity (de Vriend et al., 2011). However, groynes located in the outer bank of the river lead to a shift of the large flow velocities further towards the inner side of the river section. Typical groyne experiments resulting in these flow patterns are shown in Giri et al. (2004) and Mehraein et al. (2017). In general, the studies show that the flow characteristics depend on the radius of the bend.

2.1.3 Morphological effects of groynes

A protruding structure such as a groyne in a river results in adjusting flow patterns and morphological configurations like scour. Excessive scour is one of the major causes for failure of groynes (Zhang & Nakagawa, 2008) and, therefore, an essential aspect in designing groynes. For this reason, flow characteristics and morphological dynamics associated with the development of scours have to be reviewed before investigating the flow characteristics for various groyne configurations.

Scour around groynes

Usually, changes in flow patterns and morphological configurations inducts a scour process, which is generally divided into two categories in the presence of a groyne: constriction scour and local scour (Zhang & Nakagawa, 2008). When river bends are present, additional scours due to bending is present, which is called bend scour (van der Wal M., 2020). Constriction scour is a consequence of narrowing the river leading to upstream streamlines converting into vortexes at the bottom of the water depth. The vortices at the bottom causes scour upstream of the construction (Hoffmans & Verheij, 1997), as seen in Figure 2.4. Local scour is directly initiated by the changes in the flow patterns caused by groynes (Zhang & Nakagawa, 2008).

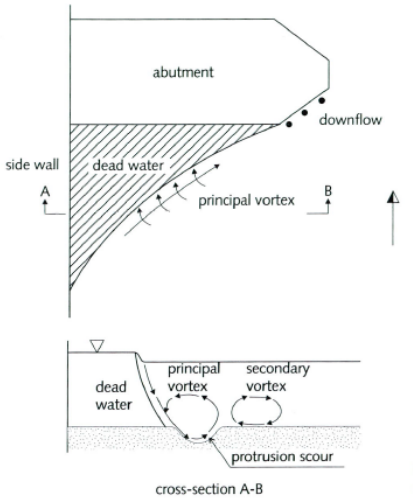

Figure 2.4: Protrusion scour due to horizontal constriction, figure from Hoffmans & Verheij (1997)

Scour is generally expressed in sediment transport, which is correlated to the mean near-bed shear stresses and mean flow velocities (Ouillon & Denis, 1997, Chrisohoides et al., 2003, Koken & Constantinescu, 2008). However, this concept is identified to be insufficient for accurate scour predictions around groyne like structures, in which turbulent behaviour is present Chrisohoides et al. (2003). Relations are observed for bed shear stresses and the scour depths around groynes, which is typically used for an indication of the scour depths Zhang & Nakagawa (2008). Another indication for scour holes around groynes, abutments, and other protruding structures is to use shape factors (Kandasamy & Melville, 1998, van der Wal M., 2020). The shape factor is an empirical expression accounting for the influence of the shape of the groyne. Eventually, many studies have indicated and visualized the scour depths around groynes. One of the indications for the scour depth around groynes, based on the equilibrium sediment transport model, is shown in Figure 2.5.

From Figure 2.5, it can be seen that the maximum values for the scours and bed shear stresses are relative dependant on each other. Hence, the maximum scour regions related to bed shear stresses have often been studied. The maximum bed shear stresses observed by Ettema & Muste (2004), Higham et al. (2017) have shown that the areas upstream, around the groyne and in the mixing layer has resulted in the most significant bed-shear stresses. These affected regions agree with the important hydrodynamic processes affected by groynes, namely, the horseshoe vortex system, the detached shear layer and the vortex shedding at the tip of the groyne. In addition, these observed areas are correlated with the largest scour hole developments, as stated in Figure 2.5.

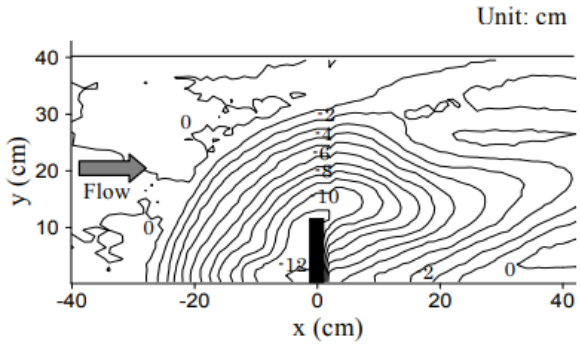

Figure 2.5: Scour around an impermeable groyne, figure from Zhang & Nakagawa (2008)

Bed shear stress

Turbulent properties are used for indicating the turbulent structures within a flow field, which leads to the bed shear stresses. Multiple options are possible to derive this. From the study of Biron et al. (2004) it is shown that Reynolds shear stresses are observed to be sufficient for indicating the bed shear stresses with great accuracy in a simple boundary layer. More information about calculating bed shear stresses is stated in the Appendix B.2.

Morphological effects in river bends

Typically, groynes are placed in river bends, where extensive erosion is present. The processes, however, are different in river bends compared to a straight open channel. Therefore, the river's bend may be an important aspect for studying flow characteristics. When concerning the scour due to the river bend, the behaviour of the river responds differently by the combination of the secondary flow and the downstream flow (de Vriend et al., 2011). The extensive flow velocities have moved more towards the river's outer side and led to bend scour combined with deepening the outer river bend. However, in cases with groynes, it is observed that river bends with a large radius manifested minimal effects of this bend scour (van der Wal M., 2020). Accordingly, neglecting the secondary flow's effect within the scour near groynes is acceptable for minor river bends. Bending is, therefore, not taken into consideration in this research.

Morphological effects for multiple groynes

Besides the fact that groynes are located in bends, they are also regularly present in series. Local scour depth for a series of groynes behaves differently than scour for single groynes. Normally, a series of groynes is seen as a constriction, which typically results in bed degradation of this river part (Yossef, 2002) (Zhang & Nakagawa, 2008). However, a slight change of behaviour is observed comparing the effects of groynes against long constrictions. Hence, a multiplication factor is used to define the river response to groynes, based on experiments for a series of groynes (Yossef, 2002) or an empirical expression is used (Przedwojski et al., 1995). As concluded in these experiments, groynes with small spacing lead to extensive degradation. This degradation is more extensive than a river with a constriction. In contrast, groynes with large spacing led to less river degradation compared to a constriction.

The flow characteristics are affected by the spacing between groynes, leading to possible river scour and degradation. Important to conclude from these researches that the spacing will lead to various effects on hydrodynamics and morphology. Therefore, the spacing is included in approaching the configurations for a series of groynes to avoid unnecessary extreme values for the degradation and thus the bed shear stresses.

Conventional groynes have been investigated heavily. However, this research wants to provide more insight in the flow characteristics for the permeability and head steepness of groynes. The next part of the literature review will include the information known for the flow characteristics for these type of groyne configurations.

2.2 Various groyne structures

2.2.1 General

Table G.1 and Table G.2 from the appendix show various studies which investigated and implemented different configurations of groynes. Frequently, studies have shown optimizations for groyne configurations in rivers, where scour and, consequently, large turbulence structures are minimized or sustained. Configuration parameters as angles, emerged and submerged, permeability, use of bed protection, spacing, slopes, or head shapes have all been investigated. Most of these studies investigated configurations focusing on one specific element. However, they have not given satisfactory results due to limitations or have specific environmental conditions, which cannot be used in this thesis.

The flexible groyne has notable characteristics of porosity and steep slopes can be applied up to 1:1 for the shank and head of the groyne. These conditions are investigated in recent studies and are concluded in the following sections 2.2.2 and 2.2.3. Based on this review, the important aspects of the hydrodynamic and morphological effects are used for obtaining more insight into the flow characteristics for the effects of permeability and head steepness of groynes.

2.2.2 Hydrodynamic effects of various groynes

Hydrodynamic effects of permeable groynes

Previous studies have shown that permeability is an important factor for optimizing groynes. A permeable groyne is mainly executed by large piles with varying openings between the piles, dependant on the required permeability. The open structure allows water to flow through the construction, hence absorbing part of the flow energy. However, the flow velocity, consequently, the sediment transport, is locally decreased, affecting sediment deposition (Raudkivi, 1996, Kang et al., 2011a, Zhang, 2020).

Investigations of the permeable pile groynes have shown that the turbulence effects have been reduced compared to conventional groynes (Uijttewaal, 2005, Yeo et al., 2005, Kang et al., 2011b). A linear correlation with increasing permeability and decreasing recirculation flow is observed until roughly 60 %, in where no recirculation flow was found (Kang et al., 2011b). An empirical relation was developed for the length of the recirculation zone associated with the permeability (Han & Lin, 2013). The width of the mixing layer, expressed in the incident angle from the tip of the groyne, is also affected by permeability. An increase in permeability led to a reduced width of the mixing layer (Yeo et al., 2005, Kang et al., 2011b). In addition, permeable pile groynes with related slopes of groynes have shown that the turbulence behaviour is decreased as well, especially in a submerged situation (Uijttewaal, 2005).

Hydrodynamic effects of sloped groynes

Slopes in groyne configurations, especially the head steepness, are significant for the behaviour of turbulent structures around groynes (Uijttewaal, 2005, Kang et al., 2011b, Ghaldarbandi et al., 2013, Koken & Constantinescu, 2014, Bahrami Yarahmadi et al., 2020). A recent study Koken & Constantinescu (2014) has shown that the slope upstream of the groyne reduces the strong adverse pressure gradients perpendicular to the core of the vortexes of the horseshoe vortex system. Less scour is expected upstream of the groyne induced by the weakened horseshoe vortex system. The appearance of the main necklace for the horseshoe vortex system has also been reduced for a sloping wall compared with vertical walls. The horseshoe vortex system remains relatively less effective, even using bed protection around sloped groynes. However, it has been observed that the flow movement with bed protections had a strong flow acceleration at regions where no bed protection was present. Also, the effectiveness of the detached shear layer and recirculation zone has been decreased by using slopes for the head of the groyne (Bahrami Yarahmadi et al., 2020, Kang et al., 2011b). For a head steepness of 45 °, the maximum values of the recirculation zone have been reduced by almost two times compared with rectangular cases. Accordingly, it is observed that sloped groynes reduce the flow velocity and turbulent behaviour around groynes.

Hydrodynamic effects of porous groynes

Porous groynes, defined as gabions or groynes with only rocks, have small, inhomogeneous gaps between the stones in which water can flow through the structure. The flow through the permeable pile groyne and a porous groyne is different, whereas the flow through a permeable pile groyne moves less unobstructed. Flow through a porous groyne behaves more as porous flow. Additionally, pile groins have much higher permeability than those with only rocks. The little research that is executed (Mioduszewski & Maeno, 2005, Muraoka et al., 2009) have concluded that porous structures tend to result in less deflection of the current and smaller ranges of the vortex shedding at the tip of the groyne compared with conventional groynes. However, these result differences were noticed as very small, and studies are limited.

Typically, flow in porous zones is computed with the Darcy-flow theory, however, small turbulent fluctuations are present in the permeable construction. Therefore, the approach of Darcy is not fully supported due to this turbulent behaviour. It is observed that the Reynolds stresses have a negligible effect on the momentum of the flow in porous media. Hence, no excessive turbulent models are necessary for these kinds of situations. The drag only produces turbulent flow, so averaged drag must be taken into account to contribute to this flow. Using the Forchhheimer equation is a possibility to solve this sort of problem Jin & Kuznetsov (2017).

2.2.3 Morphological effects of various groyne configurations

The various configurations lead to changing hydrodynamic effects and, therefore, different morphological effects. The permeability of pile groynes has led to a decrease of the scour holes as observed by Zhang & Nakagawa (2008), van der Wal M. (2020), Shampa et al. (2020). The research of van der Wal M. (2020) concluded that high permeable pile groynes reduce scour holes significantly for cases without bed protection. Permeable pile groynes with bed protection will increase scour compared to using no bed protection, however, the general decrease of scour is still present. A relation was found for the permeability and observed scour holes in a k-shape factor. Another relation was found in which a linear correlation between the permeability and the scour hole dimensions are observed (Zhang & Nakagawa, 2008), shown in figure Figure 2.6. Similarly, in this case, the important areas are defined near the essential hydrodynamic processes; the horseshoe vortex system, detached shear layer, and the vortex-shedding at the tip of the groyne.

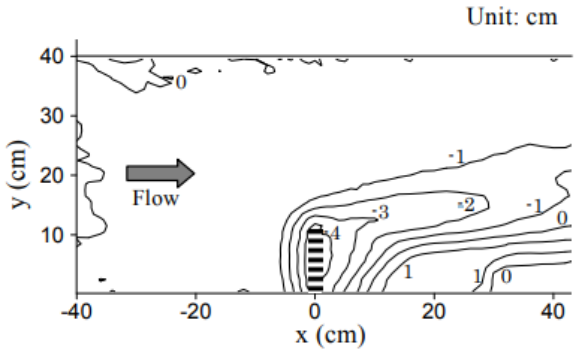

Figure 2.6: Scour around a permeable groyne construction, figure from Zhang & Nakagawa (2008)

The examination of erosion around 1:1 (45 °head steepness) sloped groynes have shown that most scour occurs around the tip of the groyne (Bahrami Yarahmadi et al., 2020) and was smaller and more asymmetrical compared to the rectangular groynes. This statement is in agreement with the observations of Ghaldarbandi et al. (2013), in where the bed shear stresses were compared with different slopes. Groynes with gentle slopes were observed with the small bed shear stresses compared with steep-sloped groynes. These results are similar to the shape-factors of groynes which are based on experimental investigations of scour depths (Kandasamy & Melville, 1998). From the investigations, it can be concluded that gentle slopes should result in minor abrupt flow movements than steep-sloped groynes. Therefore, less strong turbulent behaviour is present, which leads to reduced scour development.

2.3 Modelling various groyne structures

In this section, acknowledged information about modelling various groyne constructions is investigated. Information about the processes required in the model and turbulence modelling is specified. This investigation is executed explicitly for the characteristics of the flexible groyne, varying permeability and head steepness of the groyne.

2.3.1 Processes

Turbulence structures

Investigations Rajaratnam & Nwachukwu (1983), Chrisohoides et al. (2003), Uijttewaal (2005), Paik & Sotiropoulos (2005), Koken & Constantinescu (2008) suggest that the large turbulence structures, arising from the disturbances of the square groynes, have highly three-dimensional, non-hydrostatic flow features. Previous studies Chrisohoides et al. (2003), Paik & Sotiropoulos (2005), Koken & Constantinescu (2008) investigated the horse-shoe vortex system for groynes and observed the complexity of the various developing eddies and interactions with the shear layer upstream. It concludes that a tangled web of vortices dominates the flow upstream with axes perpendicular to either the surface or the surrounding walls. In addition, independent of time, a primary necklace vortex is present and oscillated in two states; one vortex close at the edge of the groyne and another one convected vortex away from the groyne Koken & Constantinescu (2008).

The mixing layer downstream is also heavily investigated for rectangular impermeable groynes Chrisohoides et al. (2003) and sloped permeable pile groynes Uijttewaal (2005). It concludes that the large-scale eddies and intense temporal oscillations in the horizontal plane dominate the processes in the mixing layer. The developing eddies merge with previously shedding eddies and interchange with large eddies of the recirculation zone downstream of the mixing layer, thus enhancing a sudden expansion of the shear layer Higham et al. (2017). Therefore, primarily two-dimensional patterns in the horizontal plane dominate the flow in the mixing layer. However, Reynolds shear stresses in the vertical direction are present in the mixing layer Jeon et al. (2018), which indicates that three-dimensional effects are nonnegligible.

Studies have discussed chiefly the results of turbulence structures for rectangular impermeable groynes without slopes. However, rectangular impermeable groynes show more substantial flow behaviour than that for permeable groynes Yeo et al. (2005), Mioduszewski & Maeno (2005), Kang et al. (2011b) or head sloped groynes Uijttewaal (2005), Kang et al. (2011b), Koken & Constantinescu (2014). Accordingly, implementing the highly three-dimensional, non-hydrostatic flow within the numerical model is desirable for sufficiently modelling flow characteristics around the permeable, head sloped groyne configurations.

Bottom friction

In a recent study, it shows that the two counter-rotating eddies in the recirculation zone have a relation with the shallowness of the flow Talstra (2011). Furthermore, another study concludes that bed friction contributes to the non-linear growth of the mixing layer Uijttewaal & Tukker (1998). Increasing roughness or decreasing the shallowness will enlarge the eddies' size and thus the location of the reattachment point. So in a more general manner, the sudden expansion of the mixing is a function of the bottom friction and water depth. An adequate approach of the flow near walls and bottom includes the contribution of the friction in the model.

Free surface flow

The interaction of the water and air phase is part of the flow behaviour around groynes. However, the importance of modelling this free surface flow is dependant on the objective. Including the free surface flow in numerical modelling increases the accuracy of modelling reattachment lengths downstream of the groynes (Ouillon & Denis, 1997). In addition, flow dynamics around groynes are present close to the free surface flow, such as the two counter-rotating circulations in the recirculation zone (Duan, 2009) and the formation of the vortex related to the horse-shoe vortex system upstream (Jeon et al., 2018). Hence, studies suggest that free surface modelling can not be neglected for flow around groynes.

The Froude number is the relation between the velocity by force and gravity and indicates the flow condition. It represents the relation between the velocity of the free surface flow and the velocity of an larger area due to gravitation. Hence, it is used for the representation of the free surface flow dynamics. Large Froude numbers in sub-critical flow regimes exhibit significant variations of flow surface levels (Roulund et al., 2005) and therefore simplified models may not be used, such as the rigid-lid assumptions. Hence, a numerical method that tracks the free surface flow is suggested for high Froude numbers, respectively more extensive values of 0.5 (Paik et al., 2014). For flow around an abutment in open channel flow shows a comparison for tracking free surface flow between a rigid-lid approximation and level-set method. Froude number of 0.36 shows non-negligible effects of the near bed flow statistics between the approaches and hence a more complex method for surface tracking is suggested for these small Froude numbers (Khosronejad et al., 2019).

Flow in the porous medium

For permeable groynes, an essential feature is the flow in the porous medium. Studies Mioduszewski & Maeno (2005), Jin & Kuznetsov (2017), Banerjee et al. (2018) show various approaches for the computation of turbulent flow in porous zones. Typically, turbulent flow in porous zones has non-linear behaviour and is therefore calculated using the known Forchheimer equation, which includes the inertial term in the equation (Jin & Kuznetsov, 2017). However, difficulties are present in concluding general formulations based on the Forchheimer equations for various porous mediums. One of the most widely used equations is proposed by Stephenson (1979), which is based on non-linear flow equations for rock-fill structures (Yousefi & Hosseini, 2019). The hydraulic gradient is calculated using empirical equations developed by using experimental data. This equation is stated as follows:

$$i = \frac{800v}{gnd^2}V + \frac{K_t}{n^2 gd}V^2 \tag{2.1}$$

In which the i is the hydraulic gradient, V is bulk velocity through the system, n is the porosity, v is the kinematic viscosity, d is the mean particle size and K_t is the friction coefficient in the turbulent region of the flow. Stephenson has a very general formulation for the medium particles, in which the geometry of the particles is taken into account by this K_t factor. Still, it is important to understand that this formulation differs for every case.

The study of simulating turbulent flow through coarse granular porous media within an open channel flow, shown in Banerjee et al. (2018), has implemented a slightly different approach based on the Forchheimer equation. The Forchheimer equation defines the turbulent flow process in porous media as a pressure difference over a length scale. Hence, it indicates a pressure loss, which is used within the fully Navier-Stokes equations. Results have shown that this method could analyse the flow through porous media with sufficient precision.

Geometry of the groyne

The complex geometry of groynes is another aspect of the difficulties in modelling groynes. Ambagts (2019) uses a numerical model for groynes with a slope of 1:2. The slopes' complexity uses a sub-grid parametrisation when the grid cell sizes are larger than the groyne's geometry. Another option for defining groynes' geometry is using unstructured mesh, which is used to create complex geometries for modelling groynes (Nakagawa et al., 2004). The models show satisfactory results compared with the experimental results. Hence, both approaches are applicable for relatively complex geometry, such as a sloped head groyne.

Implementation of the processes

Previous paragraphs conducted the essential processes for modelling flow around groynes and is concluded as follows:

- Free surface flow. The interaction with the air and water phase is essential due to the flow dynamics near the water surface and the increase in flow modelling accuracy.
- The three-dimensional features of the flow around groynes requires non-hydrostatic assumptions
- Variability in the geometry of the groyne and environment to implement the variation of the groynes' geometry
- Adapting the modelling of a porous zone for turbulent flow by using a macroscopic approach
- Implementation of the wall function sufficiently for including the bottom friction and wall friction
- Adaption of large turbulence structures due to the macro fluctuations

The processes stated above show from previous studies that they are essential for representing the flow around groynes. The features for the flexible groyne, variability in permeability, and steepness of groynes' head lead to a possible reduction of the turbulent flow behaviour. Hence, including these processes supports setting up a satisfactory model for a flexible groyne.

2.3.2 Turbulence modelling

The numerical approach for most engineering flow models is based on the Reynold averaged Navier-Stokes turbulence models (RANS). The Reynold-Averaging method uses the different turbulence scales on the mean flow. Past studies show that both steady and unsteady RANS models did not adequately predict essential aspects of separation flow dominated by the development of vortex shedding and large-scale vortex interactions (Rodi, 1997, McCoy et al., 2008, Koken & Constantinescu, 2008). The RANS models severely underpredict the turbulent fluctuations and width of the mixing layer. In addition, the RANS method fails in a highly three-dimensional flow that is associated with strong anisotropic turbulence (Kang & Sotiropoulos, 2012) due to the isotropic approach of most RANS models. Inaccuracies for detailed flow occur in RANS models, however, large scale turbulent structures are sufficiently captured (Chrisohoides et al., 2003) while maintaining relatively low computational costs.

Calculating turbulence

Multiple options can indicate the turbulent properties and consequently quantify the turbulent structures within a model. As already stated, the Reynolds stresses are generally used for indicating the turbulence, as shown in Duan (2009). Reynolds stresses are obtained by directly obtaining the fluctuations of the velocity. However, this method is an extensive, complicated approach in numerical and experimental studies. Hence, the Reynolds stresses can also be obtained by using the Boussinesq hypothesis, which simplifies the approaching the Reynolds stresses. More information about calculating the Reynolds stresses is stated in the appendix, shown in Appendix B.1.

Vorticity is another essential property of a fluid that describes the local spinning motion and plays a vital role in the turbulence dynamics (Perry & Chong, 1982). There is no generally accepted definition for vortices. The vorticity shows the importance of the turbulence dynamics such as turbulence generation, kinetic energy production and dissipation (Dong et al., 2016). The method chosen will be dependant on the capabilities of the numerical model.

Turbulence models

Separation flow with large turbulent structures is present for flow around groyne-like structures. This flow behaviour has to be simulated carefully to agree with the experiments and to present the bed shear stresses satisfactory. Various successful turbulent models have been derived during the past years, such as large-eddy simulations (LES), detached eddy simulations (DES)/hybrid RANS models or RANS models with turbulent closure models. For flow around groynes, LES has been applied by Koken & Constantinescu (2008), Paik & Sotiropoulos (2005) has adapted DES and a three-dimensional flow model using $k-\omega$ turbulent closure model combined with the RANS model is used by Chrisohoides et al. (2003). In a less detailed study for the turbulent quantities, a three-dimensional flow model using the standard $k-\epsilon$ turbulent closure model by Ho et al. (2007) and Zhang et al. (2005) is used with sufficient accuracies.

Lately, investigations for numerical flow models have been studied for various groyne configurations such as Choufu et al. (2019) and Saberi & Galoie (2017) by using RANS with the $k-\epsilon$ turbulent closure model or Shamloo & Pirzadeh (2014) using the RANS model with a Reynold stress model for turbulence closure modelling. Also, for modelling longshore currents on permeable groynes are investigated by Zhang (2020) using the RANS method. An overview of numerical investigations for flow around emerged groynes is seen in the appendix Table G.2.

3 Software selection

The literature review has given much information about the effects of groynes on flow characteristics. Additionally, literature is given for the applied software packages for the modelling. Most software packages vary and have limitations for modelling fluid dynamics. Therefore, it is essential to understand the various software packages and whether they are suitable for the research. Most specific cases are very distinctive and should be analysed to verify if the software is sufficient for the specific interested area. This section explains the approach and selection of various software packages, resulting in one particular software used in the study. Furthermore, the concluded software package is described for the essential processes required for the model.

3.1 Approach to software selection

The literature study, Section 2.3.2, shows multiple numerical studies using various software or codings for modelling flow around groynes. Applied software for modelling flow around groynes as stated in the literature study are Flow3D (Flow Science, 2019), OpenFOAM (OpenFOAM, 2021), Fluent (ANSYS, 2019) and Telemac3D (Telemac-3D, 2020). These models are considered and reflected on for the application of modelling the flow characteristics around a permeable, head sloped groyne. In addition, other interesting and available software packages are considered for this study. First, the required technical implementation of the software package is described. Subsequently, the software package is chosen by comparing the abilities and the possibilities.

3.1.1 Technical implementations

Computational method

The numerical discretizations of the solving equations can be executed by using various computational methods such as the finite volume method (FVM), finite element method (FEM) or finite difference method (FDM). A computational method is not defined to be better than the other one. It is dependant on multiple variables to choose the most fitted method, for instance, the area of interest, recent studies using this method or the implementation of satisfying the consistency and stability.

Solving equations

Various software packages using hydraulic models are designed for modelling free-surface flow problems occurring in a river, seas and oceans, in which they apply the shallow water equations (SWE). Non-linear effects and adverse vertical gradients are present in some cases, which is not fully solved by applying SWE. The non-hydrostatic assumptions have to be taken into account in these circumstances, and thus the fully three-dimensional Navier-Stokes (3D NS) equations are solved.

Mesh

Meshing is used to decompose the domain into smaller cells and, therefore, define the attributes of the flow in every cell. For complex geometries, the meshing becomes relatively challenging. A structured mesh is observed to be difficult to use in these cases, as stated in Section 2.3.1. Unstructured meshes are mostly used, but also curvilinear meshes could be applied. Both of these meshes are acknowledged as flexible meshes. In addition, turbulent flow is multi-scale and therefore requires a flexible mesh.

Permeability implementation

The implementation of the permeability is important for modelling a porous medium. Hence, a non-linear function for the flow in the porous medium is required for modelling the turbulent behaviour within this area as stated in Section 2.3.1.

Wall function

The importance of the bottom friction as stated in Section 2.3.1 leads to accurately modelling the flow near the walls. Therefore, a fitted function of the flow near the wall behaviour is required. Implementation of the wall functions is dependant on the implementation of the turbulence modelling. Consequently, varieties of options for the wall function is necessitated to contribute sufficient for modelling flow near the walls.

Turbulence modelling

Both models solving the SWE and 3D NS include the approach for treating the turbulence modelling. Most of these models have multiple options to implement turbulence and depend on the particular problem to implement the correct method. An interesting option for flow around groynes is the use of a DES or LES model in which the anisotropic behaviour of the flow is taken into account. Flexible options for the implementation of turbulence modelling may help in setting up a sufficient model for turbulent flow.

Free-surface flow

The free-surface flow is considered in every software package but has been implemented using various methods applicable to the model. Hydraulic models use a single-valued function for presenting the movement of the free surface. CFD software packages apply more extensive free surface tracking methods include the Volume of Fluid (VOF), level-set methods (LSM), Marker-and-Cell (MAC) or Galerkin Interface Stabilization (GIS) methods. Frequently used for flow around groynes in which turbulent free-surface flow is present is the VOF method in CFD packages. Most numerical studies with a VOF method show agreement with the experimental studies as shown in Paik et al. (2014).

3.1.2 Reference applications

Various software packages have been used for modelling flow around groynes. Hence, for specific cases, it is of additional significance that various processes are already applied and validated. Furthermore, references increase the reliability to model the flow accurately with the specific software package. The practical information is based on the manuals for every software package and the previous numerical model investigations.

The availability and practicality for every software package have to be addressed as well. The availability is specified as commercial, open-source, and available and is based on the environmental conditions of the investigation. The practicality is dependant on the interface, user-friendly software and serviceability of the software and ranges from sufficient to excellent.

3.1.3 Overview of software packages

Today, many software packages are being used for flow modelling. However, it is not practical to list every possible software package. In addition to the already presented software packages, a few more are added to the comparisons. The software packages available for this study and potentially useful is Mike3 DHI (Mike3, 2017), Finel (Finel, 2012) and Delft3D (Delft3D, 2021).

Combining all the abilities of the various software packages and reference applications results in an overview of the software packages. Two tables are presented to identify the various models used in previous studies for flow around groynes. In the first table, the technical implementations are ranged from limited capabilities to an extensive range of possibilities. In the second table, the various models are referred to the applicability, range of implementations stated in reports and validation. Also, the availability and practicality are presented to show the ability to use the software package.

Table 3.1: Overview models for modelling hydrodynamics of groynes with technical implementations

	Free-surface	Solving	Mesh	Permeability impl.	Wall func.	Turbulent impl.
Flow3D	VOF	3D NS	Flexible	non-linear eq.	limited	RANS, LES
Delft3D	Single-valued	SWE	Flexible	Simplified	limited	RANS
Mike3 DHI	Single-valued	SWE	Flexible	Porosity material	Unknown	RANS
OpenFoam	VOF, Level-set	3D NS	Flexible	Forchheimer eq.	Extensive	RANS, DES, LES
Fluent	VOF, Level-set	3D NS	Flexible	Superficial eq.	Extensive	RANS, DES, LES
Finel	GIS	3D NS	Flexible	Forchheimer eq.	Extensive	RANS, LES
Telemac3D	Single-valued	SWE	Limited	Unknown	Extensive	RANS, DES, LES

Table 3.2: Overview models for modelling hydrodynamics of groynes with reference models, applied cases and practicality

	Frequency	Permeability	Geometry	Validated	Availability	Practicality
Flow3D	Often	Yes	Flexible	Yes	Commercial	Excellent
Delft3D	Few	No	Flexible	Yes	Open-source	Excellent
Mike3 DHI	No	No	Flexible	No	Available	Excellent
OpenFoam	Often	Yes	Flexible	Yes	Open-source	Sufficient
Fluent	Often	Yes	Flexible	Yes	Available	Excellent
Finel	Few	Yes	Flexible	No	Available	Good
Telemac3D	Few	No	Limited	Yes	Commercial	Excellent

3.2 Result software selection

3.2.1 Assessment of software selection

Table 3.1 and Table 3.2 show that all models have some advantages and possible disabilities for modelling flow around groynes. Hence, considerations are made for choosing the most fitted software package. In the literature study, essential processes are stated for the flow around groynes with variation in permeability and head steepness. However, to improve the consideration of choosing a model, the most critical processes are identified, which are required of the software package. The most critical implementations are inclusion of non-hydrostatic effects, adapting the large turbulent structures and implementing the porous zone using a non-linear function based on the Forchheimer equation.

Hydrostatic assumptions are used in the SWE, and thus hydraulic models neglect the non-hydrostatic effects. Hence, Delft3D, Mike3 DHI and Telemac3D are not chosen for this study. For the implementation of the large turbulent structures, RANS modelling should be sufficient, as stated in 2.3.2. However, to increase the model's accuracy, more minor turbulent scales have to be resolved. A more non-isotropic approach to turbulence closure modelling is required. LES or DES models are used in those cases, whereas the LES models require extensive computations resources. Therefore, software packages including DES models for turbulence modelling are preferred. OpenFOAM and Fluent have shown both the ability to solve the 3D NS using a DES or LES model. In addition, both have shown implementations of solving the flow in a porous medium using equations based on the Forchheimer equation.

Both OpenFOAM and Fluent show the ability to implement all the identified important processes for the flow around groynes. OpenFOAM is an open-source software package in which the program is handled with a text-based interface, and much coding is required. Fluent is a commercial software package from ANSYS with a straightforward graphical user interface and an extensive support desk. Both software packages are available for this study and have shown remarkable results in previous numerical studies for turbulent flow. The practicality and user-friendly interface of Fluent is the decisive factor in choosing this program for further studying.

3.2.2 Background of model

Ansys Fluent is the chosen software for applying the various groyne configurations. Hence, it is essential to have some basic understanding of the composition of the solution for a specific model. The general solution for the motion of fluids is based on the Navier-Stokes equation and expresses the momentum and mass balance. However, due to the equations' complexity, many versions exist to describe the phenomena for specific engineering areas.

Ansys Fluent solves the complete set of three-dimensional equations of the Navier-Stokes equations in combination with an appropriate turbulent representation. This method may describe any kind of complicated flow phenomenons. It uses the finite-volume method (FVM) to discretize the governing Navier-Stokes equations. Conservation of mass, which is the first part of the Navier-Stokes equation, is described by the differential equation as follows:

$$\frac{\partial \rho}{\partial t} + \nabla \cdot (\rho \vec{v}) = S_m \tag{3.1}$$

where ρ is the density of the fluid. $\vec{v}$ is the velocity, and S_m is the source term, which can be used for adding mass or any user-defined sources. The differential equation for the conservation of momentum, is written as follows:

$$\frac{\partial}{\partial t}(\rho\vec{v}) + \nabla \cdot (\rho\vec{v}\vec{v}) = -\nabla \cdot p + \nabla \cdot \left[\mu\left(\nabla\vec{v} + \nabla\vec{v}^T\right)\right] + \rho\vec{g} + \vec{F} \tag{3.2}$$

where p is the static pressure, $\vec{v}$ is the velocity, g is the gravity. $\mu = \mu_0 + \mu_t$, where μ_0 is the viscosity of the fluid, μ_t is the turbulence viscosity, and $\vec{F}$ is the external body force.

Turbulence model

Dealing with turbulence effects in the Navier-Stokes equations can be solved using four different methods: Empirical relations (1), methods using the Reynolds-averaged Navier-Stokes (RANS) equations in which a time-averaged approach is used (2), direct numerical simulations (DNS) (3), and large-eddy simulations (LES) (4) Rodi (2017). A variety of the LES and RANS methods are available in ANSYS Fluent ANSYS (2019) and are considered in this research.

RANS models consider the effect of turbulence on the mean flow while not resolving the actual turbulent motion. The averaging process from the Navier-stokes equations to the RANS equations leads to additional terms correlated with the unknown fluctuation velocities, also known as the Reynolds stresses. Hence, the equations are not fully closed, and a turbulence model is required for the unknown quantities. The foundation of most turbulence closure models is based on introducing the turbulent viscosity, which takes the turbulent effects into account. This quantity depends on the turbulent properties, and it is assumed locally that the turbulence has isotropic behaviour. On the other hand, LES resolved the turbulent motion for the scale dependant on the grid size of the numerical domain and resolves the isotropic behaviour for these motions. DES employs the eddy-viscosity models as RANS near walls and further away resolves the turbulent motion for large scales as LES.

Most calculations in hydraulics have been carried out with the use of RANS models Rodi (2017). This is also shown in the Table G.2, in where most studies for flows around groynes have used a RANS model or a hybrid RANS model for solving the turbulent effects. Many researchers have investigated the various turbulence model options for RANS in the software Yazdi et al. (2010), Ghaldarbandi et al. (2013), Kumar & Malik (2016) for flow around groynes, in which both the $k-\varepsilon$ models and $k-\omega$ models have been used with satisfactory results. By testing in the present numerical model, it has also been found that the $k-\omega$ models have been most accurate. Furthermore, these types of models are often used by adverse-pressure gradient flows Rodi (2017). However, it is known that Large Eddy Simulations (LES) have very accurate results for turbulent flow Koken & Constantinescu (2008). Using the LES approach is considered for composing this model, yet it is a time-consuming process and therefore not applied in this research Spalart (2000).

Free surface flow

Free surface flow is essential for modelling flow around groynes, as seen in Ouillon & Denis (1997), Duan (2009), Higham et al. (2017). Commonly, two approaches are used for modelling the interaction between the water phase and air phase. The first approach is a rigid-lid assumption, in which the water surface elevation does not change in time. A rigid-lid approximation typically represents a river flow in a sub-critical condition. The second approach tracks the surface flow numerically by expressing the properties of the air-water interface Katopodes (2019).

The rigid-lid assumption can be used in every software package. For the free surface tracking method, Fluent has the ability to use the VOF method, level-set method and a combination of both methods. Various studies for flow around groynes have used different methods for solving the free surface flow. Mostly VOF models or rigid-lid assumptions have been used, as seen in the appendix Table G.2.

Non-hydrostatic

Hydrostatic pressure assumption is based on the neglection of the acceleration and eddy viscosity terms in the momentum equation for the vertical component of the differential equations stated in Section 3.2.2. However, it is already mentioned that three-dimensional effects are nonnegligible in Section 2.3.1 for flow around groynes and, therefore, a hydrostatic assumption is not applicable. Hence, the fully 3D Navier-Stokes equations must be solved in order to maintain an accurate representation of the flow around the various configurations of groynes in this research.

Porous zone

In the software program ANSYS Fluent, the porous zone is calculated by using a source term in the momentum equation of the Navier-Stokes differential equations stated in Section 3.2.2 and is referred to as the pressure drop. The pressure drop is based on the Darcy-equation though it added a part in the source term. Hence, the source term is composed of two parts: the viscous loss term and the inertial loss term. The total pressure drop is stated as follows:

$$\Delta P = D\mu V + C\frac{1}{2}\rho V^2 \tag{3.3}$$

where $D = \frac{1}{\alpha}$ with α is the permeability, C is the inertial loss and V is the velocity through the porous media. It must be noted that both coefficients (C and D) have to be calculated divided by the thickness.

The coefficients D and C are known as the viscous resistance factor and inertial resistance factor and must both indicated in the model as input parameters. For the known media, the pressure drop must be calculated through the porous medium from experimental results. The pressure drop data must be matched with a curve fit, so coefficients for the linear and quadratic term will be generated.

However, it must be noted that the fluid will also flow parallel over the porous media. Study of Prinos et al. (2003) uses the 'microscopic approach' to investigate for turbulent flow regimes the characteristics of flow over and within the porous media. The 'microscopic approach' is based on using low-Reynolds number with the $k - \epsilon$ turbulence model. This study shows that this approach's results are in satisfactory agreement with the experiments for turbulent flow. A conclusion was made that the porous layer structure (both staggered as non-staggered arrangement) have little effect on the flow characteristics near the fluid and porous interface. In addition, the mean flow velocities for the turbulent flow near the porous structure tends to decrease significantly for increasing permeability.

Roughness

The roughness is present in both the bed and wall frictions. In Fluent, many options are available to model this aspect. In recent numerical studies, default settings have widely been used for solving this problem. The standard formula for the wall function is based on Nikuradse experiments. For smooth walls, the velocity profile normal to the walls follows:

$$U^+ = \frac{1}{\kappa} log(Ey^+) \qquad 30 < y^+ < 300 \tag{3.4}$$

However, for an increase in roughness, an increase of the wall shear stress is present. The profile of the velocity will increase, and therefore, a modification is present. The modification of the velocity profile is achieved by adding a function ΔB based on the size and shape of the roughness elements:

$$U^+ = \frac{1}{\kappa} log(Ey^+) - \Delta B \tag{3.5}$$

The roughness height and roughness constant are the inputs for this standard wall function. Uniform roughness elements result in a roughness constant value of 0.5, and non-uniform elements may be as high as 1.0 (ANSYS, 2019).

Geometry

ANSYS Fluent options various types of mesh for modelling in Computational Fluid Dynamics (CFD). Both structured as unstructured meshes are possible. The meshes vary from simple rectangular meshes as hexahedral or tetrahedral mesh formations. Improvements around walls and objectives are possible by using refinements.

4 Validation

This chapter is the validation of the numerical model by comparing the experimental results with the numerical results. The validation approach is the first part. The set-up of the model is explained, and the optimization of the three models is described. The results of the various models are stated in the following part, in which extensively the results are extensively investigated for validation purposes.

4.1 Approach to validation

This section explains the set up and approach for validating the numerical model which is used for obtaining a conclusion of the objective. Hence, the numerical model represents the turbulent flow around the groyne. The approach of setting up this model and choosing the various input parameters are extensively discussed.

The validation is executed for three different cases before concluding a complete numerical model for the research. At first, the models should be validated for a conventional groyne construction, in which the turbulent properties of the flow, flow patterns and flow velocities must be included. Secondly, a coupled system of the flow in a porous zone and open channel flow should be validated. Lastly, the third case is verifying the geometry of the groyne, resulting in flow around groynes with slopes. Additionally, this case features the turbulent properties, flow patterns and flow velocities to have more insight into the 3D flow characteristics. The set-ups slightly vary from each other due to presenting various implications and computational domains. Nevertheless, the combination of these models results in the final numerical model used further in the research.

4.1.1 General input

Setting up this model in ANSYS Fluent is stated as a time-dependent flow problem in an open channel, on which the controlling factors are based. The amount of modifying parameters are dependant on the software program used. For ANSYS Fluent, this may be listed as:

- Mesh properties
- Various input parameters such as operational conditions, materials, interaction conditions, cell zone conditions
- Boundary conditions such as inflow, outflow, friction, surface condition
- Turbulence model
- Solving methods

Each controlling factor is discussed and concluded for this specific numerical model in the next few sections.

Mesh properties

In Fluent ANSYS (2019), a general approach to determining an adequate type of mesh is by analyzing the geometry and the complexity of the model. In this case, the model could be classified as relatively complex because of the multiple refinements and obstacles within an open channel domain. Hence, tetrahedral meshing is advised. The mesh size depends on the required solution of the model and is directly related to the computing time and Courant number.

The Courant number is present for every numerical simulation and shows the amount of convergence by the model. In a three-dimensional case, the Courant number becomes:

$$C = \frac{u_x \delta t}{\delta x} + \frac{u_y \delta t}{\delta y} + \frac{u_z \delta t}{\delta z} \tag{4.1}$$

The implicit method in Fluent suggests to have Courant number below 20 for a stable system. Explicit methods in Fluent suggests a Courant number below $1$for stable solutions.

Another essential property of the mesh is the skewness. The skewness defines the amount of mesh quality and stability of the grid. In default, the maximum skewness is defined as 0.9. Closer to zero is preferable for an accurate solution. In relatively complex geometries, the skewness may become a problem, and therefore the solver methods have to be adapted to the amount of skewness. A standard option 'improve mesh quality' is used for improving the mesh skewness with maximum skewness of the cells of around 0.5.

For validation purposes, the numerical models are based on experimental studies, so sizes of flumes in water labs are used. The mesh sizes are dependant on this matter. However, they are also heavily dependant on solving turbulence modelling adequately, showing sufficient resolution of the horse-shoe vortex system, the development of vortex shedding and mixing-layer. For an initial mesh size, the use of the y^+ value is applied. The y^+ value is an important parameter for indicating the correct behaviour of the wall function for flow near the walls. This parameter should have a minimum value of 30 and around a maximum value of 300, when using the standard formula for the wall function, as stated in Section 3.2.2.

The formula for the y^+ is defined as:

$$y^+ = \frac{u_\tau y}{\nu} \tag{4.2}$$

where u_τ is the friction velocity, and y is the distance of the wall to the centre of the first cell. The unknown friction velocity is based on the wall shear stress, and accordingly, the skin friction has to be calculated as well. For an initial value, the skin friction coefficient is calculated based on Halleen-Johnston's correlation with experiments in channels, as proposed in Wilcox (2006). The friction coefficient and wall shear stress are described as follows:

$$c_f = 0.0706 \cdot RE_H^{-1/4} \tag{4.3}$$

$$\tau = 0.5 \cdot H \cdot \rho \cdot u^2 \cdot c_f \tag{4.4}$$

Consequently, the friction velocity can be computed with

$$u_\tau = \sqrt{\frac{\tau}{\rho}} \tag{4.5}$$

Based on these aspects and equations, mesh sizes for the numerical models in this report are specified and are approximately $\Delta x = 0.03\ m$. Furthermore, the amount of cells are also heavily dependant on the computational cost and thus the cell size is optimized for the specific model by using a grid dependency test.

Input parameters

Various starting input parameters are identified for the numerical model, stated as operational conditions, characteristics of the materials, interaction conditions and cell conditions. In general, this will not differ between each model when a multi-phase approach is used for water-air modelling.

The operational conditions are parameters for the operating conditions of the model. The operating parameters for gravity, density, temperature and pressure are identified and specified as in figure Fig. 4.1.

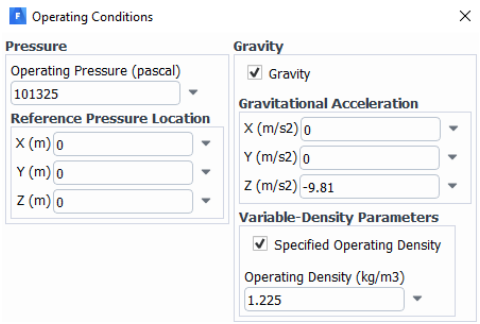

Figure 4.1: Input settings for the operational conditions in ANSYS Fluent

Both materials, air and water are specified for the numerical model. Default values are used, which are already stated in the library of ANSYS Fluent. The order of the phases are important for solving the model. ANSYS Fluent calculates the second phase material as the main flowing property and therefore the phase of water is used as the second phase. The interaction between the materials is specified as surface tension and has a constant value of $0.072\ N/m$.

The cell conditions are only used for defining the porous media. Cell conditions for the porous media is already discussed in the Section 3.2.2. However, the specific input parameters are dependant on the material of the porous media. Hence, the input settings is discussed in the specific numerical model set up.

Boundary conditions

The boundary conditions in ANSYS Fluent is specified to create an open channel flow. The standard formulation for open channel boundary conditions is based on known properties of the fluid and assumptions of the flow conditions. The open channel flow conditions are defined for sub-critical flow, thus requires one boundary condition upstream and one boundary condition downstream. Furthermore, the boundary conditions for the walls and the free surface has to be defined for completing the definition of the model.

Upstream boundary condition

The upstream boundary condition is defined for the water and air phase. However, by using the open channel condition in ANSYS Fluent, both materials are defined in the upstream boundary condition without dividing the boundary into two sections. Hence, only one boundary condition is stated for the whole plane upstream. The upstream boundary condition is defined as a pressure inlet, and therefore the pressure has to be indicated. Though, due to the open channel condition, the water velocity and water level must be specified. These parameters define the properties of the flowing water in the channel. Other parameters such as turbulent intensities and viscosities are using default values. Specific boundary conditions per numerical model are stated in the validation.

Downstream boundary condition

The downstream boundary condition is also combined with the sub model of the open channel condition. Hence, the downstream boundary is indicated as a pressure outlet, with specified parameters for the water level. For free open flow conditions in the outlet, the pressure is indicated as zero.

Wall and surface boundary condition

Both wall and surface boundary conditions use default values. The wall condition is based on the standard wall function, as stated in 3.2.2. Using default values is considered to be a smooth wall without any roughness height. The surface condition is in contact with the air layer, and therefore, default values should be sufficient. Optimizing these values is recommended when specific problems occur at the boundaries of the model.

Turbulence model

Various studies have shown satisfactory results for modelling flow around groynes using different turbulent models, as shown in the literature study. Several studies Paik & Sotiropoulos (2005), Koken & Constantinescu (2009, 2014) have shown extensive interest in turbulent flow around groyne-like structures and resulted in satisfactory results compared to the experiments. The initial turbulence model used in these studies is the Detached Eddy Simulation (DES) model. RANS with turbulence closure models have also been used for flow around groynes with sufficient accuracy Chrisohoides et al. (2003), Yazdi et al. (2010), Shampa et al. (2020) by using the $k-\omega$ model. As a result of the literature study, both models solve the large turbulent structures, and hence both models are initially used for this model. In the sensitivity analysis executed for the square groyne, the most fitted turbulence model is identified.

The DES model is introduced to use in this report. Solving the DES model is not executed for the whole domain, which is computationally very extensive. Therefore, a RANS model is selected for the remaining solving part of the model, in which the SST $k-\omega$ model is used. Modelling flow separation from smooth surfaces is favoured using the SST $k-\omega$ model based on most numerical studies and stated in the ANSYS Fluent manual ANSYS (2019). However, modelling the flow with the DES model should be applied when the turbulent length scale is larger than the mesh size. Otherwise, the model calculates the whole domain with the RANS model; therefore, no specific advantage is obtained. DES simulations have no limitations, yet more small mesh sizes result in more accurate solutions of the turbulence motion.

Additionally, various options are available to complete the turbulence model. In specific for the turbulent flow, the curvature correction is a possibility to enhance the model. Therefore, a sensitivity analysis is used for the curvature correction, whether this option is appropriate for the model. Usually, the curvature correction is used for high swirling flow and flow in curvature regions.

At last, the volume-of-fluid model (VOF) is adapted. This multi-phase approach is used to model the air-water interaction sufficiently, as stated before in Section 3.2.2. The VOF model is executed with a sub-model called open channel flow, favoured for modelling open channel flow. The formulation of modelling with the open channel model is implicit and uses implicit body forces.

Solving methods

In ANSYS Fluent, various solution methods can be used to calculate the momentum and conservation equations, also known as the Navier-Stokes equations, as stated before. The solving methods vary for each different case to improve the stability of the numerical model. Hence, the aim is to increase the stability by choosing the correct method. These equations have to be discretized for solving the equations numerically. A control-volume-based technique (Finite-volume method) converts a general scalar transport equation to an algebraic equation. By default, the stored discrete values are placed in the centre of a cell, however, the equation is solved using the discrete values at the face of a cell. Constructing scalar values at the cell faces requires gradients to discretize the convection and diffusion terms. Typically the Least Squares Cell-Based Gradient method is used for irregular, unstructured meshes and is less extensive to compute than other methods. Hence, this model uses complex meshing in which the Least Squares Cell-Based Gradient method is used for better stability of the model.

The software package solves the discretized equations in two approaches, a pressure-based solver and a density-based solver. Usually, turbulent flow in open channels is solved by using a pressure-based approach. A pressure-based approach for transient flow in Fluent may split into multiple subsections, which altogether describes the full momentum and conservation equations:

- Discretization of the Momentum Equation
- Discretization of the Continuity Equation
- Pressure-Velocity Coupling
- Time-Advancement Algorithm

The most suitable options for the numerical model are presented here, which should improve the stability and accuracy of the numerical model. More explanation about the various solution methods are stated in the Appendix A.1.

The discretization of the momentum equation is solved with the PRESTO! scheme, which is preferred due to the accuracy for high swirling flow. The discretization of the continuity equation has a default approach for incompressible flow. An arithmetic averaging method is used in this case. For the pressure-velocity coupling, two algorithms are mainly used for open channel flow. Therefore, both will be analyzed in a sensitivity analysis further on. The time-advancement algorithm uses second-order schemes resulting in the most accurate solutions.

4.1.2 Validation criteria

Sensitivity analyses are used to improve the model to increase the accuracy with the experimental data, i.e. the validation. The sensitivity analysis compares various parameters within the model, which is expected to improve the stability and accuracy of the model. The validation analysis compares the numerical results directly with the experimental data. Both analyses require criteria aspects to determine the conclusion of the analysis transparently. The sensitivity analysis is used to determine the most fitted model, while the validation analyses the whole model and shows the model's accuracy with the experimental data. Three points are considered for the criteria:

- Maximum and minimum values and locations of the velocity and Reynold shear stresses
- The Root mean square error (RMSE) and Percentage bias (PBIAS) average statistics within a cross-section line
- The streamwise and lateral velocities near the bed-plane

The maximum and minimum values of the flow characteristics and their locations are directly related to the large turbulent structures. So, these results determine the conclusions of the research questions. The RMSE and PBIAS define the validity of the model statistically. Hence, the sufficiency of the model for predicting flow characteristics compared to the experiments. The last criterion states that the streamwise and lateral velocities are crucial in the numerical flow model. It is shown in the literature that the flow in the horizontal plane (x - y-direction) is more dominant for flow around groynes. In addition, the research is focused on the turbulent structures near the bed plane. Therefore, the horizontal flow near the bed plane is a critical aspect of the analysis.

Maximum and minimum values

The maximum and minimum values in the model is determined by using visualisations. The results of these visualisations determines the maximum and minimum values and their locations. By observation, the comparison with the experimental results is made and thus determining the most fitting model.

RMSE and PBIAS

The statistical part is defined by two statistics. RMSE is a well known statistical criteria in the flow dynamics and river field. PBIAS is more used in large scale flow events, however, is still very useful to determine the bias of the model.

RMSE is defined as the root mean square error and formulated as follows:

$$RMSE = \sqrt{\frac{\sum_{i=1}^{n}(Y_i^{sim} - Y_i^{exp})^2}{n}} \tag{4.6}$$

With Y^{sim} and Y^{exp} as the simulated and experimental data set.

For calculating the percentage of the RMSE, the absolute maximum value of the data is used (for the specific location). Most numerical studies of flow dynamics in rivers are sufficient for a RMSE percentage beneath the 30 % value.

PBIAS is defined as the percentage bias of the model. A very simplistic formula which is a very common statistical parameter for validation purposes.

$$PBIAS = \frac{\sum_{i=1}^{n}(Y_i^{sim} - Y_i^{exp}) \cdot 100}{\sum_{i=1}^{n} Y_i^{exp}} \tag{4.7}$$

With Y^{sim} and Y^{exp} as the simulated and experimental data set. The PBIAS shows statistics of the model in which the bias of the model is given. This statistic is mostly used in large river simulations and is mostly sufficient beneath a percentage of 25 for the streamwise flow velocities.

Streamwise and lateral velocities

The streamwise and lateral velocities are most important in determining the flow dynamics around a groyne. Besides the large velocity values, the horizontal circulations are most critical in modelling the flow. Therefore, these particular features are taken into account for determining the most fitted model.

4.1.3 Rectangular conventional groyne structure

For the conventional groyne construction, various experimental studies have been studied. A complete and extensive study is executed in Jeon et al. (2018), where shear stresses, turbulent properties and long-range flow patterns are shown with extensive data for flow around groynes in rectangular form.

Hence, in this case, the following parameters will be validated:

- Contour lines
- Mean values velocities
- Reynold shear stresses

The geometry of this study is shown in figure Fig. 4.2 and shows a lot of data points around the groyne. Furthermore, various settings for the boundary conditions of the numerical model are specifically specified for validation purposes. These are as follows:

Parameters	Values
Flow depth [m]	0.215
Flume width [m]	0.9
Flume length [m]	7
Length of groyne in x-direction [m]	0.04
Length of groyne in y-direction [m]	0.3
Initial velocity [m/s]	0.144
Froude number	0.10
Reynolds number	3.00 x 10^4
Kinematic viscosity [m^2/s]	1.03 x 10^-6

Still, some input parameters are unknown for the numerical model, and therefore sensitivity analyses are made to verify the proper settings of the model. These are stated in the following section. After these analyses, the resulting model is applied and shown in Section 4.2.

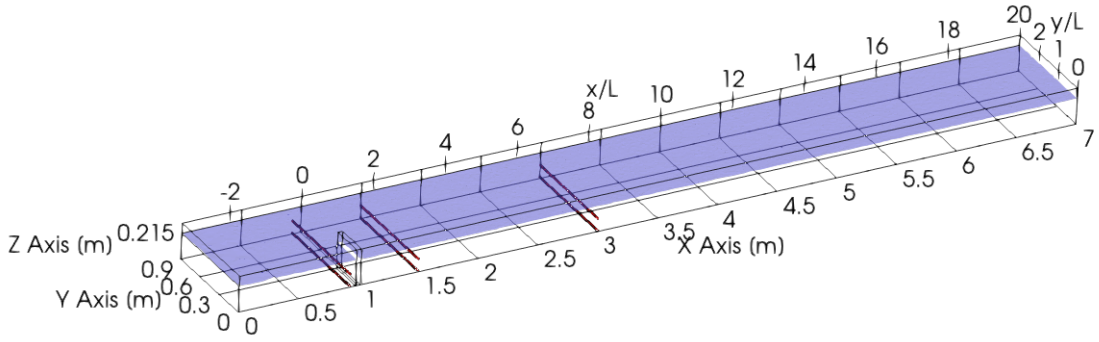

Figure 4.2: Geometry of the square groyne with the dimensions of the experiment from Jeon et al. (2018) in the numerical model. The locations of the validation and sensitivity analysis are shown in red, respectively $-0.23\ x/L$, $1.67\ x/L$ and $6.67\ x/L$; near the bed $0.01\ m$, $0.05\ z/D$ and in the mid-plane $0.11\ m$, $0.51\ z/D$

Sensitivity analysis for the input parameters

The sensitivity analyses investigate various settings to optimize the model. The following options are evaluated:

- Turbulence models
- Use of a curvature correction
- Solver algorithm

In previous studies, a lot of different turbulent models have been used. Mostly, the $k-\omega$ SST and DES models are used with sufficient accuracies compared to the experimental studies. Therefore, a comparison is made to optimize the model and compare which turbulent model favours the flow around groynes for this specific case.

The curvature correction is an option in ANSYS Fluent in which the curvature flow is optimized. Normally, the production term in the Navier-Stokes equation is damped for flow with small turbulent structures. The curvature correction enhances the production term, which increases the turbulent properties for curvature flow. The manual of ANSYS Fluent stated that this option is considered to be an addition for strong rotational, separating flow.

PISO and SIMPLE are considered to be general algorithms to solve the Navier-Stokes equation in an iterative manner. Both have benefits and disadvantages as stated in Appendix A.1. For this reason, it is worthwhile to investigate which algorithm optimizes the model for this research.

An essential area is directly downstream of the groyne, where the large turbulent structures and velocities are expected to be significant. Data is available at $0.5\ m$ downstream of the groyne, approximately $1.67\ x/L$ downstream of the groyne. In addition to the criteria list stated in Section 4.1.2 is that the sensitivity analyses limit the investigation to the flow velocities downstream of the groyne, in which the settings should improve the model. Visualisations of the flow characteristics are very extensive and therefore only used for validation purposes.

Turbulence model

Based on the square groyne from Jeon et al. (2018), the DES model and $k-\omega$ SST model is compared. The comparison is made at $0.5\ m$ downstream of the groyne, which is approximately $1.67\ x/L$ downstream of the groyne. The figures are shown in the Appendix C.

From the results of Fig. C.1, Fig. C.2 and Fig. C.3 it is shown that the DES model follows the data of the experiment better compared to the $k-\omega$ SST model. Specifically, the figures showing the mean-y-velocity near the bed and the mean-z-velocity near the bed show better results for the DES model. Therefore, in the following numerical models, the DES model is applied.

In addition, the turbulent length scale is small enough in comparison with the mesh size. The turbulent length scale is calculated with:

$$T_L = \frac{k^{3/2}}{\epsilon} \tag{4.8}$$

Table 4.1: Overview statistical average values for the comparison of the $k-\omega$ SST model and DES model

	RMSE [m/s]	RMSE [%]	PBIAS [m/s]	PBIAS [%]
Mean-x-velocity Bedplane KWSST	0.046	15.29	-0.029	-18.49
Mean-x-velocity Bedplane DES	0.034	11.32	-0.022	-13.82
Mean-x-velocity Midplane KWSST	0.025	7.81	-0.0059	-3.67
Mean-x-velocity Midplane DES	0.033	10.42	-0.007	-4.34
Mean-y-velocity Bedplane KWSST	0.016	29.25	-0.0012	-5.90
Mean-y-velocity Bedplane DES	0.014	24.52	0.0042	20.88
Mean-y-velocity Midplane KWSST	0.018	44.76	-0.0043	-28.30
Mean-y-velocity Midplane DES	0.012	30.27	-0.0024	-15.83
Mean-z-velocity Bedplane KWSST	0.0039	32.82	0.0026	84.31
Mean-z-velocity Bedplane DES	0.0033	27.46	0.0022	71.31
Mean-z-velocity Midplane KWSST	0.0036	30.83	0.0024	73.08
Mean-z-velocity Midplane DES	0.0036	30.72	0.0018	55.07

where k is the turbulent kinetic energy and ϵ is the turbulent dissipation rate. A mean value for the turbulent kinetic energy of $0.0028 m^2/s^2$ and a dissipation rate of $0.00151/s$, calculated from the simplified model, results in an approximately turbulent length scale of $0.1m$. These values lead to the computation of the turbulent flow with the DES model. Hence, the large eddy simulation further away from the wall is adequately used for this specific model.

The curvature correction is analysed as well. The DES model is used to verify the curvature option in the turbulence model and is visualised in Appendix C.

Table 4.2: Overview statistical average values for the comparison of using the curvature correction option in the DES model

	RMSE [m/s]	RMSE [%]	PBIAS [m/s]	PBIAS [%]
Mean-x-velocity Bedplane DES curve	0.034	11.24	-0.022	-14.17
Mean-x-velocity Bedplane DES	0.034	11.32	-0.022	-13.82
Mean-x-velocity Midplane DES curve	0.031	9.80	-0.007	-4.46
Mean-x-velocity Midplane DES	0.033	10.42	-0.007	-4.34
Mean-y-velocity Bedplane DES curve	0.014	25.03	0.0041	20.11
Mean-y-velocity Bedplane DES	0.014	24.52	0.0042	20.88
Mean-y-velocity Midplane DES curve	0.012	31.21	-0.00311	-20.66
Mean-y-velocity Midplane DES	0.012	30.27	-0.0024	-15.83
Mean-z-velocity Bedplane DES curve	0.0033	27.35	0.0021	67.57
Mean-z-velocity Bedplane DES	0.0033	27.46	0.0022	71.31
Mean-z-velocity Midplane DES curve	0.0034	28.38	0.0021	65.00
Mean-z-velocity Midplane DES	0.0036	30.72	0.0018	55.07

The statistical values are in a small favour of the curvature correction model. However, from Fig. C.4, Fig. C.5 and Fig. C.6 stated in the appendix, it shows that the DES model without the curvature correction has a slightly better fit with the experimental data. Specifically, the mean-y-velocities and mean-z-velocities have a better fit with the experimental data. Hence, the curvature correction will not be used in the numerical model.

Solver methods

Based on the square groyne from Jeon et al. (2018), the PISO algorithm and SIMPLE algorithm is compared.

Table 4.3: Overview statistical average values for the comparison of using the SIMPLE algorithm and PISO algorithm in the DES model

	RMSE [m/s]	RMSE [%]	PBIAS [m/s]	PBIAS [%]
Mean-x-velocity Bedplane DES SIMPLE	0.051	16.96	-0.038	-24.06
Mean-x-velocity Bedplane DES PISO	0.034	11.32	-0.022	-13.82
Mean-x-velocity Midplane DES SIMPLE	0.035	10.83	-0.0018	-1.12
Mean-x-velocity Midplane DES PISO	0.033	10.42	-0.007	-4.34
Mean-y-velocity Bedplane DES SIMPLE	0.017	30.76	0.0043	21.21
Mean-y-velocity Bedplane DES PISO	0.014	24.52	0.0042	20.88
Mean-y-velocity Midplane DES SIMPLE	0.019	47.92	-0.0073	-48.84
Mean-y-velocity Midplane DES PISO	0.012	30.27	-0.0024	-15.83
Mean-z-velocity Bedplane DES SIMPLE	0.0038	32.20	0.0026	83.36
Mean-z-velocity Bedplane DES PISO	0.0033	27.46	0.0022	71.31
Mean-z-velocity Midplane DES SIMPLE	0.0056	47.72	0.0033	101.80
Mean-z-velocity Midplane DES PISO	0.0036	30.72	0.0018	55.07

Fig. C.7, Fig. C.8 and Fig. C.9 from the appendix are showing that both the algorithms for the DES model differ a lot with each other. In all three direction of the velocities the PISO algorithm shows a more accurate result compared with the experimental data. It is known that for better mesh, the PISO algorithm will solve the equations more accurately. Therefore, the PISO algorithm is used in further modelling.

Grid dependency test

An initial mesh size is obtained, following the principles of Section 4.1.1. For a value for y^+ of 120 results in a cell size of approximately $0.32\ m$. However, a more refined mesh could result in a better solution of the turbulent flow. Hence, the grid dependency test is executed to verify the mesh size. The grid dependency test is verified with mean velocities of the flow for a specified simulation time of 60 s.

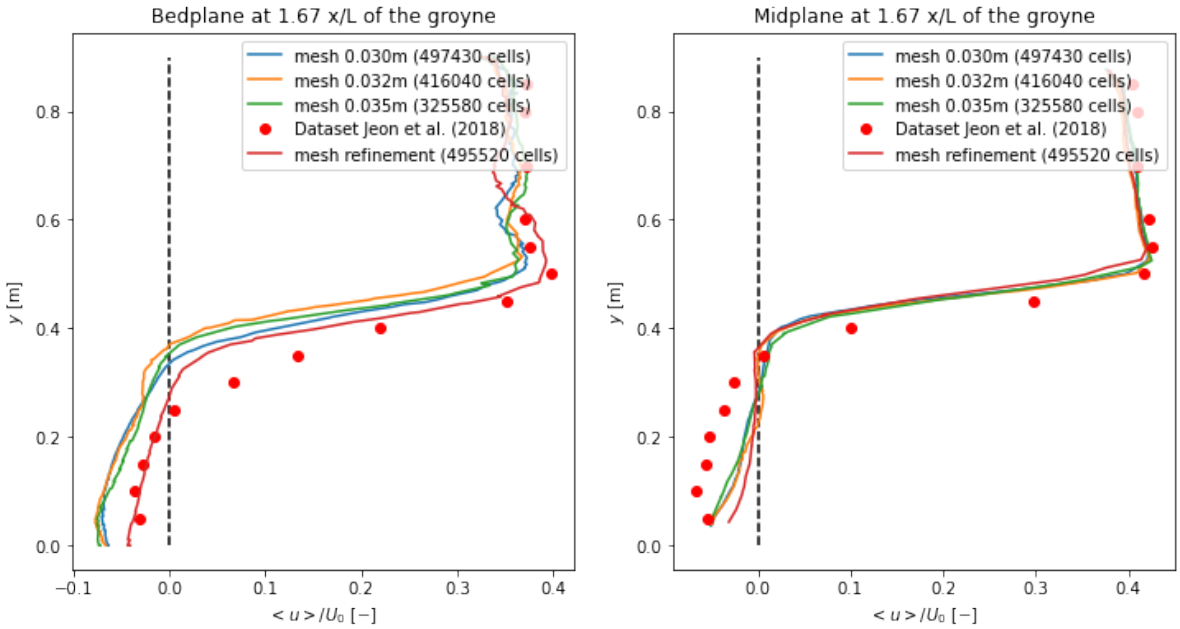

Figure 4.3: Grid dependency test for the mean-x-velocity for a time simulation of 60 s

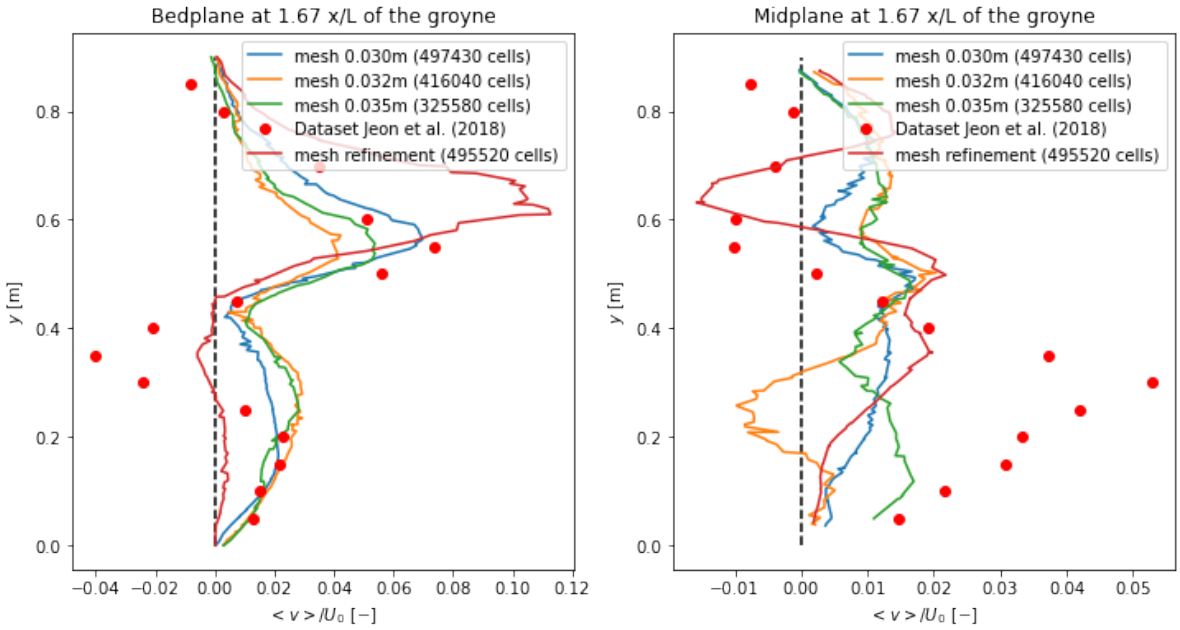

Figure 4.4: Grid dependency test for the mean-y-velocity for a time simulation of 60 s

The sensitivity of the grid is visible. For the mean flow velocities, it is not always accurate for the more fine mesh. However, it is observed that the flow is more reactive in the fine mesh. Besides the standard increase of the mesh size, a refinement is used around the groyne, where the flow characteristics are crucial. For the most refinement around the groyne, a smaller length of the whole domain is used while still maintaining the same computational force. It is observed during the modelling that shifting the boundary conditions more upstream did not affect the flow characteristics. The figures show that the model with the refinement leads to the most fitted model, especially the flow near the bed.

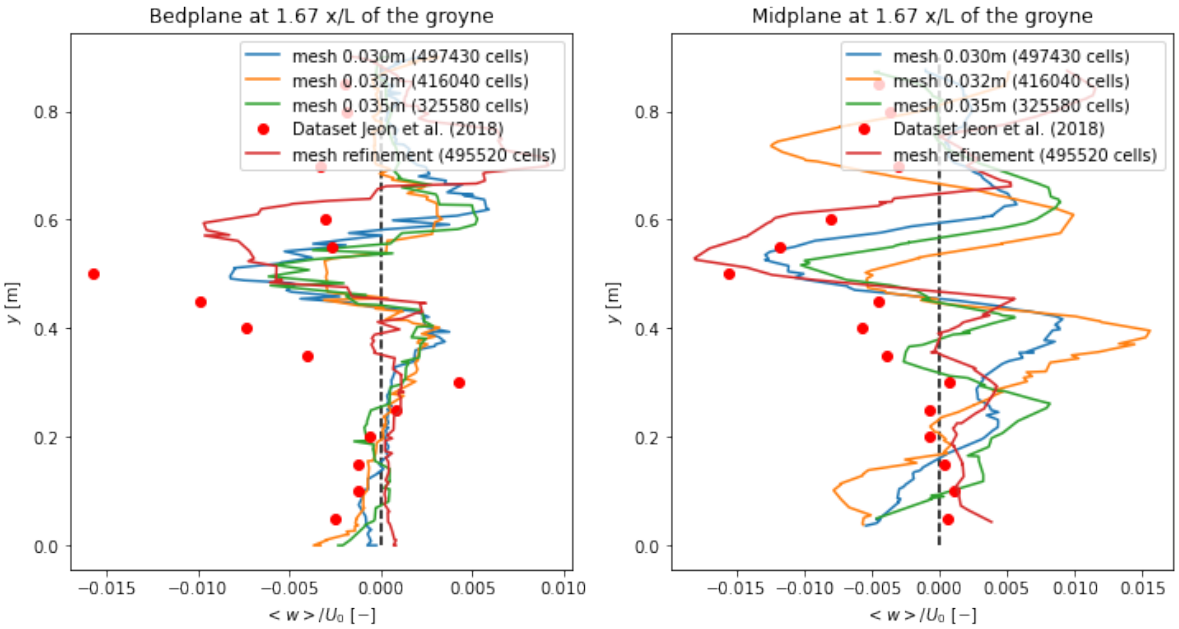

Figure 4.5: Grid dependency test for the mean-z-velocity for a time simulation of 60 s

Overview adjusted input settings and case specific settings

The sensitivity analyses are executed and thus the resulted input settings are justified. These settings are as follows:

Input settings	Values/setting
Turbulence model	DES with KW-SST
Turbulence options	Without curvature correction
Pressure-velocity solver	PISO
Grid size [m]	0.030 with refinement
CFL [-]	4
Simulation time [s]	300

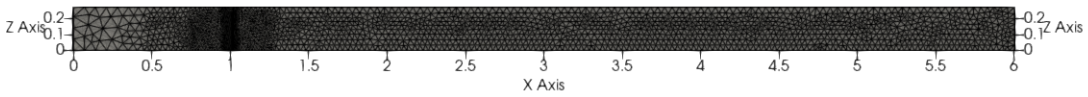

Figure 4.6: Mesh with refinement around the square groyne in the numerical model

4.1.4 Coupled system for porous medium

The coupled system of the porous zone with the open channel flow must be validated. The study of Mohammadpour et al. (2013), Banerjee et al. (2018) has shown models that sufficiently present the flow through coarse granular porous media. Also, experiments for coarse granular porous media have been executed Mioduszewski & Maeno (2005). However, little data about turbulent properties and velocity vectors are known from these experiments. Therefore, data from Leu et al. (2008) will be used for validating a numerical model coupled with the free surface flow and a porous medium. In this experimental study, a porous weir is investigated that resulted in many features of the flow.

As stated previously, this validation is focused on the experimental study from Leu et al. (2008). The experimental study is focused on the mean flow properties and the turbulent properties around the porous weir. Furthermore, the mean velocity profile within the porous structure is analysed as well. Hence, the following parameters will be validated:

- Vertical Velocity profile
- Vertical Reynold shear stresses profile
- Mean velocity profile above and within the porous structure

The geometry and domain of the model are shown in Fig. 4.7. Additionally, the input settings are arranged as follows:

Parameters	Values
Flow depth [m]	0.242
Flume width [m]	0.3
Flume total length [m]	1.5
Length of weir in x-direction [m]	0.15
Length of weir in y-direction [m]	0.3
Initial velocity [m/s]	0.206
Froude number	0.13
Reynolds number	4.97 x 10^4
Kinematic viscosity [m^2/s]	1.03 x 10^-6

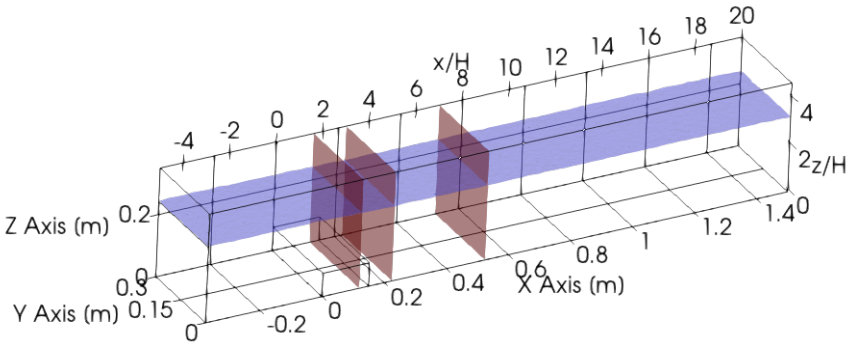

Figure 4.7: Geometry of the porous structure with dimensions of the experiment from Leu et al. (2008) in the numerical model. The location of the validation and sensitivity analysis are shown in red, respectively $0.40\ x/H$, $3.00\ x/H$ and $7.00\ x/H$

Sensitivity analysis for the input parameters

From the previous validation approach, most input settings are optimized. However, one important input setting for this particular model is the porous settings, which has not been used at all. A sensitivity analyses will be used. In addition, domains vary and therefore the mesh size is optimized for this model in combination with the computational costs. A grid dependency test is used to verify the optimal mesh size.

Porous setting sensitivity test

As stated before in section Section 2.3.1 of the literature study, the porosity settings can be estimated by using the formula of Stephenson. However, because the settings of the porosity is still an uncertainty, a sensitivity analysis is used. The formula will be used with an external factor in front of the linear and non-linear term. Therefore, some kind of coefficient is made to improve the settings for this specific case. This sensitivity analysis is defined on the porous weir $0.03\ m$ from the zero axis or $0.40\ x/H$.

The Stephenson formula is optimized by using a coefficient C1 and C2 as follows:

$$\Delta P = \left(C1 \frac{800v}{gnd^2} V + C2 \frac{K_t}{n^2 gd} V^2 \right) \cdot \rho g D \tag{4.9}$$

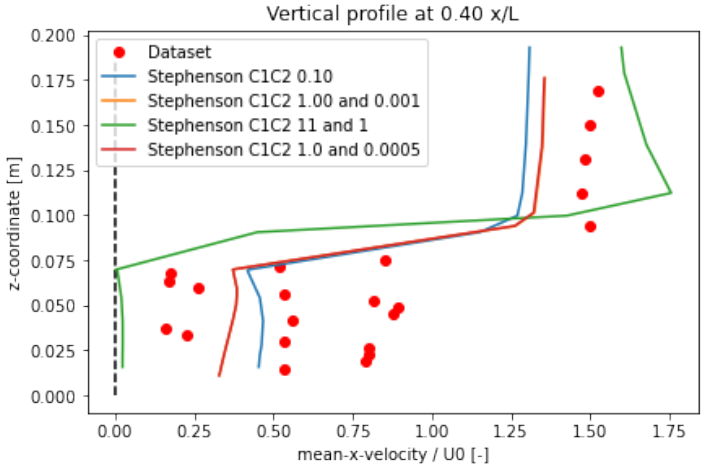

Figure 4.8: Sensitivity analysis porous settings at $x = 0.40\ x/H$

The most optimized setting is the combination of C1 and C2 of 0.10 and 0.10 or 1.0 and 0.001. The general formula by Stephenson is already investigated many times, and therefore it is essential not to change the formula a lot. Therefore, the settings for C1, C2 is defined as 1 and 0.001. This sensitivity analysis concludes that the linear term stays the same, and the non-linear term leads to a coefficient for K_t as 0.001.

Grid dependency test

An initial mesh size is obtained, following the principles of Section 4.1.1. For a value for y^+ of 120 results in a cell size of approximately $0.24\ m$. The grid dependency test is verified with mean velocities of the flow for a specified simulation time of 60 s. In addition, this dependency test is defined on the porous weir $0.12\ m$ from the zero axis or $1.60\ x/H$, $0.225\ m$ from the zero axis or $3.00\ x/H$ and $0.525\ m$ from the zero axis or $7.00\ x/H$, as shown in the overview in Fig. 4.7.

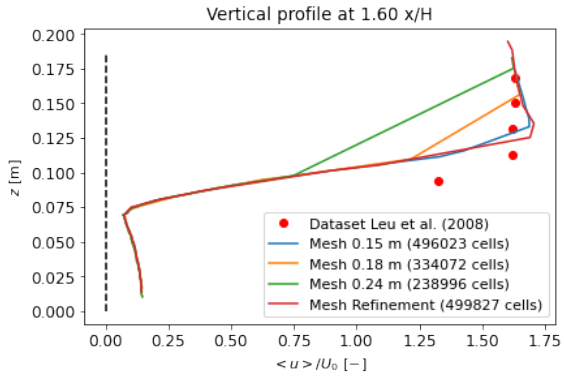

Figure 4.9: Grid dependency test for the mean-x-velocity for a time simulation of 60 s at $0.40\ x/L$

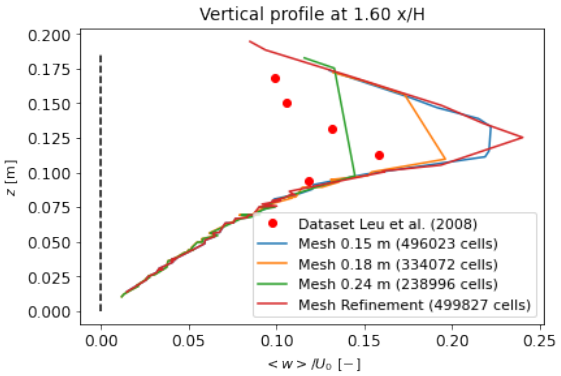

Figure 4.10: Grid dependency test for the mean-z-velocity for a time simulation of 60 s at $0.40\ x/L$

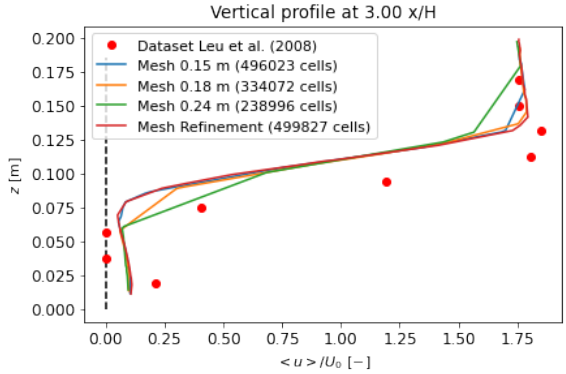

Figure 4.11: Grid dependency test for the mean-x-velocity for a time simulation of 60 s at $3.00\ x/L$

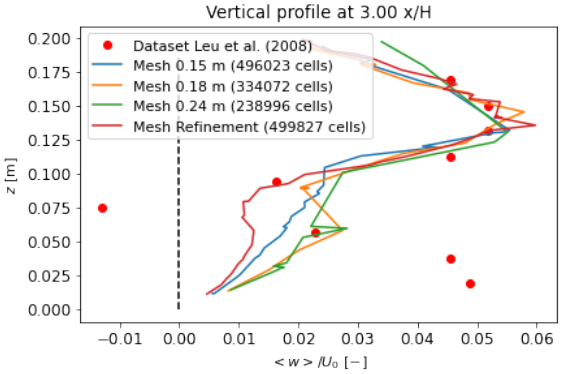

Figure 4.12: Grid dependency test for the mean-z-velocity for a time simulation of 60 s at $3.00\ x/L$

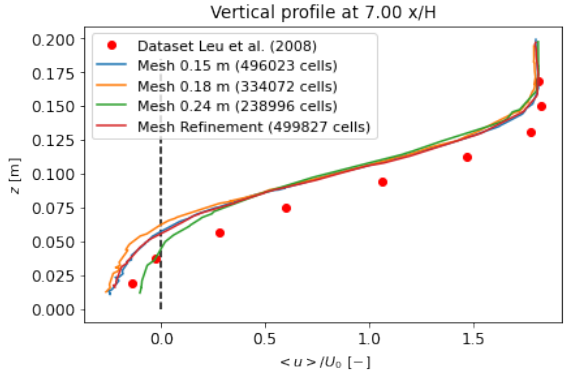

Figure 4.13: Grid dependency test for the mean-x-velocity for a time simulation of 60 s at $7.00\ x/L$

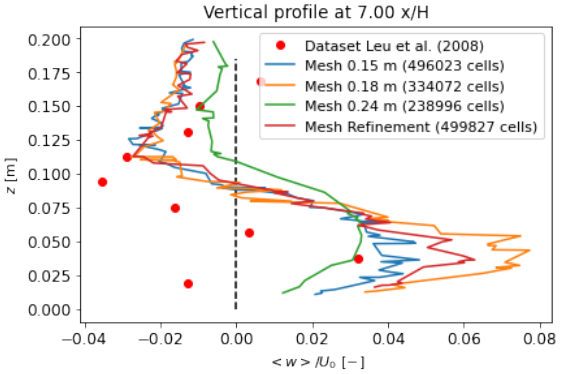

Figure 4.14: Grid dependency test for the mean-z-velocity for a time simulation of 60 s at $7.00\ x/L$

From the figures of the grid dependency test it is shown that the largest mesh size does not react adequately to the experimental data set. Both the refinement and the mesh size of $0.15/m$ show the most accurate solutions, especially for the streamwise velocity. For the vertical velocity, the most accurate solution is obtained by using a mesh size of $0.015/m$. Thus the mesh with the most optimized mesh cell size, $0.015/m$ is observed to be the most fitted model, compared with the actual experimental data.

Overview adjusted input settings

The sensitivity analyses are executed and thus the resulted input settings are justified. These settings are as follows:

Input settings	Values/setting
Turbulence model	DES with KW-SST
Turbulence options	Without curvature correction
Pressure-velocity solver	PISO
Grid size [m]	0.015
CFL [-]	4
Simulation time [s]	300

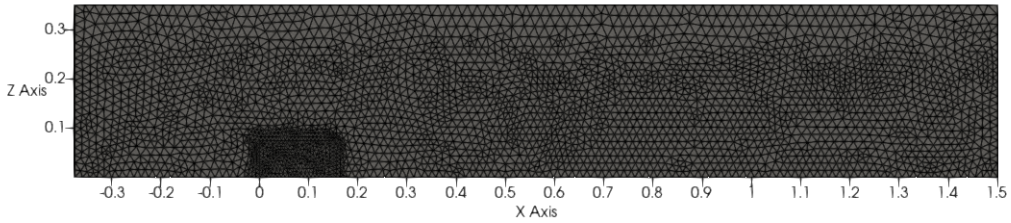

Figure 4.15: Mesh around the porous weir

4.1.5 Sloped groyne

Slopes groynes are validated by the study of Bahrami Yarahmadi et al. (2020). This study investigated the development of scouring and flow patterns around a sloped groyne. Mean flow velocities are reported for various depths over the whole domain. However, no information is available about the turbulent properties around the groyne. Therefore, this study only validates the flow patterns and mean flow velocities around a sloped groyne.

This model is validated for the following parameters:

- Contour lines
- Re-circulation flow length scales
- Mean flow velocities

Parameters	Values
Flow depth [m]	0.15
Flume width [m]	0.8
Flume total length [m]	2.5
Length of groyne in x-direction [m]	0.04
Length of groyne in y-direction [m]	0.16
Angle groyne [degrees]	43
Initial velocity [m/s]	0.208
Froude number	0.14
Reynolds number	4.97 x 10^4
Kinematic viscosity [m^2/s]	1.03 x 10^-6

The geometry of the experiment is shown in figure Fig. 4.16.

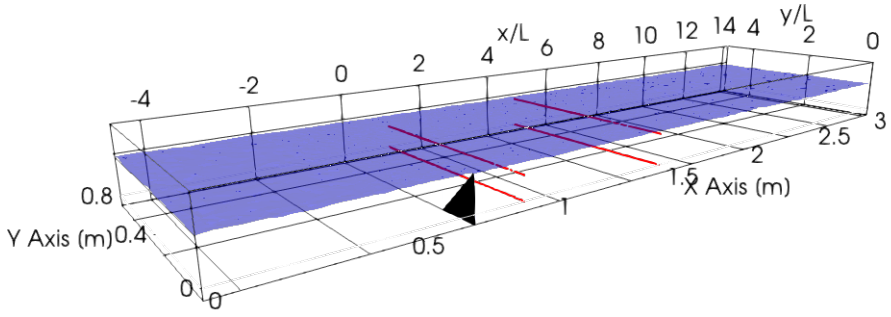

Figure 4.16: Geometry of the sloped groyne with dimensions of the experiment from Bahrami Yarahmadi et al. (2020) in the numerical model. The locations of the validation and sensitivity analysis are shown in red

Grid dependency test

The grid dependency test for the sloped groyne is analyzed downstream of the groyne, approximately $0.18m$ or $1.13\ x/L$ as shown in Fig. 4.16.

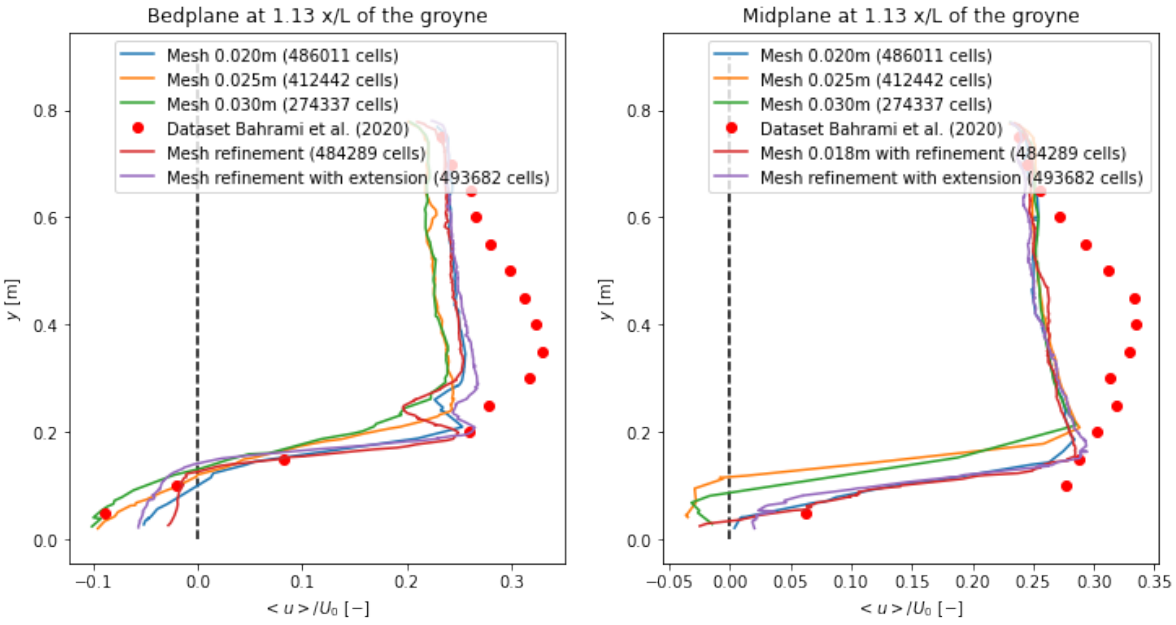

Figure 4.17: Grid dependency test for the mean-x-velocity for a time simulation of 60 s at 113 x/L

From the figures, it is shown that the models with the fine mesh sizes and refinement around the groyne, have the best fitted models compared with the experimental data. Especially the CFD model with the refinement has the most accuracy for the mean velocities near the bed. Therefore, the refinement model will be used in the validation model.

Overview adjusted input settings and case specific settings

The sensitivity analyses are executed and thus the resulted input settings are justified. These settings are as follows:

Input settings	Values/setting
Turbulence model	DES with KW-SST
Turbulence options	Without curvature correction
Pressure-velocity solver	PISO
Grid size [m]	0.020 with refinement
CFL [-]	4
Simulation time [s]	300

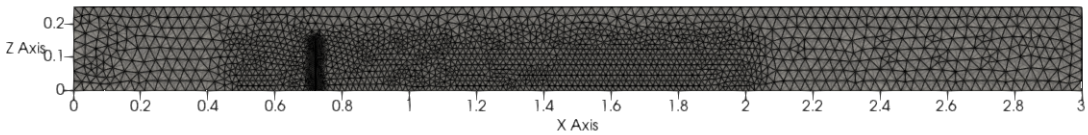

Figure 4.18: Mesh of the sloped groyne

4.2 Validation results

This section describes the validation results for obtaining a validated numerical model to contribute in the study. The input settings are stated and verified in Section 4.1.

4.2.1 Rectangular conventional groyne structure

Contour lines

The contour lines are defined for two planes; mid-plane and near the bed, respectively $0.11\ m$ or $0.51\ z/D$ and $0.01\ m$ computed from the bottom or $0.1\ z/D$.

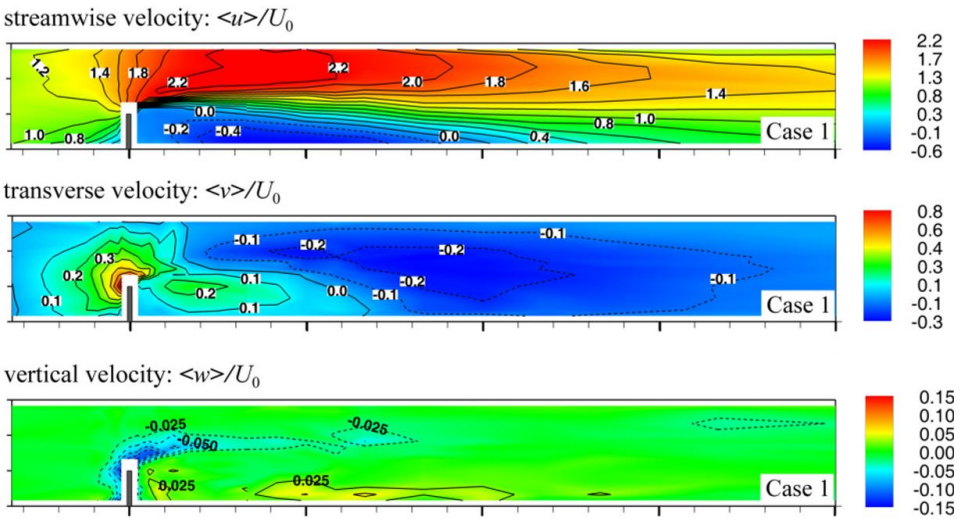

Figure 4.19: Dimensionless mean velocity fields at mid-plane (0.11m) from experiment Jeon et al. (2018)

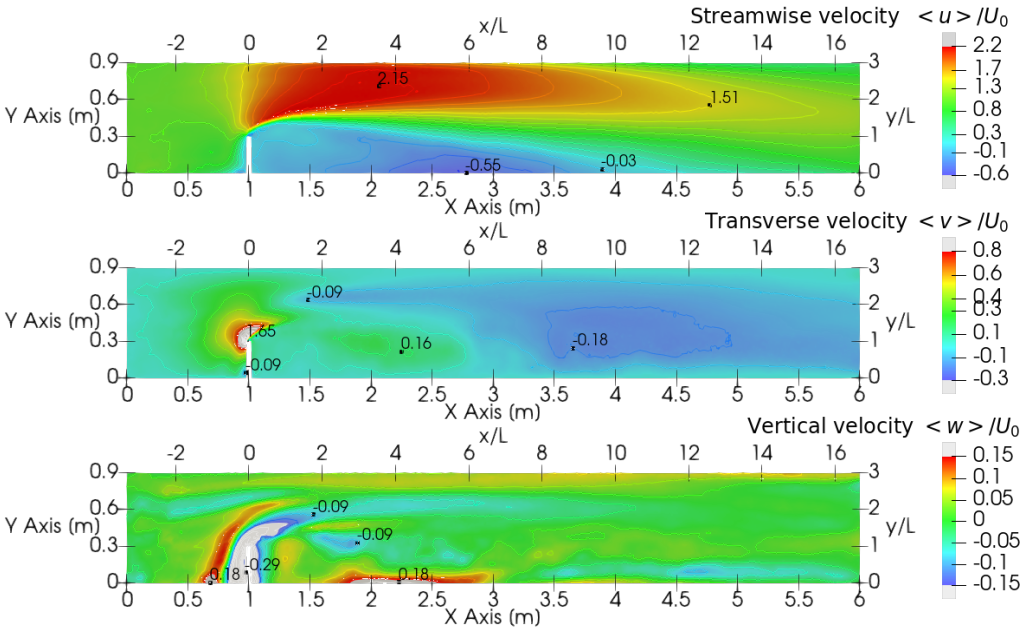

Figure 4.20: Dimensionless mean velocity fields at bed-plane ($0.11\ m$ or $0.51\ z/D$) from the numerical model

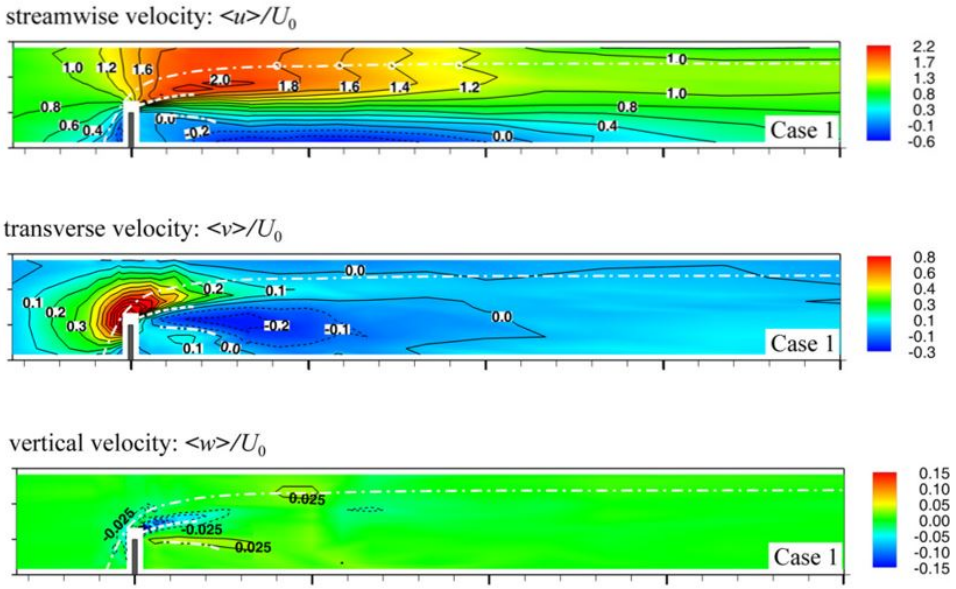

Figure 4.21: Dimensionless mean velocity fields at near bed-plane (0.01 m) from experiment Jeon et al. (2018)

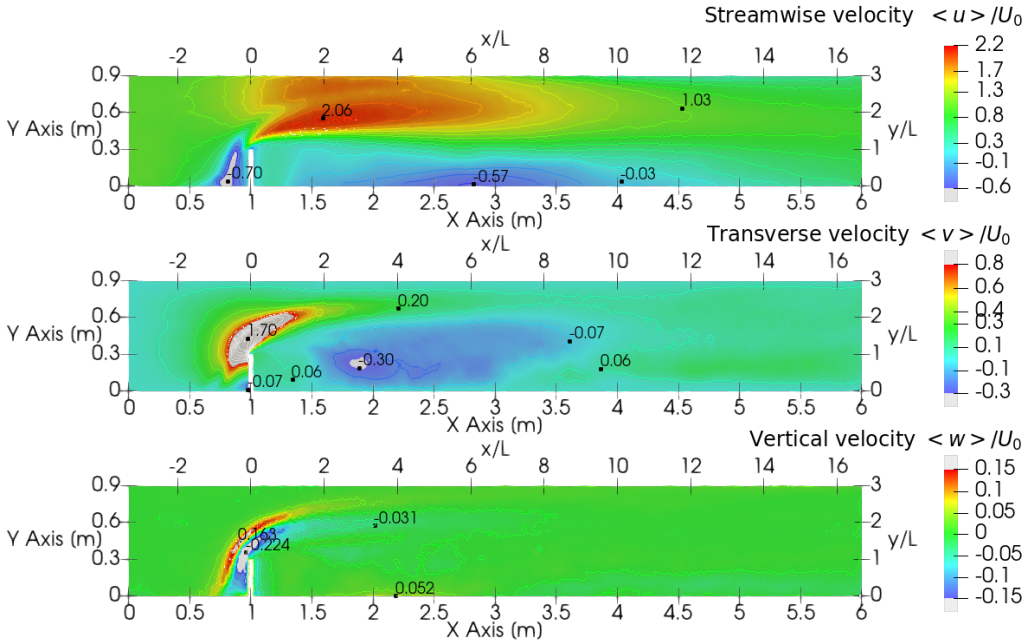

Figure 4.22: Dimensionless mean velocity fields at bed-plane ($0.01\ m$ or $0.1\ z/D$) from the numerical model

The contour lines of the numerical model have many similarities with the experiment. The maximum and minimum values and the locations for the velocities are in agreement. However, certain aspects, such as the y-velocity contour in the recirculation zone and the z-velocity contour near the reattachment location are reasonable points of attention.

Mean values

Comparison of the specific data points from the experiments with the numerical model is executed using cross lines for various x-values in the domain. The cross lines are present 0.07 m upstream of the groyne, 0.5 m downstream of the groyne and 2 m downstream of the groyne. Respectively, in a length order of $-0.23\ x/L$, $1.67\ x/L$ and $6.67\ x/L$ from the groyne. The first position is stated in this section, while the two other positions are shown in the appendix.

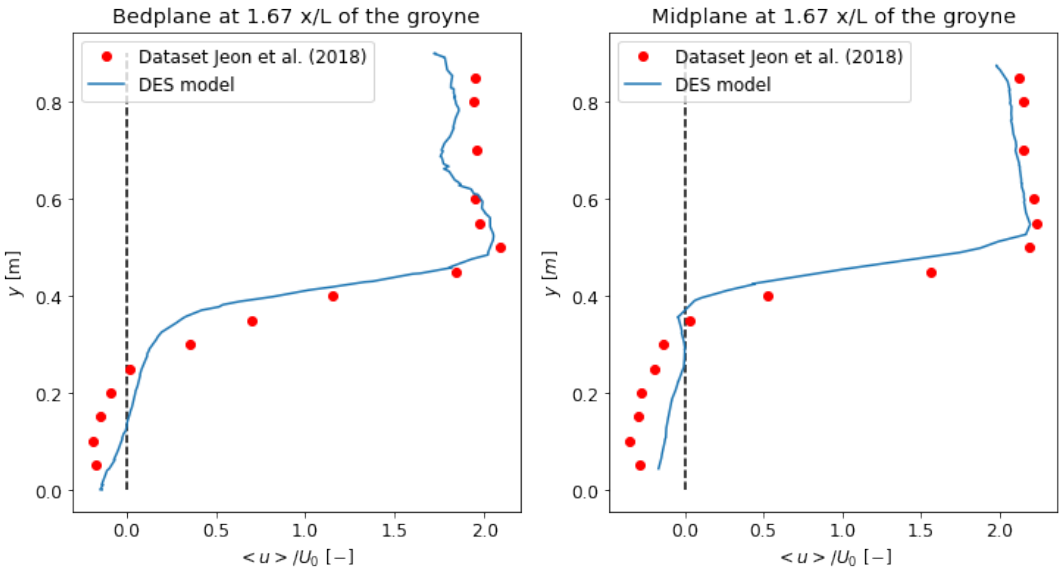

Figure 4.23: x-velocity for $1.67\ x/L$, downstream of the groyne

The mean velocities for x and y-direction over the cross lines are comparable to each other near the groyne. This comparison is also in agreement with the contour levels and visualisations. The lateral and vertical velocities far downstream showing less comparable results. This is also shown in the visualisations. However, it can be seen that the results of the numerical model at the important areas for the horse-shoe vortex system, vortex shedding at the tip of the groynes and the mixing layer are mostly in agreement with the experimental studies.

Turbulent properties

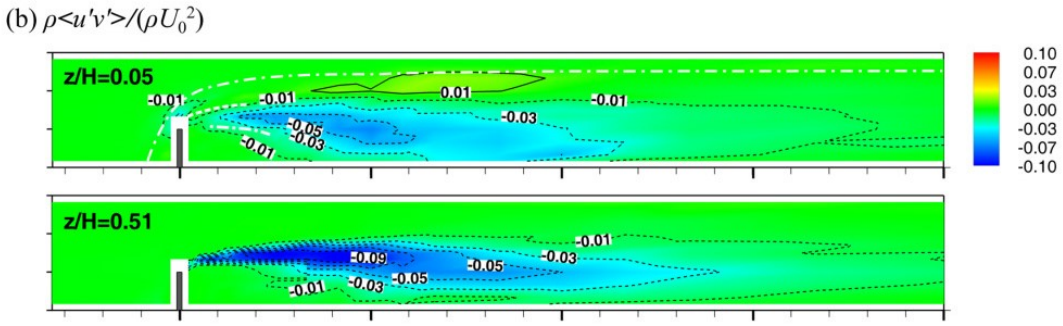

Figure 4.24: Dimensionless mean Reynold stresses UV at bed-plane ($0.01\ m$ or $0.1\ z/D$) and mid-plane ($0.11\ m$ or $0.51\ z/D$) from the experiment Jeon et al. (2018)

Table 4.4: Overview statistical average values for the validation of the numerical model by using mean flow velocities within the squared groyne application

	RMSE [m/s]	RMSE [%]	PBIAS [m/s]	PBIAS [%]
Mean-x-velocity Bedplane DES $-0.23\ x/L$	0.041	19.67	-0.024	-18.20
Mean-x-velocity Bedplane DES $1.67\ x/L$	0.025	8.47	-0.008	-5.08
Mean-x-velocity Bedplane DES $6.67\ x/L$	0.01	4.4	0.0041	2.67
Mean-x-velocity Midplane DES $-0.23\ x/L$	0.021	8.75	-0.0015	-8.46
Mean-x-velocity Midplane DES $1.67\ x/L$	0.035	10.81	-0.0061	-3.82
Mean-x-velocity Midplane DES $6.67\ x/L$	0.021	6.94	-0.017	-8.49
Mean-y-velocity Bedplane DES $-0.23\ x/L$	0.028	14.59	0.014	18.68
Mean-y-velocity Bedplane DES $1.67\ x/L$	0.017	31.35	-0.00023	-1.15
Mean-y-velocity Bedplane DES $6.67\ x/L$	0.014	94.71	-0.0056	-78.13
Mean-y-velocity Midplane DES $-0.23\ x/L$	0.013	9.50	0.011	23.24
Mean-y-velocity Midplane DES $1.67\ x/L$	0.016	40.50	-0.0062	-40.86
Mean-y-velocity Midplane DES $6.67\ x/L$	0.0085	25.91	-0.0045	-25.59
Mean-z-velocity Bedplane DES $-0.23\ x/L$	0.014	138.38	0.0023	43.60
Mean-z-velocity Bedplane DES $1.67\ x/L$	0.0046	38.91	0.0024	77.20
Mean-z-velocity Bedplane DES $6.67\ x/L$	0.0041	66.51	0.0036	106.54
Mean-z-velocity Midplane DES $-0.23\ x/L$	0.0019	86.43	0.00044	-4.94
Mean-z-velocity Midplane DES $1.67\ x/L$	0.0055	46.32	0.0031	93.38
Mean-z-velocity Midplane DES $6.67\ x/L$	0.0062	65.77	0.0046	102.87

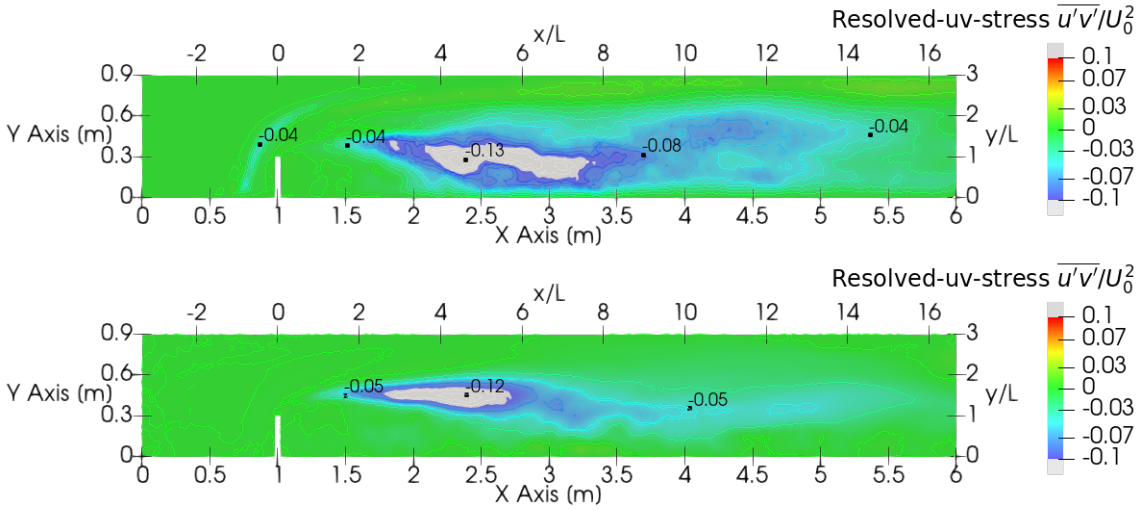

Figure 4.25: Dimensionless mean Reynold stresses UV at bed-plane ($0.01\ m$ or $0.1\ z/D$) and mid-plane ($0.11\ m$ or $0.51\ z/D$) from the numerical model

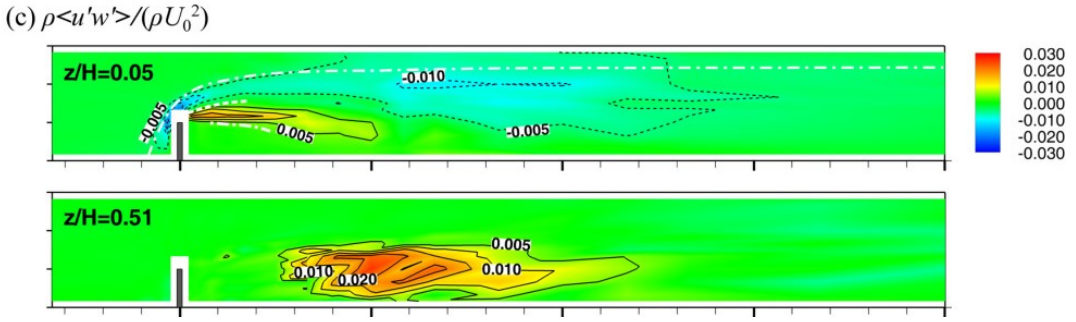

Figure 4.26: Dimensionless mean Reynold stresses UW at bed-plane ($0.01\ m$ or $0.1\ z/D$) and mid-plane ($0.11\ m$ or $0.51\ z/D$) from the experiment Jeon et al. (2018)

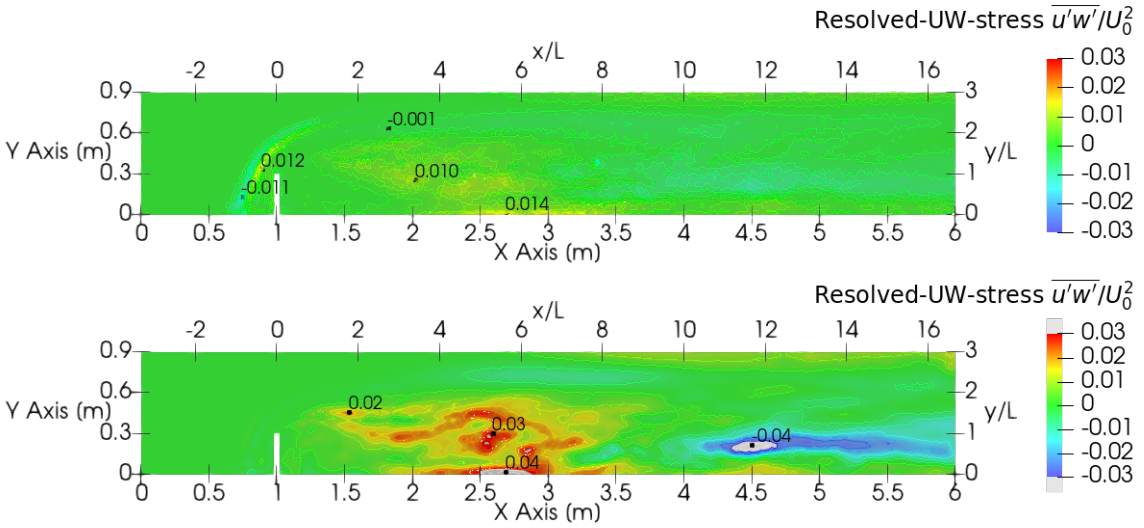

Figure 4.27: Dimensionless mean Reynold stresses UW at bed-plane ($0.01\ m$ or $0.1\ z/D$) and mid-plane ($0.11\ m$ or $0.51\ z/D$) from the numerical model

Comparison of the specific data points from the experiments with the numerical model is executed using cross lines for various x-values in the domain. The cross lines are present $0.5\ m$ and $2\ m$, respectively $1.67\ x/L$ and $6.67\ x/L$ downstream of the groyne.

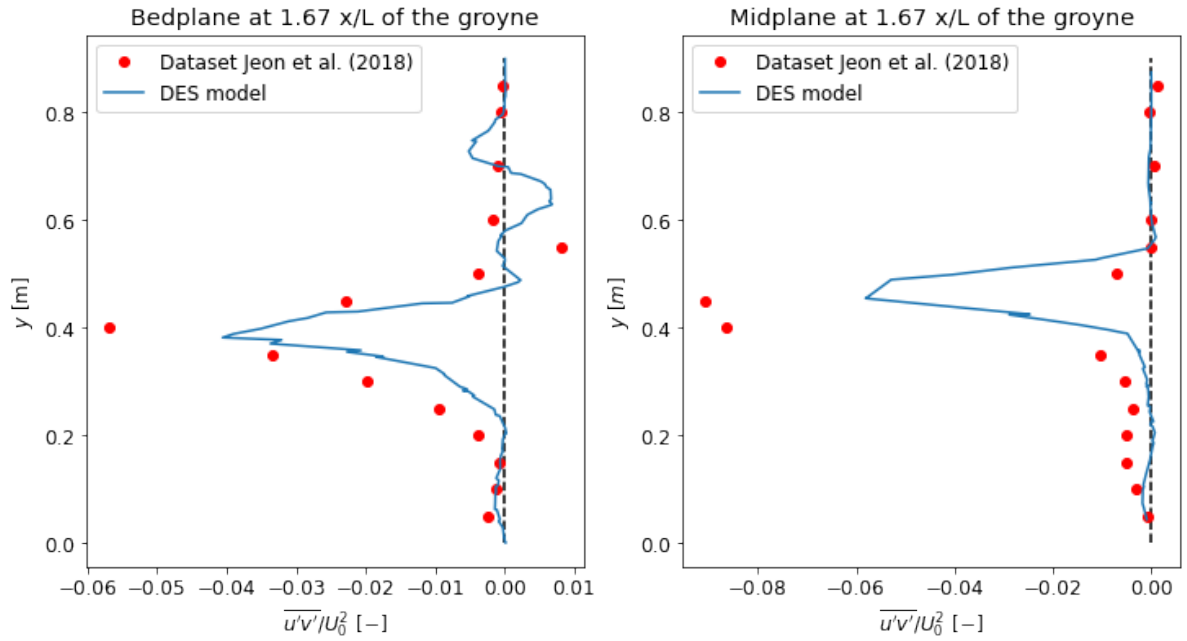

Figure 4.28: UV stress for $1.67\ x/L$, downstream of the groyne

Table 4.5: Overview statistical average values for the validation of the numerical model of the squared groyne

	RMSE $[m^2/s^2]$	RMSE [%]	PBIAS $[m^2/s^2]$	PBIAS [%]
UV stress Bedplane DES $-0.23\ x/L$	0.00021	42.94	-0.000012	-8.78
UV stress Bedplane DES $1.67\ x/L$	0.00019	16.35	-0.00011	47.47
UV stress Bedplane DES $6.67\ x/L$	0.00081	83.86	-0.00066	-140.45
UV stress Midplane DES $-0.23\ x/L$	0.000022	31.06	-0.0000019	-8.27
UV stress Midplane DES $1.67\ x/L$	0.00049	25.85	0.000015	48.15
UV stress Midplane DES $6.67\ x/L$	0.00029	21.76	-0.00011	-20.58
UW stress Bedplane DES $-0.23\ x/L$	0.00017	56.38	0.0000085	109.12
UW stress Bedplane DES $1.67\ x/L$	0.000096	27.45	-0.00000028	0.36
UW stress Bedplane DES $6.67\ x/L$	0.00014	60.759	0.00012	94.98
UW stress Midplane DES $-0.23\ x/L$	0.000027	32.77	0.000018	77.70
UW stress Midplane DES $1.67\ x/L$	0.00016	220.14	0.00011	601.66
UW stress Midplane DES $6.67\ x/L$	0.00017	37.56	-0.00008	-61.33

The Reynolds shear stresses directly downstream of the groyne (at $0.5\ m$, respectively $1.67\ x/L$) agrees with the experimental data set. Further downstream, the numerical model over predicts the Reynolds shear stresses UV. The UV Reynolds shear stresses are the most significant values compared to the other Reynolds shear stresses and therefore has much influence on the bed shear stresses. It can be stated that the model over predicts the Reynolds shear stresses. In addition, most Reynolds shear stresses resolved further downstream from the groyne and are extended much deeper downstream.

4.2.2 Coupled system for porous medium

Vertical velocity profile

The vertical velocity profiles are defined for three locations; one above the porous structure and two after the porous structure, where large velocity gradients are expected, respectively $1.6\ x/H$, $3\ x/H$ and $7\ x/H$ as stated in Fig. 4.7.

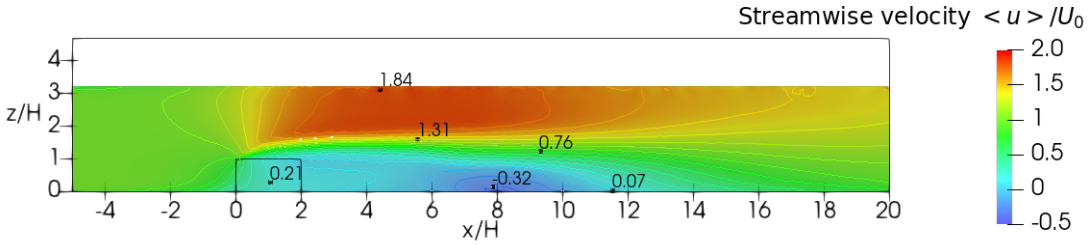

Figure 4.29: Streamwise velocity around the porous weir

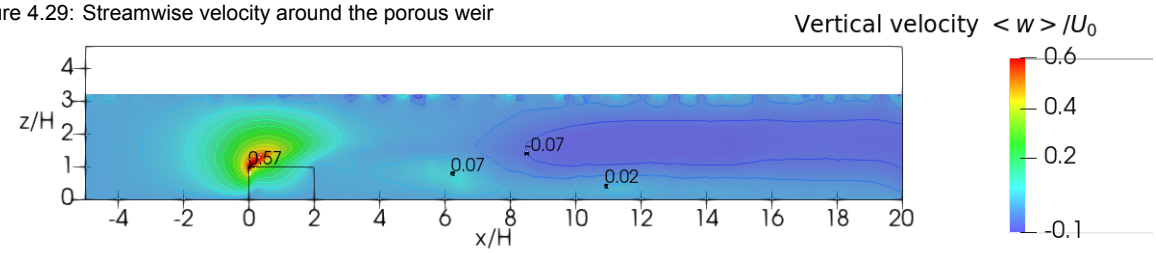

Figure 4.30: Vertical velocity around the porous weir

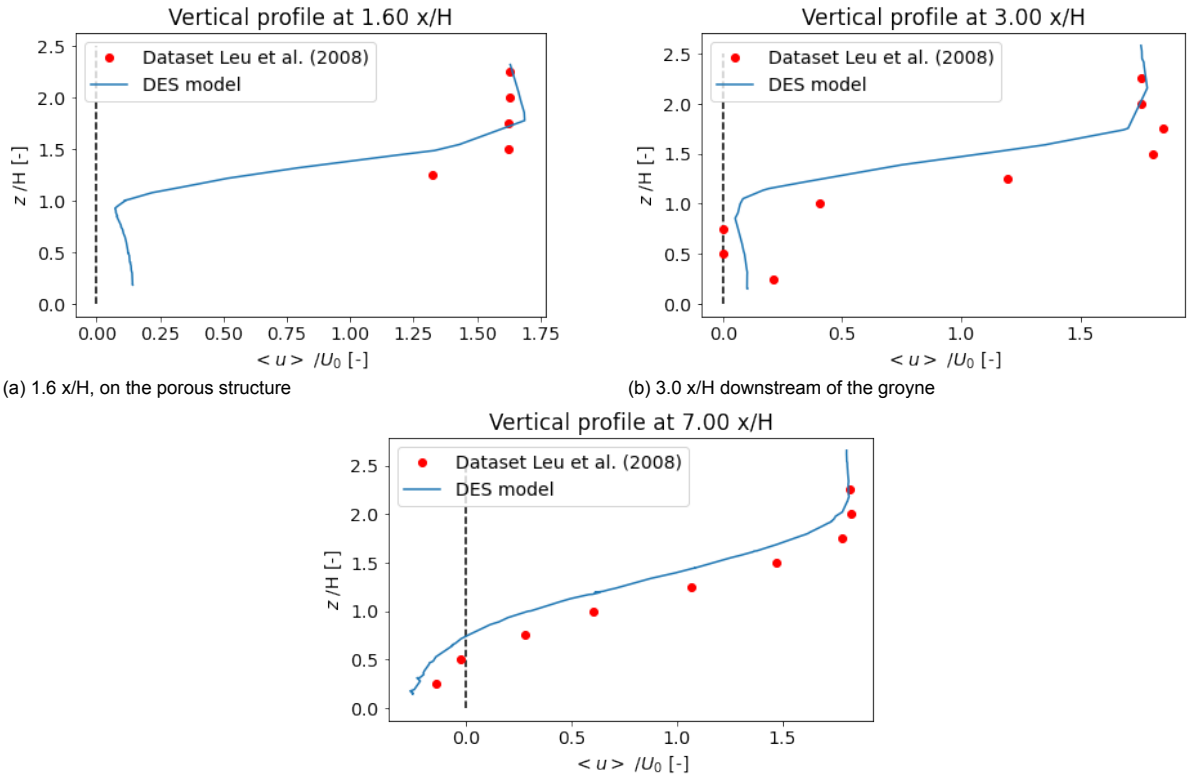

(a) 1.6 x/H, on the porous structure

(b) 3.0 x/H downstream of the groyne

(c) 7.0 x/H downstream of the groyne

Figure 4.31: The streamwise velocity for specified vertical profiles in the numerical model

From Fig. 4.31 it is shown that the mean streamwise velocity profile near the weir is in an acceptable range. However, the mean vertical velocity profile, as shown in Fig. D.14 in the appendix, shown less accuracy, especially the profile most downstream of the weir. The statistics follow this up.

Vertical Reynold shear stresses profile

The vertical Reynold shear stresses profiles are defined for three locations; one above the porous structure and two after the porous structure, where large velocity gradients are expected, respectively $1.6\ x/L$, $3\ x/L$ and $7\ x/L$.

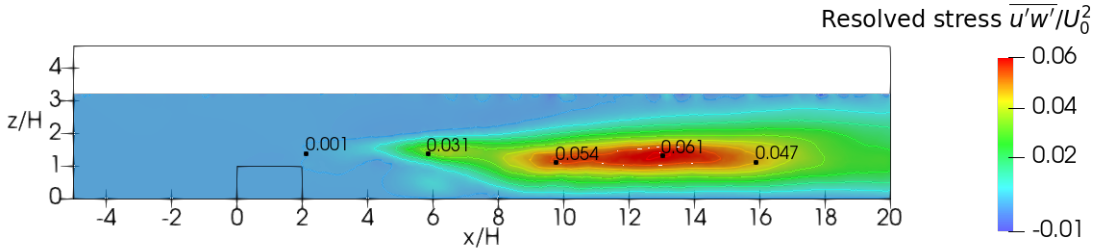

Figure 4.32: Reynolds shear stresses UW around the porous weir

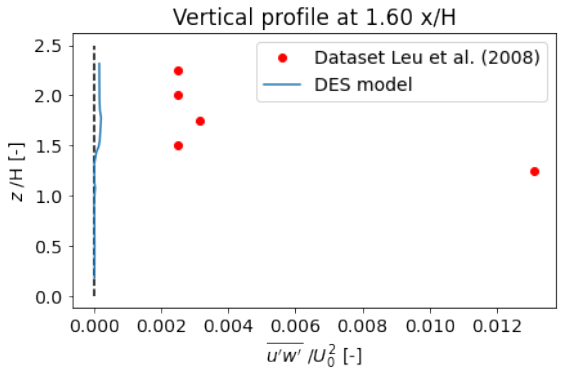

(a) 1.6 x/H, on the porous structure

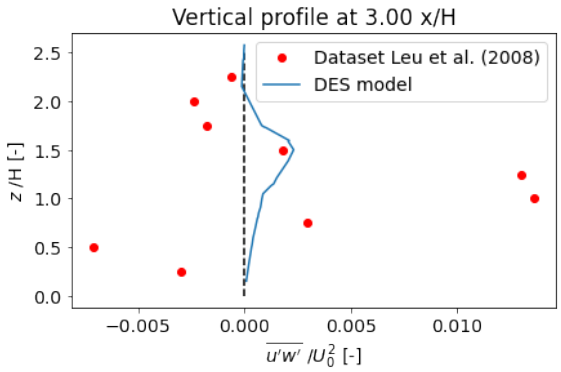

(b) 3.0 x/H downstream of the groyne

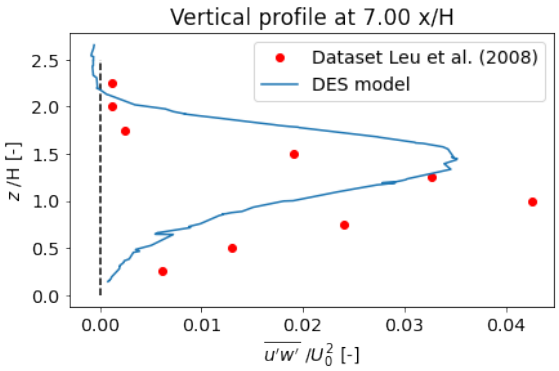

(c) 7.0 x/H downstream of the groyne

Figure 4.33: The Reynold shear stress $\overline{u'w'}$ for specified vertical profiles in the numerical model

Table 4.6: Overview statistical average values for the validation of the numerical model of the porous weir

	RMSE [m/s]	RMSE [%]	PBIAS [m/s]	PBIAS [%]
Mean-x-velocity DES 1.6 x/H	0.07	20.85	-0.037	-11.37
Mean-x-velocity DES 3 x/H	0.077	20.24	-0.044	-21.26
Mean-x-velocity DES 7 x/H	0.045	12.05	-0.039	-18.76
Mean-z-velocity DES 1.6 x/H	0.0013	40.23	0.012	46.88
Mean-z-velocity DES 3 x/H	0.0044	41.55	-0.0013	-16.35
Mean-z-velocity DES 7 x/H	0.0046	62.44	0.0019	52.21

	RMSE [m^2/s^2]	RMSE [%]	PBIAS [m^2/s^2]	PBIAS [%]
UW stress DES 1.6 x/H	0.00027	47.87	-0.00020	-97.32
UW stress DES 3 x/H	0.00027	47.61	-0.000046	-21.18
UW stress DES 7 x/H	0.00055	30.39	-0.000077	-11.50

The maximum Reynolds shear stresses from the experiment are observed around 7 x/L. From the resulting figures, it can be concluded that the Reynold shear stresses follow the experiments' data-set sufficiently. However, it stands out that the most significant values for the numerical model are observed to be from 9 x/L to 14 x/L. Therefore, the numerical model estimates the Reynolds shear stresses to over-predict and extend further downstream. A small note can be made that the maximum Reynolds shear stresses are observed at 10 x/L for the numerical model.

4.2.3 Sloped groyne

In this case, the following parameters are validated:

- Contour lines
- Re-circulation flow length scales
- Mean flow velocities

Contour lines

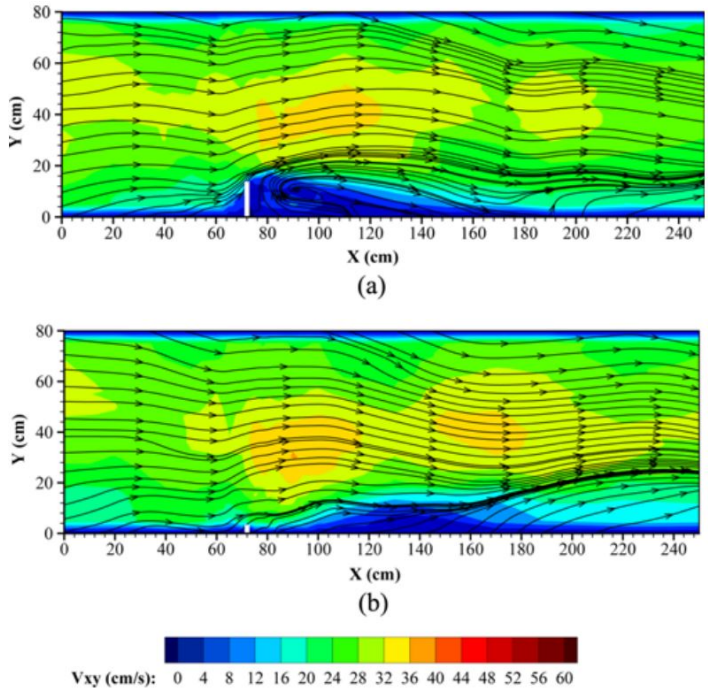

Figure 4.34: Mean velocity field over the whole domain near the bed plane (0.03m) and mid plane (0.14m) Bahrami Yarahmadi et al. (2020)

The contour lines based on the mean velocity magnitude is compared with the experimental study Bahrami Yarahmadi et al. (2020). Contour lines for the flow in the main channel are comparable. However, the numerical results slightly under-predicts the mean values. The contour lines for the recirculation zone is near the bed very much alike. The numerical model results in the mid-depth contours conclude more effects by the sloped groyne, in which the values are approximately zero.

Re-circulation zone

The length of the recirculation zone can be identified by the zero values of the streamwise velocities (x direction) and lateral velocities (y direction) at the bank of the domain. It is observed in the experimental studies that the recirculation length scale is various over the water depth. Near the bed plane, the length scale is approximately $0.68\ m$ or $4.25\ x/L$. And in the mid-plane, the streamwise and lateral velocity is positive at almost every x position. The only exception is directly downstream of the groyne, approximately $0.06\ m$ or $0.375\ x/L$. The general flow field is shown by the velocity magnitude, as shown in Fig. 4.34.

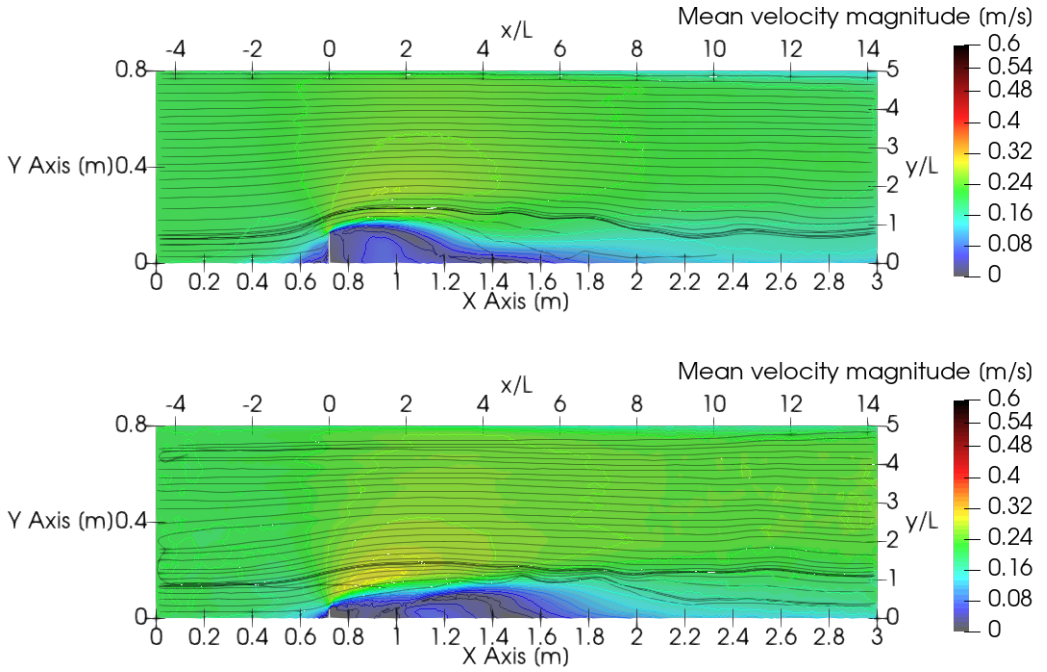

Figure 4.35: Mean velocity field over the whole domain near the bed plane (0.03m) and mid plane (0.14m) from the numerical model

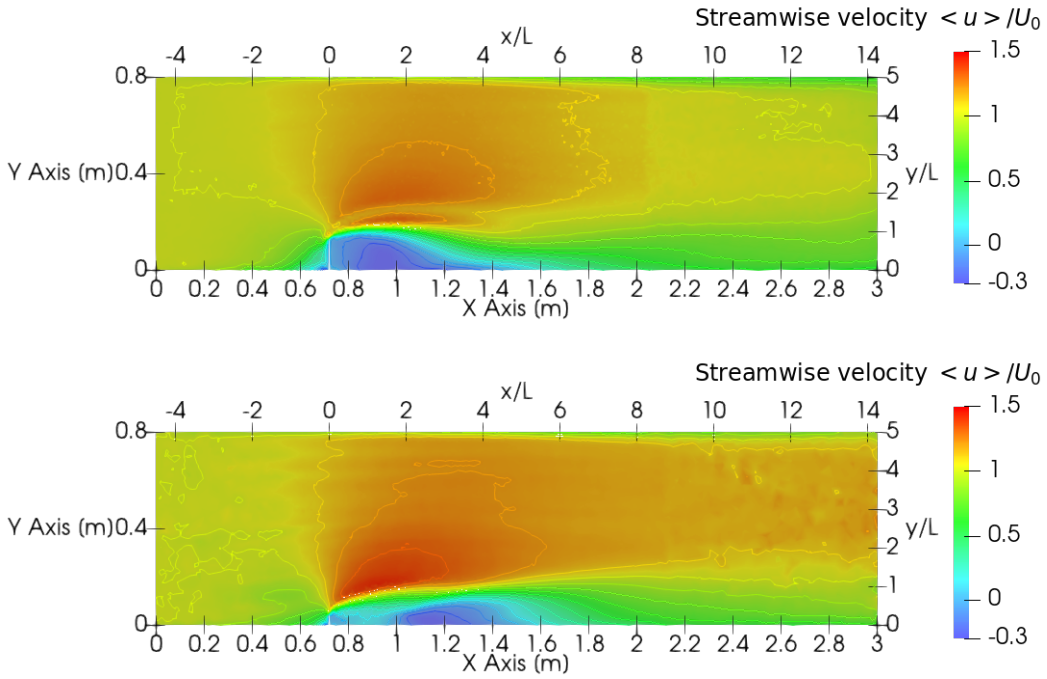

Figure 4.36: Mean x velocity over the whole domain near the bed plane (0.03m) and mid plane (0.14m) from the numerical model

From the numerical model as shown in Fig. 4.36 and Fig. D.15 from the appendix, the recirculation zone are roughly the same lengths.

Mean flow velocities

Comparison of the specific data points from the experiments with the numerical model is executed using cross lines for various x-values in the domain. The cross lines are present at $0.18\ m$ and $0.78\ m$ downstream of the groyne. Respectively, in a length order of $1.13\ x/L$ and $4.88\ x/L$ from the groyne.

The graphs for the cross lines are stated in the Appendix D.3.

Table 4.7: Overview statistical average values for the validation of the numerical model of the sloped groyne

	RMSE [m/s]	RMSE [%]	PBIAS [m/s]	PBIAS [%]
Mean-x-velocity Bedplane DES $1.13\ x/L$	0.042	12.89	-0.031	-12.87
Mean-x-velocity Bedplane DES $4.88\ x/L$	0.030	10.08	-0.021	-8.58
Mean-x-velocity Midplane DES $1.13\ x/L$	0.058	17.20	-0.043	-15.46
Mean-x-velocity Midplane DES $4.88\ x/L$	0.054	16.20	-0.046	-17.72
Mean-y-velocity Bedplane DES $1.13\ x/L$	0.021	30.54	-0.016	-54.30
Mean-y-velocity Bedplane DES $4.88\ x/L$	0.040	59.05	0.034	63.00
Mean-y-velocity Midplane DES $1.13\ x/L$	0.044	40.51	-0.030	-59.31
Mean-y-velocity Midplane DES $4.88\ x/L$	0.041	48.17	0.030	76.60
Mean-z-velocity Bedplane DES $1.13\ x/L$	0.025	69.19	0.016	79.26
Mean-z-velocity Bedplane DES $4.88\ x/L$	0.023	82.09	0.022	104.10
Mean-z-velocity Midplane DES $1.13\ x/L$	0.020	63.19	-0.016	-101.52
Mean-z-velocity Midplane DES $4.88\ x/L$	0.014	83.16	-0.0079	90.86

5 Effects of permeability and head steepness

5.1 Approach to model for the effects of permeability and head steepness

5.1.1 Setup

The general model set-up and approach is extensively discussed in the previous section. However, more insight into the flow characteristics around porous, sloped head groynes is required. This investigation describes a new model for these particular characteristics of the groyne. Hence, the validation models are the foundation of this numerical model, in which these characteristics are validated.

The general set-up of this model has an initial concept of a small scale experimental set-up in a water flume, in which the conditions are based on the IJssel. This model simulates four different configurations for the analysis of the flow around groynes. The representation of the four simulations follows Table 5.1, while Figure 5.1 and Figure 5.2 defining the domain of the model. More extensive information about the set-up of the domain of the model is stated in Appendix E.

Table 5.1: The four configurations of the numerical model

	Porosity 0 %	Porosity 60 %
Slope 1:1	A	B
Slope 1:3	C	D

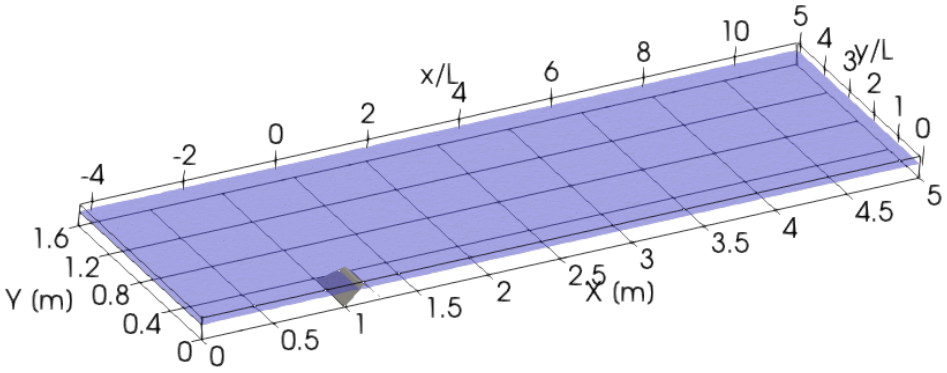

Figure 5.1: Domain of the numerical model for a groyne with a slope of 1:1

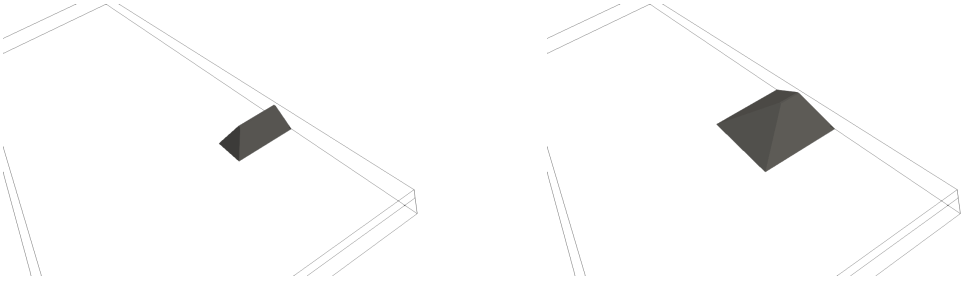

(a) Slope 1:1

(b) Slope 1:3

Figure 5.2: 3D sketch of the various sloped groynes

Porous settings

The porous settings of model B and D are calculated from experimental studies with the Xstream blocks shown in Wetser (2016). Section 3.2.2 described the procedure of achieving the input settings by analyzing the pressure drop against the velocity through the system. This is shown in figure Figure 5.3.

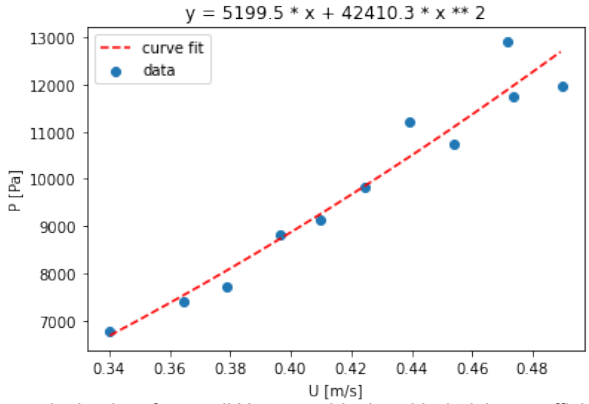

Figure 5.3: Pressure drop against velocity data for small X-stream blocks with deriving coefficients for a curve fit with linear and non-linear coefficients

The parameters solved by fitting a curve with the data are the coefficients for a non-linear curve. However, viscous resistance and inertial resistance are required in the model. Hence, converting these terms is executed by following the orders in the subsection Section 3.2.2. For these specific Xstream blocks, the viscous resistance and inertial resistance are stated in table Table 5.2. Note that the input values in Fluent have to be divided by the thickness of the porous zone.

Table 5.2: Values of the viscous and inertial resistance for Xstream blocks

Xstream media size [m]	Porosity [%]	Darcy coefficient [kg/sm2]	Non Darcy coefficient [kg/m3]	Viscous resistance [1/m]	Inertial resistance [-]
0.029	60	5199.5	42410.3	5189121.8	85.25

Grid dependency test

An initial mesh size is obtained, following the principles of Section 4.1.1. For a value for y^+ of 120 results in a cell size of approximately $0.030\ m$. However, a more refined mesh could result in a better solution of the turbulent flow. Hence, a grid dependency test is executed to verify the validity of the mesh size. The grid dependency test is verified with mean velocities of the flow for a specified simulation time of 120 s.

Figure 5.4, Figure 5.5 and remaining figures in the appendix in Appendix E show that both the finest mesh ($0.028\ m$ and the refinement mesh has the most reactive results. The mesh refinement at the bed-plane $1.16\ x/L$ downstream of the groyne stands out with a negative value for the lateral velocity. The negative value for the lateral velocity near the head of the groyne is in agreement with the mixing layer and the experimental study from the first validation model of the square groyne. In addition, outlaying results are observed from the coarse mesh models in both bed-plane as mid-plane velocities, which concludes less favourable for the model. Hence, the numerical model uses the refinement mesh in this study. The refinement is present $1\ m$ around the groyne in the streamwise direction and over the whole lateral section, as shown in Figure 5.6.

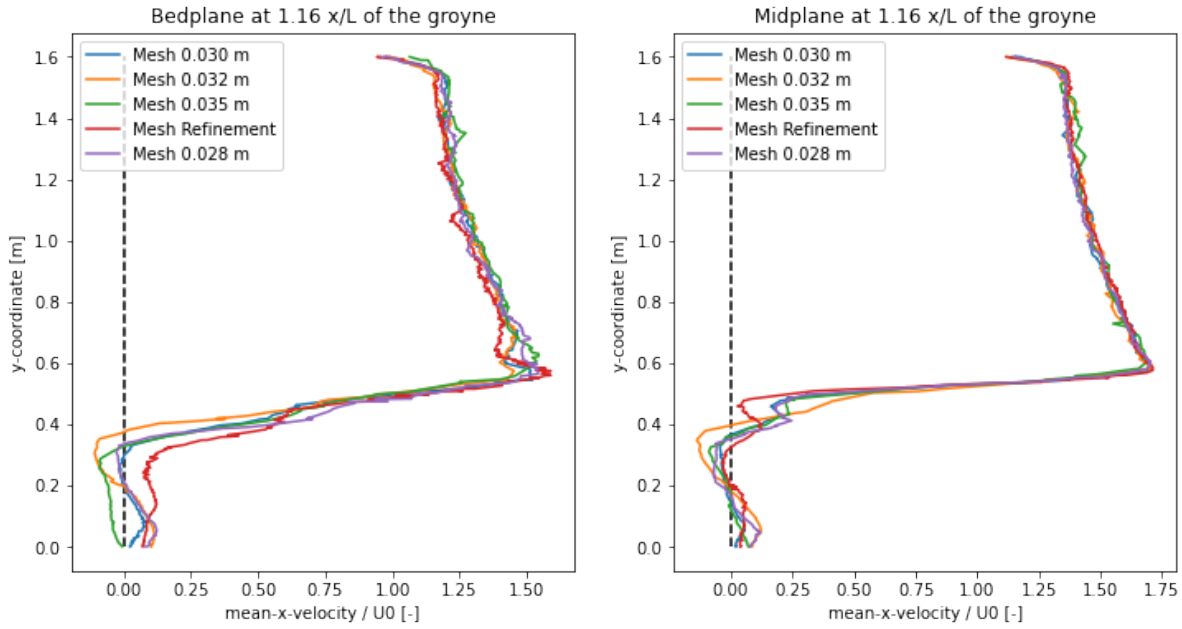

Figure 5.4: Grid dependency test for the mean-x-velocity for a time simulation of 120 s

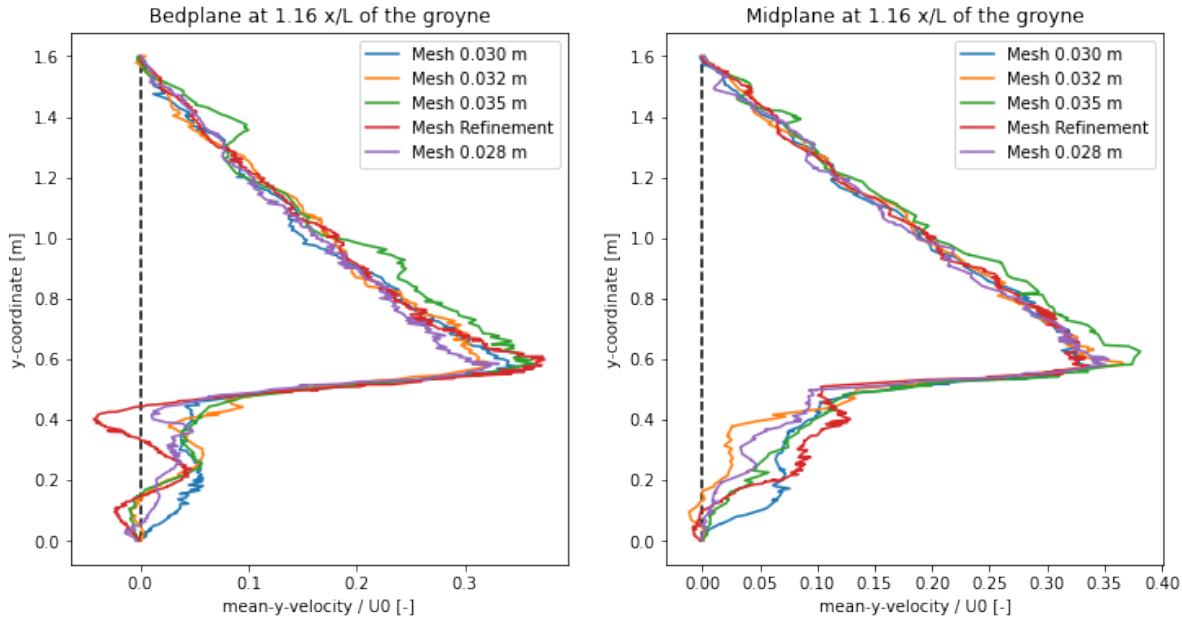

Figure 5.5: Grid dependency test for the mean-y-velocity for a time simulation of 120 s

5.1.2 Velocity contours

The contour lines show the velocity profile near the bed-plane, approximately $0.01\ m$, respectively $0.1\ z/D$ and in the mid-plane, approximately $0.05\ m$, respectively $0.5\ z/D$. Hence, the main important processes, such as the horseshoe vortex system, vortex shedding and detached shear layer are observed close to the bed and in the mid plane.

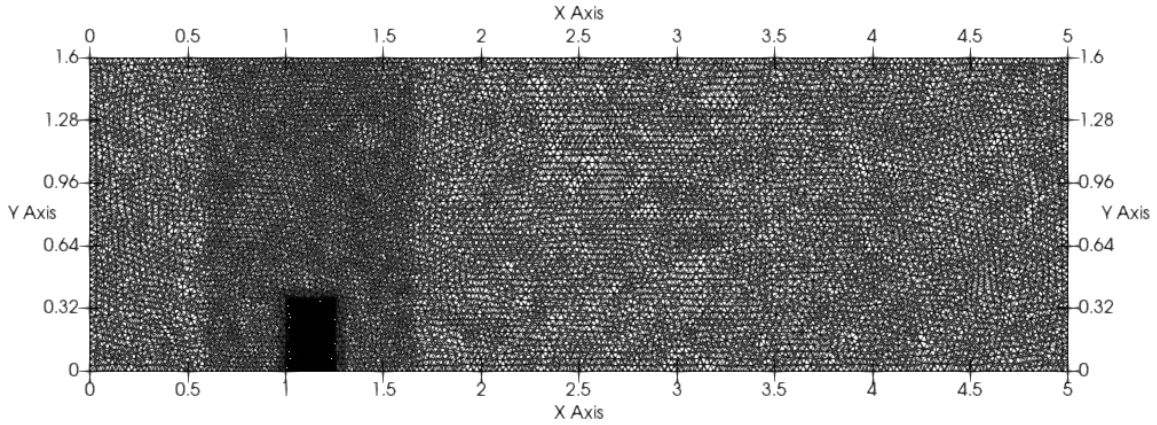

Figure 5.6: Refinement of the mesh with an average mesh size of $0.02\ m$ in the refinement zone, and $0.03\ m$ overall

5.1.3 Large turbulent structures

According to the literature, Reynolds stresses may define the turbulent structures in flow dynamics. Additionally, vorticity is a turbulent property that is broadly used for the visualisation of these time-dependent structures. The Reynolds stresses are widely used to quantify and analyse the turbulent behaviour of the flow. However, Reynolds stresses are properties obtained from fluctuations in the velocity, which the model approximates to a definite length scale. Therefore, it is essential to understand the approach of calculating the Reynold shear stresses. An extensive explanation may be found in the Appendix B.1. In DES simulations, the Reynold shear stresses are resolved directly from the fluctuating quantities of the flow.

In Fluent, the model may calculate the vorticity in two approaches; the Lambda two method and the Q criterion. Both have some benefits and are widely used in turbulence flow structures. The Q-criterion is commonly used for in-stream structures in open channel flow to visualise the vortex structures. Comparing the two methods, the Q-criterion measures the turbulence in all directions, while the Lambda two method defines the turbulence in the most dominant plane direction Dong et al. (2016). Therefore, in this model, the Q-criterion is used to visualise the complete turbulent structure. The vorticity is shown for both the bed plane as mid plane.

5.1.4 Bed shear stresses

This model calculates the bed shear stresses using an indirect method from the flow properties. The detailed, enhanced information of turbulent properties of the fluid leads to the calculation of the bed shear stresses. Two methods calculated from the flow properties may be distinguished in the Reynolds shear stresses and the Turbulent kinetic energy. However, the validation is executed by analyzing the turbulent properties as Reynolds shear stresses. These were acceptable within the range of sufficiency. Hence, the model calculates bed shear stresses at the bed level using the resolved Reynolds shear stresses, directly calculated from the instantaneous velocity. From the Reynold stresses, the bed shear stress equations are as follows:

$$\tau_x = \rho\sqrt{\overline{u'v'}^2 + \overline{u'w'}^2} \tag{5.1}$$

$$\tau_y = \rho\sqrt{\overline{u'v'}^2 + \overline{v'w'}^2} \tag{5.2}$$

$$\tau_z = \rho\sqrt{\overline{u'w'}^2 + \overline{v'w'}^2} \tag{5.3}$$

in which ρ is the density of the water, $\overline{u'v'}$ is the Reynolds shear stresses for the streamwise and lateral direction, $\overline{u'w'}$ is the Reynolds shear stresses for the streamwise and vertical direction, and $\overline{v'w'}$ is the Reynolds shear stresses for the lateral and vertical direction. The general formula for the bed shear stresses follows:

$$\tau_{total} = \sqrt{\tau_x^2 + \tau_y^2 + \tau_z^2} \tag{5.4}$$

The dimensionless values of the bed shear stresses are calculated by using the initial bed shear stress ($\tau = \frac{\tau_{total}}{\tau_0}$). The initial bed shear stress is obtained by using the method for calculating the average bed shear stress, stated in the appendix Equation (B.1). For this model, the initial bed shear stress is $0.076\ N/m^2$.

Overview adjusted input settings

By using the sensitivity analyses, the input settings are confirmed and justified. This concludes the input settings for the four configurations, which are as follows:

Parameters	Values model A	Values model B	Values model C	Values model D
Flow depth [m]	0.10	0.10	0.10	0.10
Flume width [m]	1.6	1.6	1.6	1.6
Flume total length [m]	5	5	5	5
Total length of groyne in x-direction [m]	0.26	0.26	0.74	0.74
Total length of groyne in y-direction [m]	0.38	0.50	0.50	0.50
Average length of the groyne in y-direction [m]	0.32	0.32	0.32	0.32
Angle groyne [degrees]	45	45	18.43	18.43
Porosity [%]	0	60	0	60
Initial velocity [m/s]	0.14	0.14	0.14	0.14
Initial bed shear stress [N/m^2]	0.076	0.076	0.076	0.076
Froude number	0.14	0.14	0.14	0.14
Reynolds number	1.4 x 10^4	1.4 x 10^4	1.4 x 10^4	1.4 x 10^4
Kinematic viscosity [m^2/s]	1.03 x 10^-6	1.03 x 10^-6	1.03 x 10^-6	1.03 x 10^-6

Input settings	Values/setting
Turbulence model	DES with KW-SST
Turbulence options	Without curvature correction
Pressure-velocity solver	PISO
Mean Grid size [m]	0.020
CFL [-]	4
Simulation time [s]	300

5.1.5 Comparison with conventional groyne

The flexible groyne is mainly similar to model B, whereas the conventional groyne is related to model C. So, for comparing the results, both models are shown with the most outstanding features from the visualisations.

5.2 Results from model for the effects of permeability and head steepness

5.2.1 Velocity profile

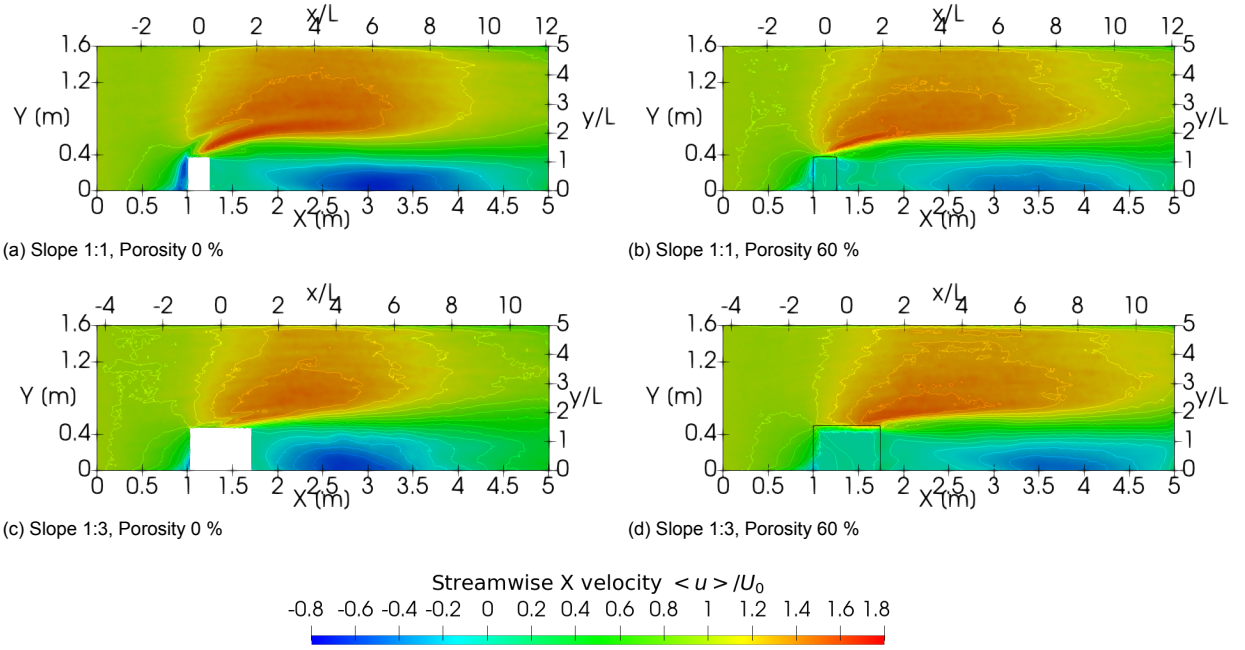

(a) Slope 1:1, Porosity 0 %

(b) Slope 1:1, Porosity 60 %

(c) Slope 1:3, Porosity 0 %

(d) Slope 1:3, Porosity 60 %

Figure 5.7: Mean X velocities near the bed plane for the numerical model in non-dimensional units

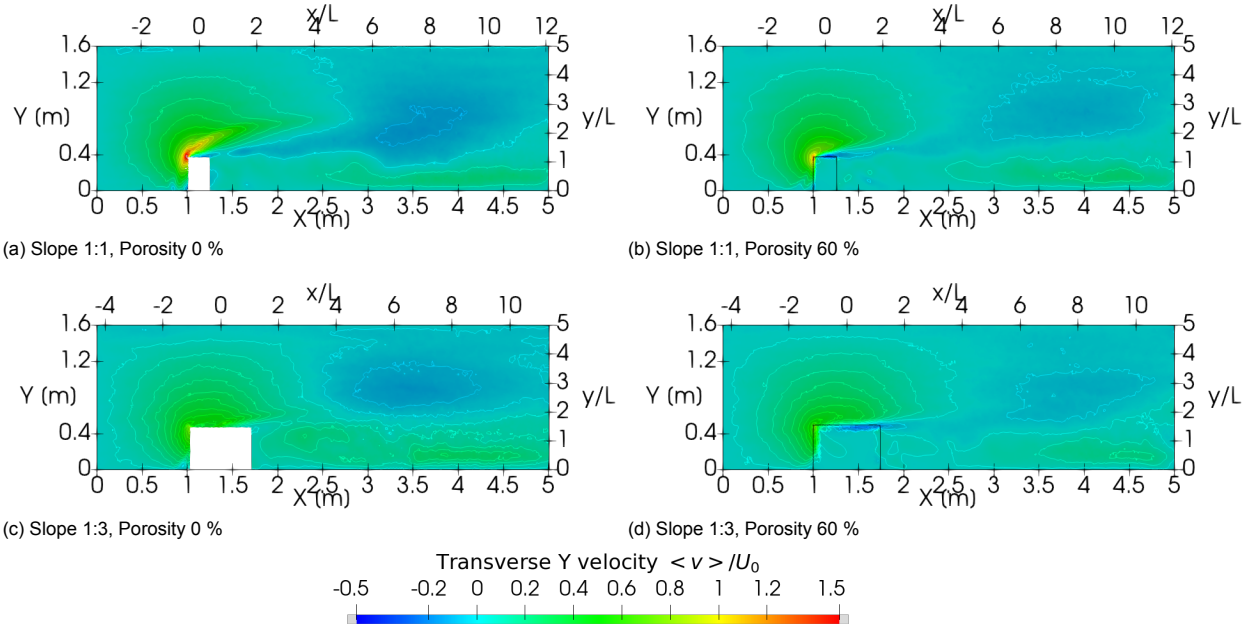

(a) Slope 1:1, Porosity 0 %

(b) Slope 1:1, Porosity 60 %

(c) Slope 1:3, Porosity 0 %

(d) Slope 1:3, Porosity 60 %

Figure 5.8: Mean Y velocities near the bed plane for the numerical model in non-dimensional units

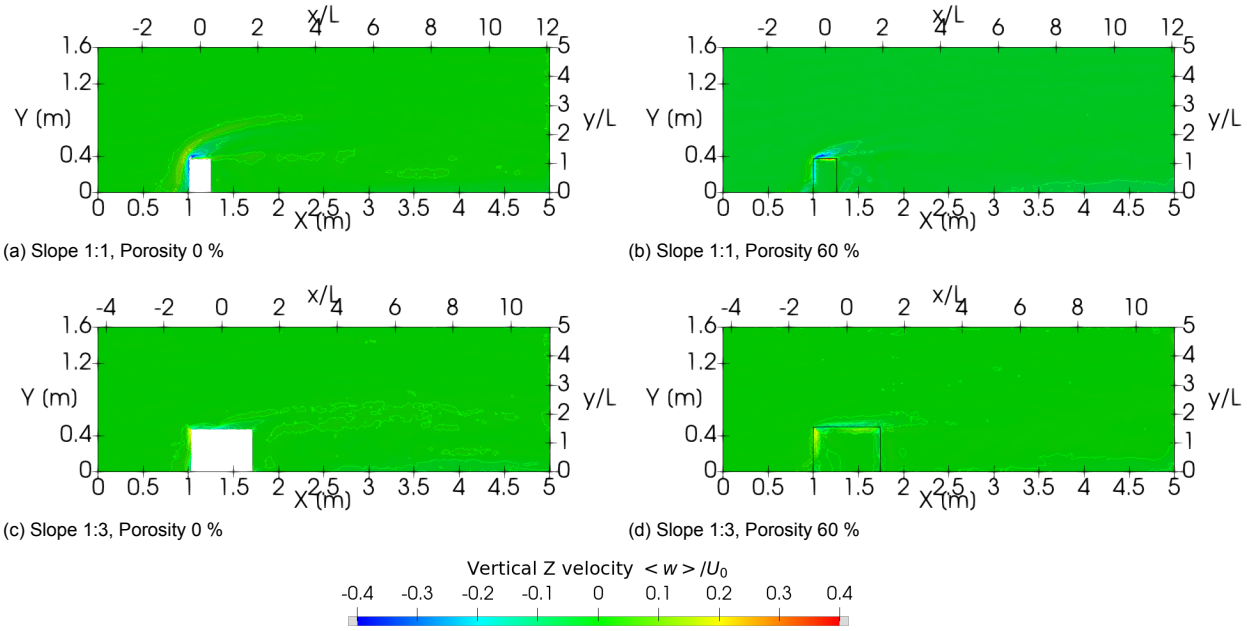

(a) Slope 1:1, Porosity 0 %

(b) Slope 1:1, Porosity 60 %

(c) Slope 1:3, Porosity 0 %

(d) Slope 1:3, Porosity 60 %

Figure 5.9: Mean Z velocities near the bed plane for the numerical model in non-dimensional units

The figures show that the recirculation zone near the bed has a reattachment length of approximately $9\ x/L$ for model A. For model B this is roughly $10\ x/L$, model C $7\ x/L$ and D $9.5\ x/L$. Most intensities for the streamwise velocities in the main channel are observed in the steep, impermeable groyne model A. These strong streamwise velocities are less noticeable in model B, and even less present for the gentle groynes. Though, significant reverse velocities near the bank are most observed for the impermeable groynes whereas in the porous groynes, it remains less noticeable. The transverse velocities for the gentle groynes have resulted in less strong mean flow velocities than the steep head sloped groynes. At the same time, the steep slopes observe to have extensive flow dynamics, especially upstream. Strong flow is also recognised in the vertical velocities, in which flow features of the horseshoe vortex system is observed for the steep groynes.

Additional results for the mid plane mean flow velocities are shown in the Appendix F. Extensive differences are not observed, when comparing the results with the bed plane results. However, the horseshoe vortex system in models A, B and C are more distinguished compared to the results in the bed plane by having large negative vertical velocities in front of the groyne.

5.2.2 Large turbulent structures

Model A shows large $\overline{u'v'}$ around $3\ m$ of the x-axis, respectively $6\ x/L$ downstream of the groyne. These maximum Reynolds stresses are extending to respectively $9\ x/L$. The results in model B are comparable to a lesser extent with model A, however, the $\overline{u'v'}$ show maximum values more downstream in the mixing layer, respectively $9\ x/L$. Gentle groynes, models C and D, were observed to have less strong values of $\overline{u'v'}$. It is shown in model C that large values of $\overline{u'v'}$ are presented more closely to the groyne, yet, the intensity is less than the steep-sloped groynes. The gentle head sloped groyne with porosity showed maximum values far downstream of the groyne, approximately $9\ x/L$ comparable with model B. Hence, it is observed that the porosity decreases the $\overline{u'v'}$ and shifts the peak values more downstream than the steep, impermeable groynes.

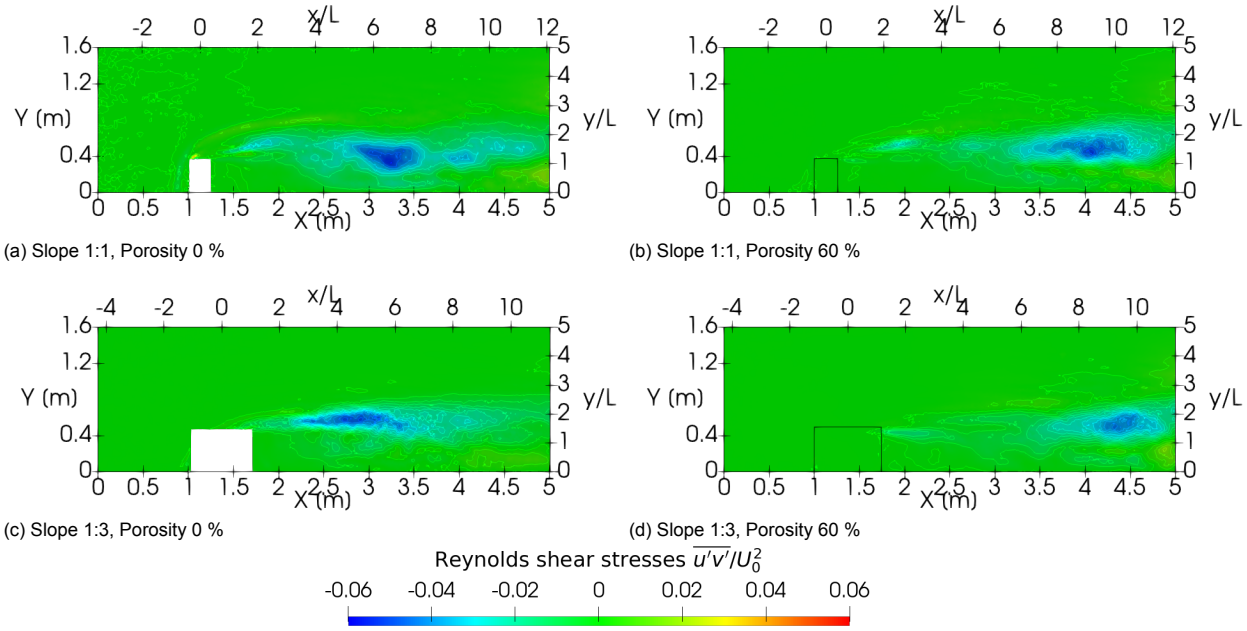

(a) Slope 1:1, Porosity 0 %

(b) Slope 1:1, Porosity 60 %

(c) Slope 1:3, Porosity 0 %

(d) Slope 1:3, Porosity 60 %

Figure 5.10: Reynolds shear stresses in horizontal and lateral direction ($\overline{u'v'}$) near the bed plane for the numerical model

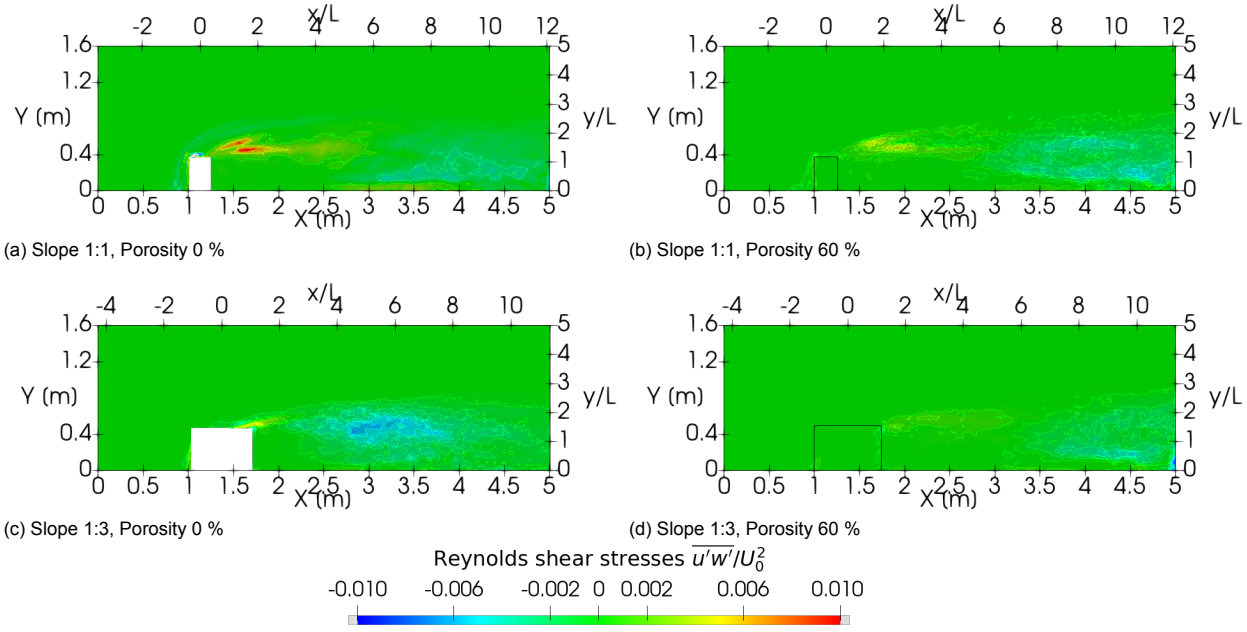

(a) Slope 1:1, Porosity 0 %

(b) Slope 1:1, Porosity 60 %

(c) Slope 1:3, Porosity 0 %

(d) Slope 1:3, Porosity 60 %

Figure 5.11: Reynolds shear stresses in horizontal and vertical direction ($\overline{u'w'}$) near the bed plane for the numerical model

The $\overline{u'w'}$ are primarily present in the solid groynes, models A and C. The significant values are found in the mixing layer, respectively $5\ x/L$ and near the head of the groyne. These indicate the vortex shedding at the head of the groyne, which is related to the highly 3D flow features. In addition, the horse-shoe vortex system is present in model A due to the prominent negative values of $\overline{u'w'}$ shown upstream of the groyne. This observation is similar to the vertical velocity. Extensive flow features are observed for the steeply sloped groynes, which are related to the horse-shoe vortex system.

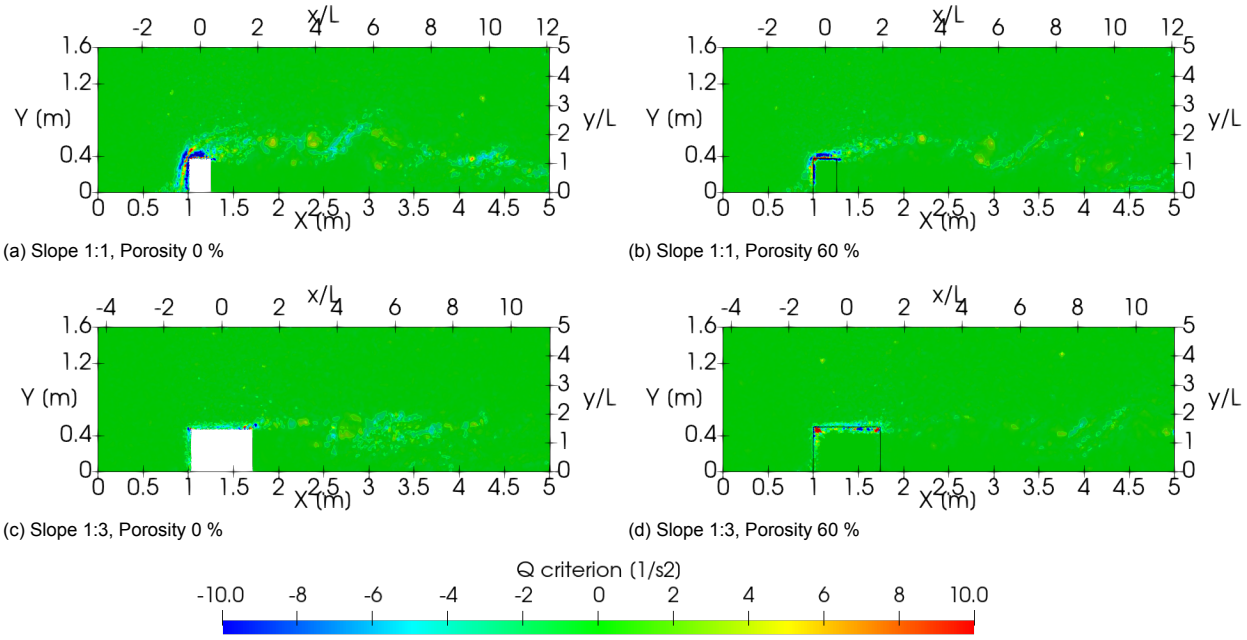

(a) Slope 1:1, Porosity 0 %

(b) Slope 1:1, Porosity 60 %

(c) Slope 1:3, Porosity 0 %

(d) Slope 1:3, Porosity 60 %

Figure 5.12: Vortical structures near the bed plane by using the Q criterion

The vorticity shows the development and intensities of the swirling eddies in the flow around the groyne. It is observed in model A that many eddies upstream and downstream of the groyne are present, indicating the vortex shedding around an obstacle in the open channel flow. Vortex shedding is shown to a lesser extent for the impermeable gentle groyne, model C. For the permeable steep groyne, model B, it is observed that there are many similarities for the eddy formations with the steep, impermeable groyne. However, the intensities are much less. In general, the results of the models have indicated that the eddy formations are less extensive for permeable groynes, especially downstream of the groyne. This is in agreement with the results in the mid plane, shown in Appendix F.

5.2.3 Bed shear stresses

The bed shear stresses are closely related to the two most dominant Reynolds shear stresses. As shown in the large turbulent structures, the most significant values are observed downstream of the groyne in the mixing layer. Hence, it is expected that the large bed shear stresses are present in the mixing layer. From Fig. 5.13 it is observed that the locations of the bed shear stresses are similar with the locations of the peak values for $\overline{u'v'}$ and $\overline{u'w'}$.

The output of the models showed that the maximum bed shear stresses are primarily in the mixing layer. Although, for the impermeable groynes, it is observed that significant values are relatively close to the head of the groyne. The extreme values for the impermeable groynes are both 20, whereas the maximum values of the porous groynes are rough 5 % smaller, resulting in a range of maximum values between 20 and 18 for the bed shear stress. This is especially shown within model D, in which a gentle slope is used with the porosity. The peak values' location was shifted more downstream from 6 x/L to 9 x/L, which is a downstream movement of approximately 1.5. By comparing the locations and intensities of the Reynolds shear stresses with the bed shear stresses, it is observed that the most dominant shear stress is defined by $\overline{u'v'}$.

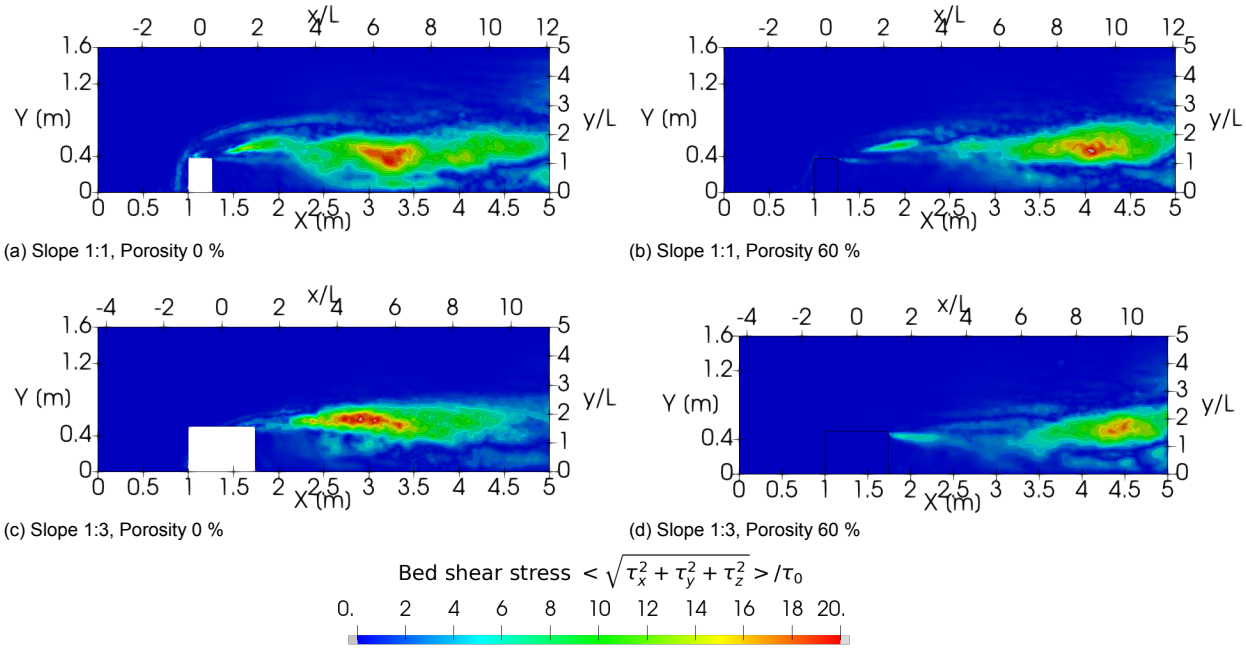

(a) Slope 1:1, Porosity 0 %

(b) Slope 1:1, Porosity 60 %

(c) Slope 1:3, Porosity 0 %

(d) Slope 1:3, Porosity 60 %

Figure 5.13: Bed shear stresses ($\sqrt{\tau_x^2+\tau_y^2+\tau_z^2}/\tau_0$) at the bed plane for the numerical model

5.2.4 Comparison with conventional groyne

Model C is relatable with the conventional groyne structure. Some remarkable flow dynamics are observed, such as the relatively short recirculation zones, the minor transverse and vertical velocities, and large turbulent structures are observed for both $\overline{u'v'}$ and $\overline{u'w'}$. In addition, several eddy formations are present near the groyne. The strong Reynolds shear stress values are primarily located at $3\ x/L$, in which the large bed shear stresses are observed as well.

Model B is referred to as the flexible groyne and is noted to have a small flow velocity through the structure, approximately 5 %. However, the flow has still enormous dynamics around the groyne. The most notable features are observed in the transverse and vertical velocities, in which the horse-shoe vortex system is visible due to the large negative vertical velocities upstream of the groyne. The Reynolds stresses are relatively low compared to the solid configurations, and therefore more minor fluctuations are present. Still, it shows that strong $\overline{u'v'}$ are present in the mixing layer further downstream. In addition, the $\overline{u'w'}$ shows some positive large shear values near the head of the groyne. Most bed shear stresses are observed far downstream of the groyne, approximately $9\ x/L$. Thus, it can be indicated that the shear stresses near the head of the groyne have a relatively low impact.

Significant differences observed are predominantly shown in the lateral and vertical velocities and the $\overline{u'v'}$. The strong positive values for the lateral velocities upstream of the groyne are almost not shown in the conventional groyne. These small lateral velocities result in less strong curving flow around the groyne. Nevertheless, the recirculation zone is more strongly for the conventional groyne, which is located closer to the groyne. The edges of both models' recirculation zone are similar to the areas with the peak values of the Reynolds stresses. It is shown that the bed shear stresses for the conventional groyne are close to the groyne. In contrast, the bed shear stresses in the flexible groyne extend more downstream within the mixing layer. The maximum values for the bed shear stresses are relatively similar for both simulations, approximately 20. However, more intensities of the bed shear stress are shown within the simulation of the conventional groyne.

6 Application of multiple groynes

The general model setup and approach is extensively discussed in the previous sections. This model is an extended version of the previous model B. In the IJssel, the particular groynes are executed in series. Hence, this model simulates as a two series groyne, which has similar features of the groynes placed in the IJssel.

6.1 Approach for the application of multiple groynes

6.1.1 Setup

The characteristics of the groynes in the IJssel are as follows:

- The blocking part of the groyne is 1/5 of the width of the river
- The spacing between groynes is approximately three groyne lengths
- The scaling is approximately 1:50 compared with the IJssel length scales

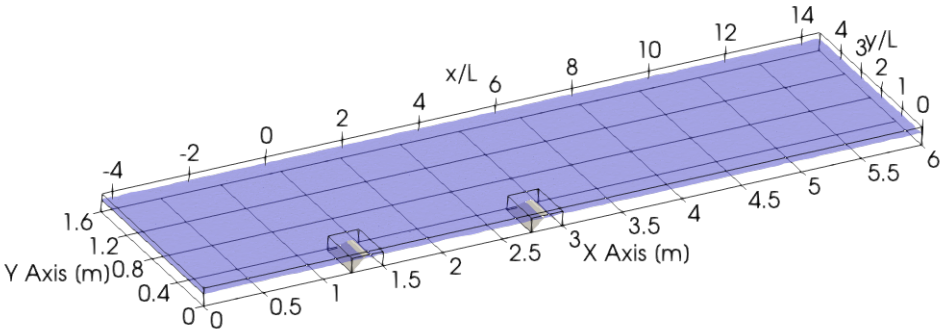

Figure 6.1: Domain of the application of multiple groynes in the numerical model

The objective of this model is to increase the knowledge of the flow features for groynes in a more suitable application. More insight in the flow dynamics around a series of groynes is therefore supplementary to the four simulations. The general setup of this model has an initial concept of a small scale experimental setup in a water flume, in which the conditions are based on the IJssel. This section investigate model A and B in a series of two groynes.

Porous settings

This model uses the parameters of model B and C. Therefore, the same porous settings will be used as approached in section Section 5.1.1.

6.1.2 Velocity contours

The contour lines show the velocity profile near the bed-plane, approximately 0.01 m, respectively 0.1 z/D.

6.1.3 Large turbulent structures

According to the previous sections, the turbulent structures will be calculated using Reynolds shear stresses and vorticity.

6.1.4 Bed shear stresses

This model calculates the bed shear stresses by using an indirect method from the flow properties using Reynold shear stresses on the bed level.

Overview adjusted input settings

The input settings for the two configurations are as follows:

Parameters	Values model A	Values model B
Flow depth [m]	0.10	0.10
Flume width [m]	1.6	1.6
Flume total length [m]	6	6
Total length of groyne in x-direction [m]	0.26	0.26
Total length of groyne in y-direction [m]	0.50	0.38
Average length of the groyne in y-direction [m]	0.32	0.32
Axial location of first groyne in x-direction [m]	1.37	1.37
Axial location of first groyne in x-direction [m]	2.87	2.87
Angle groyne [degrees]	18.7	45
Porosity [%]	0	60
Initial velocity [m/s]	0.14	0.14
Froude number	0.14	0.14
Reynolds number	1.4 x 10^4	1.4 x 10^4
Kinematic viscosity [m^2/s]	1.03 x 10^-6	1.03 x 10^-6

Input settings	Values/setting
Turbulence model	DES with KW-SST
Turbulence options	Without curvature correction
Pressure-velocity solver	PISO
Mean Grid size [m]	0.020
CFL [-]	4
Simulation time [s]	300

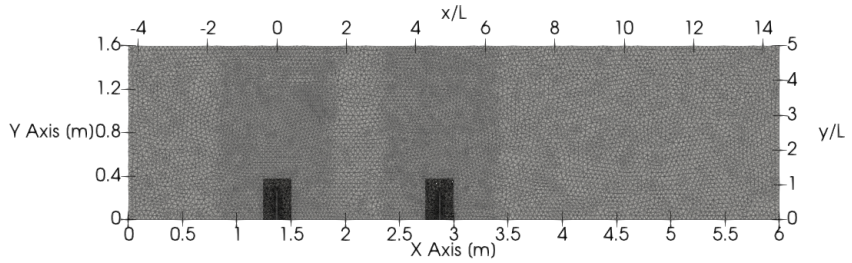

Figure 6.2: Refinement of the mesh with an average mesh size of $0.02\ m$ in the refinement zone, and $0.03\ m$ overall

6.2 Results for the application of multiple groynes

6.2.1 Velocity profile

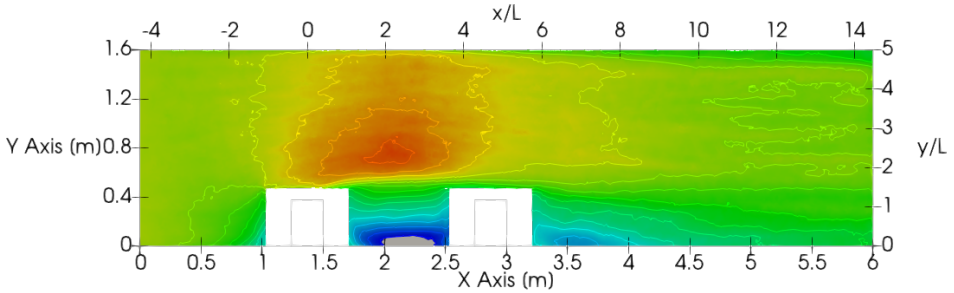

(a) Slope 1:3, Porosity 0 %

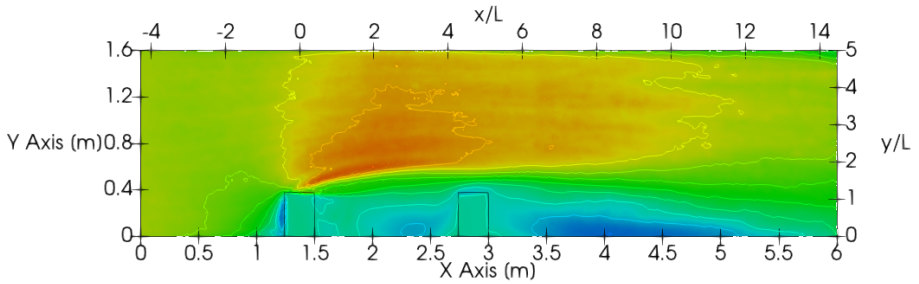

(b) Slope 1:1, Porosity 60 %

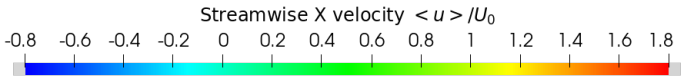

Figure 6.3: Mean X velocities near the bed plane for the numerical model in non-dimensional units

The results intend to show a decrease in the intensity of the recirculation zone for porous groynes. Especially, the negative streamwise flow values in the groyne field is outstanding for the conventional groyne simulation. The streamwise velocity in the main channel is somewhat similar. In contrast, the overall intensity of the re-circulating zone has increased compared with the single groyne simulations as shown in Fig. 5.7. The increase from single groyne to the series groynes is approximately -0.8 to -1.0 in dimensionless units $< u > /U_0$. Extra visualizations are found in the Appendix F.

6.2.2 Large turbulent structures

The Reynolds stresses indicate that the horseshoe vortex system is present for the porous groyne simulation, however minor, as shown in the single groyne results. $\overline{u'w'}$ are primarily identified for the horseshoe vortex system. The conventional groyne is observed to have large turbulent structures close to the head of both groynes, which is expected to be closely related to the strong re-circulation zone. The maximum values of both Reynolds shear stresses are displayed to have a value of roughly $0.02\ \overline{u'w'}/U_0^2$.

The porous groyne shows less extreme values in both presentations of the Reynolds shear stresses. The maximum values for the Reynolds shear stresses are remarkable further downstream of the second groyne. However, the eddy formations visualized by the vortical structures are more present close to the porous groynes. The eddy formations are especially observed near the first groyne, where extensive vortex shedding is expected.

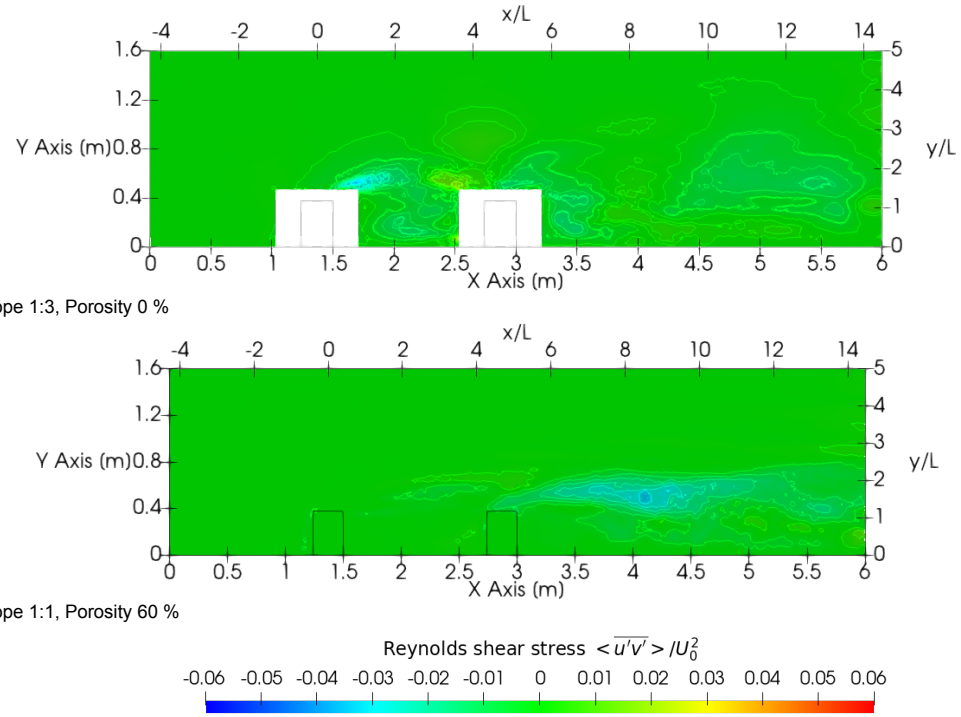

(a) Slope 1:3, Porosity 0 %

(b) Slope 1:1, Porosity 60 %

Figure 6.4: Reynolds shear stresses in horizontal and lateral direction ($\overline{u'v'}$) near the bed plane for the numerical model

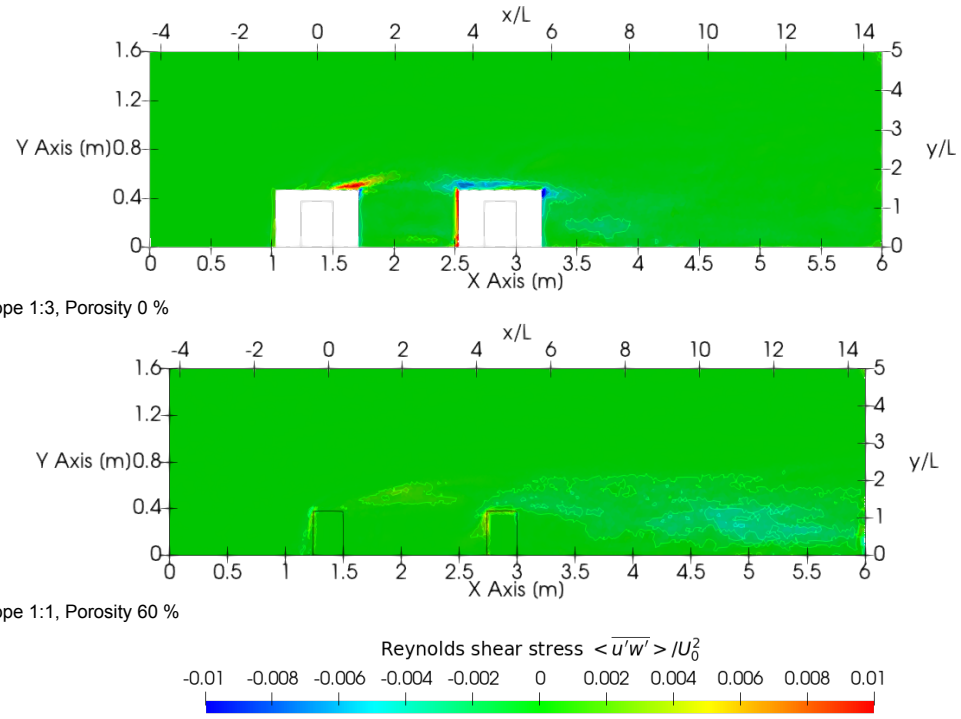

(a) Slope 1:3, Porosity 0 %

(b) Slope 1:1, Porosity 60 %

Figure 6.5: Reynolds shear stresses in horizontal and vertical direction ($\overline{u'w'}$) near the bed plane for the numerical model

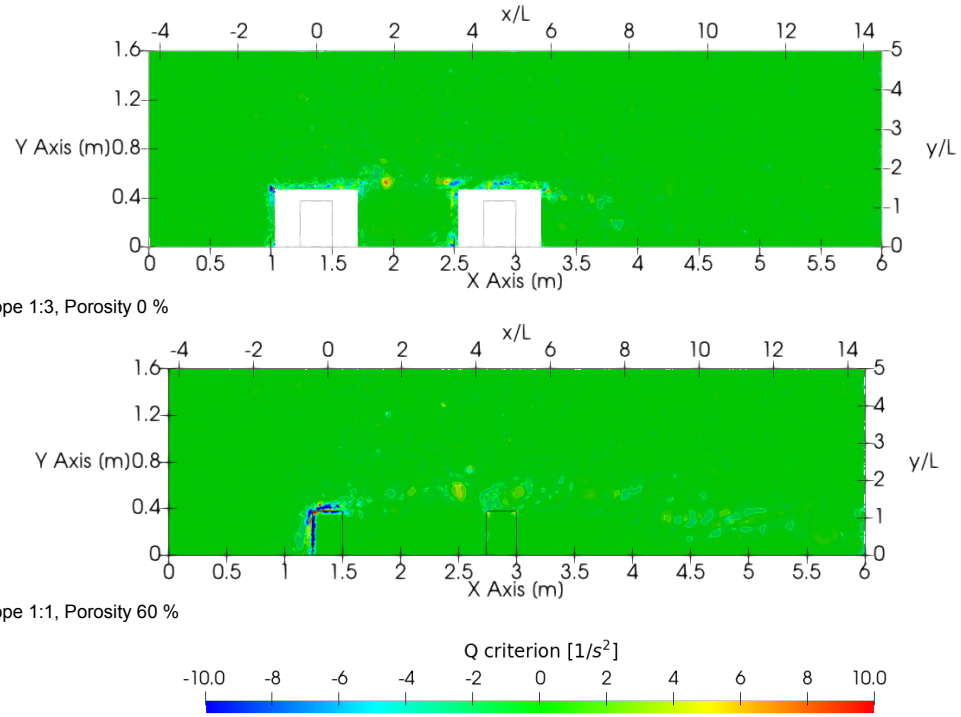

(a) Slope 1:3, Porosity 0 %

(b) Slope 1:1, Porosity 60 %

Figure 6.6: Vortical structures near the bed plane using the Q criterion

6.2.3 Bed shear stresses

The bed stresses are presented, which are primarily related to the $\overline{u'v'}$. However, by the visualizations from the Reynolds shear stresses of the impermeable groyne simulation, the $\overline{u'w'}$ have shown to be explicit present. The figures have shown that the intensities of the bed shear stress near the groyne for the flexible groynes simulation are decreased. There is almost no bed shear stress present near the groynes. Instead, the bed shear stresses have been shifted more downstream of the second groyne. The conventional groyne is showing large bed shear stresses close the groyne, which is also observed for impermeable groynes in the single groyne models. For both simulations, the maximum bed shear stresses are approximately 14, and thus the maximum intensities have not been decreased for applying porosity within the groyne.

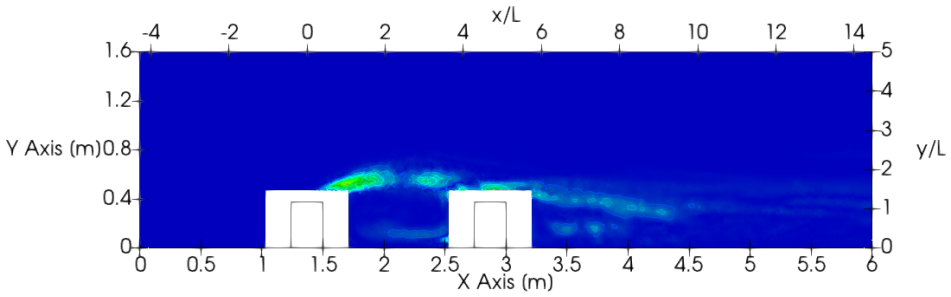

(a) Slope 1:3, Porosity 0 %

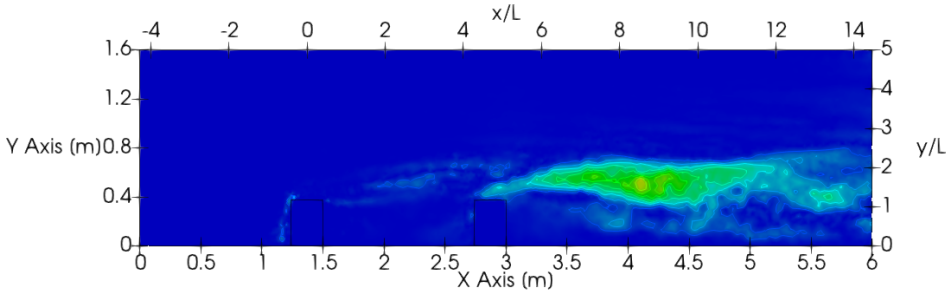

(b) Slope 1:1, Porosity 60 %

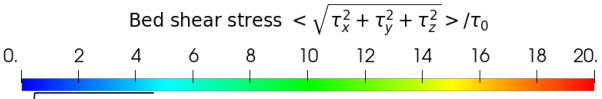

Figure 6.7: Bed shear stresses ($\sqrt{\tau_x^2+\tau_y^2+\tau_z^2}/\tau_0$) for the numerical model

7 Discussion

A numerical model is developed to model flow around groynes and is validated against experimental studies with sufficient accuracy. Important observations include the limitations of the software package and numerical model, and the effects of permeability and head steepness of groynes on local flow characteristics. Also, several indications are observed for the highly three-dimensional flow around multiple groynes. At last, the locations of the bed shear stresses are observed to be of interest for the possible development of local scour, with focus on the comparison between the configuration of the flexible groyne and the conventional groyne.

7.1 Software selection

From the study, it is shown that the required processes for modelling flow dynamics around groynes is capable within the software programme Fluent. However, within any software package and CFD model, there are some limitations for modelling turbulent flow.

In Fluent, it is not possible to combine a porous zone with friction at the edge of the zone. A zone can only exist in a single contact region, which in this case, is permeable. Therefore, no additional features such as friction can be assigned to the transition between the open channel flow and the porous flow within the structure.

Fluent solves the 3D flow using the completed set of the Navier-Stokes equation in combination with a turbulence closure model. However, the many implementations and possibilities within the software package give the modeller extra problems to tackle and distinguish unnecessary options for achieving the objective. Therefore, it is challenging for the modeller to improve the model by detaching various implementations and using the necessary options.

7.2 Validation

The validation of the model is divided into three experimental studies due to the absence of an extensive experimental study for flow characteristics around the flexible groyne. The validation models are split between a squared groyne, a porous weir structure and a sloped groyne. Hence, questions can be asked for validating the flow around a flexible groyne within one model. Uncertainties of the validation of the models are present. However, due to the extensive validation of the numerical model, it is expected that the amount of uncertainty is reduced within acceptability.

Various input settings and implementations of sub-models are used in the numerical model within the possibilities of the software package. A large number of the implementations is investigated or has already been studied. However, some critical implementations imply simplifications of real cases scenarios. In this model, the roughness is simplified. The large stones from the X-stream blocks act as the groyne medium and top layer, thus affecting the friction. From the study of Prinos et al. (2003) for flow near permeable structures, it is shown that friction has some importance for the flow characteristics near the interface and the mean flow properties in the free flow region. For simplifications, the wall roughness is defined as a smooth wall corresponding to default values in Fluent. A more actual representation of the walls could benefit the solution, though only a slight increase will presumably be observed. For most experimental studies, however, groynes are created using PVC or plexiglas, which act as a smooth wall.

The turbulence closure model is considered to be an important implementation for numeral modelling. For this study, it is critical to capture the large turbulent structures. From recent studies both DES models (Paik & Sotiropoulos, 2005, Koken & Constantinescu, 2014) and $k - \omega$ (Chrisohoides et al., 2003, Shampa et al., 2020) are used for separation flow around groynes with great accuracy. Furthermore, Fluent's manual (ANSYS, 2019) suggests using the $k - \omega$ SST model for separation shear flows. Therefore, both the $k - \omega$ SST and the DES SST model are investigated with a sensitivity analysis. The DES SST model is observed to be the best-fitted model compared to the experiments, which from the author's understanding, has not been used before in this specific combination for flow around groynes. Using the benefits of the $k - \omega$ SST model and the DES model, it is analyzed that it is the best-fitted model within the scope of this research. In addition, other implementations in the model are analyzed using sensitivity analyses to improve the solution of the model.

The sensitivity analyses are used for specific implementations of the model. Most of this validating is done by using statistical parameters, in which both RMSE and PBIAS are used in this study. The main focus for these statistics is on the streamwise and lateral velocities near the bed plane. The acceptability range of the RMSE value is dependant on the situation and case of the model. Hence, a standard value is difficult to give. For the PBIAS a satisfactory range beneath the absolute value of 25% is acceptable for mean velocities in river flow (Shampa et al., 2020).

The numerical results are compared to the experimental data. Most data-sets are obtained by using Acoustic Doppler velocimetry (ADV) measurements. The literature shows that the ADV measurements undervalue the actual turbulent properties for free-stream flow. An increase in inaccuracies is shown for measurements near the bed. Further away from the bed, the ADV becomes much more reliable and may be approximated as within 5 % accuracy (Dombroski & Crimaldi, 2007). For complex flow structures, even 20 % measurement errors may be achieved for turbulent properties (Duan, 2009).

Still, most numerical models cannot fully simulate the measured turbulent flow perfectly. In general, numerical models underestimate the mean flow velocities and overestimate the Reynolds stresses (Koken & Constantinescu, 2014, Herrera-Granados, 2018, Chang et al., 2020). In particular, being very close to the groyne increases the errors in the measurements. Hence, when comparing the validation results with the simulated data, one must be aware of the measurement errors.

Rectangular conventional groyne structure

A grid dependency test is used for defining an optimal mesh size. The results favour the mesh with a refinement around the groyne. However, this model does have some drawback in which the model has not the exact length of the total measuring domain. The original domain for the experimental study Jeon et al. (2018) has a total of 7 m, while the numerical domain is 6 m. Therefore, a critical observation has to be made at the location of the boundary conditions. After comparing the numerical models for both 6 m and 7 m, it could be stated that the boundary conditions less downstream of the groyne, do not affect the flow dynamics. Hence, the model with the refinement around the groyne is used for further validation. Still, it is observed that much finer mesh could result in great accuracy of the solution such as shown in Kang et al. (2021).

The results of the model show that streamwise and lateral velocities are within great accuracy of the experiments. The RMSE is nearly everywhere beneath 30 % and the PBIAS is almost everywhere beneath 25 %. Compared to the magnitude of the streamwise and vertical velocity, vertical velocities are not that important. Still, for the best solution of the model, this should be considered for further investigations to increase the solution's accuracy and obtain the 3D flow features.

Results of the numerical models show that the intensity of the $\overline{u'v'}$ Reynolds shear stresses overestimates compared with the results of the experiment. This observation agrees with recent studies for turbulent flow modelling (Koken & Constantinescu, 2014, Herrera-Granados, 2018, Chang et al., 2020). In addition, a downstream shift of the peak Reynolds shear stresses is observed, which is presumably the effect of numerical diffusion. Numerical diffusion may be obtained by skewed, inappropriate mesh or unsuitable discretization schemes.

Coupled system for porous medium

The porous weir has no accurate data-sets available with extensive visualisations and the data is only available digital without data sets. Consequently, validating the results by using contour lines is difficult to use. However, the vertical profiles for various flow characteristics have been expressed for many x-positions. Thus, a general view of the flow dynamics around a porous weir is present. The absence of any visualisation is observed in the model for the porous weir, in which only graphs in dimensionless numbers are given. By using digitising tools, the experimental data is obtained. It must be noted that this process decreases the accuracy of the experimental data set above the general measurements errors. Therefore, it could be questioned whether the validation material is accurate enough.

The input settings for the permeability of the flow through the porous medium is an approximation. All the formulations stated in the literature study, are focused for specific cases and therefore no general formulation has a very accurate solution. Hence, a sensitivity analysis is used to understand these parameters and conclude a more fitted approach for the porosity. The results are compared with the actual experimental data and optimized for the velocity through structure. However, it must be noted that this is a more practical approach. A more well defined formula based on experimental studies for porous groynes supports a more scientific approach.

The numerical model results compared with the experimental data-set show agreement for the streamwise velocities with approximately 20 %. In addition, the locations are similar. Both peak values for the vertical velocities, and the maximum Reynolds stresses $\overline{u'w'}$ are shifted downstream for the numerical model, which is similar to the results of the numerical model for the square groyne. Still, the peak values are observed, and the vertical profiles show similar patterns with the measurement data. Hence, it is concluded that the numerical model shows the results with acceptable accuracy, though it has some lagging factor in which most maximum values are shifted downstream.

Sloped groyne

This model presents a groyne with a head slope and vertical side walls. Therefore, a sloped groyne with side slopes is not taken into account. The importance of this model is the geometry of the groyne, particularly the importance of the head slope. Therefore, it may be stated that this model suffices the requirements. However, a more suited model with sloped sides would increase the validity of the model.

The model has 3D velocity measurements on four different water depth levels. The measurement accuracy is approximately 0.005 m/s, which is 2 % of the average initial velocity. Compared to the mean-z-velocity, this error could vary around the 25 % and for the mean-y-velocity around 10 %. Errors this large could disadvantage the model comparisons and validation, as shown in comparison with the mean-y-velocities and mean-z-velocities.

The results for the RMSE and PBIAS are shown to be slightly out of the acceptable range, especially for the lateral and mean vertical velocities. Sloped groynes should induce more 3D flow features, and therefore most velocities must be within an acceptable error. However, it is noted that many exceptional values are observed downstream of the groyne for both lateral and vertical velocities. From literature studies, it is shown that the intensity of the recirculation zones decreases for decreasing the slope's steepness and the reverse flow near the bank appears to be weakened (Kang et al., 2011b). Hence, lateral velocity should be smaller than the lateral velocities downstream of the rectangular, impermeable groyne. However, this is not the case. The lateral velocities in the square model are approximate 10 % far downstream of the groyne, and in the triangular groyne model, these are approximate 30 %. The measurements errors may be present in these areas.

Remarks numerical model

The validation concludes the validity of the model. However, some remarks are stated for the model. Due to model domain differences, the various uses of the mesh size and the variation of the domain lengths are not considered. However, the boundary conditions, the turbulence model and other important implementations such as the mesh size and solving methods are validated. The numerical model tends to overestimate the Reynolds shear stresses and shifts the peak values more downstream of the groyne. The mean flow velocities are shown to be underestimated, especially the streamwise flow.

7.3 Results from model for the effects of permeability and head-steepness

Velocity profile

The velocity profiles show the distinct differences between the mean velocities of the configurations. One of the essential aspects of these results is the various high mean velocities produced from the turbulent macro structures. The horseshoe vortex system is shown in model A (impermeable 1:1), which has flow characteristics of negative streamwise velocities near the bed and downward flow upstream of the groyne. The velocities are shown on a smaller scale are these flow characteristics in model B (porous 60 %, 1:1). Therefore, it may be deduced that porous groynes still initiate the horseshoe vortex system, however, more gentle sloped groynes results in the absence of this turbulent macro-structure.

Re-circulation zones are clearly present for flow around impermeable groynes. Still, a remarkable feature occurs when the groyne has a permeable characteristic. An increase in porosity results in a shift of the re-circulation zone downstream and decreases the intensity of this flow pattern. This feature is similar to the validation material of the porous weir, in which the porosity of the weir also resulted in shifting the re-circulation zone more downstream (Leu et al., 2008). The re-circulation zone also shows the intensity of the deflection of the average flow direction. Hence, porosity decreases the deflection of the flow, in which the re-circulation zone is observed more downstream. It is shown in Ettema & Muste (2004) that the deflection of the thalweg flow is related to the maximum streamwise velocities. Less intense deflection is related to smaller peak values of the streamwise velocity, and thus a more extended re-circulation zone is observed. This is observed for porous groynes, in which the deflection is reduced.

The decrease of deflection is also observed in the transverse flow around the head of the groyne. An increase of the groyne porosity leads to an increase in negative transverse velocities at the head of the groyne. Normally, the flow results in a curving flow around the obstacle due to the contraction of the main flow. However, due to the permeability of the groyne, the flow streamline can go through the structure. This is a distinct feature of porous structures. Momentum transfer is present by the penetration of the turbulence through the porous structure, and thus it reduces the mean flow velocities within the free flow region (Prinos et al., 2003). The reduced mean flow velocities are shown around the porous groyne. In addition, the flow through the groyne also exits the groyne, in which generally the re-circulation zone is present. Hence, the flow through the groyne pushes the re-circulation zone downstream.

For the decrease of the steepness, a shift of the re-circulation zone is observed towards the groyne. This is most likely occurring due to the flow that smoothly follows the groyne's geometry. Hence, the deflection of the mean flow decreases, and the re-circulation zone's length scale is reduced. Still, the velocity gradient is present near the groyne, and thus, large turbulent structures are expected.

Macro turbulent structures

Very large Reynolds shear stresses are seen in the mixing layer, which is also very much in agreement with both the validation material from Jeon et al. (2018) Leu et al. (2008). In addition, much turbulence is observed from the vortex shedding in the vorticity figures, but these are not well defined in the Reynolds shear stresses. Still, the vortex shedding is observed but may be less critical as expected for developing large eddy fluctuations. Nevertheless, both the horseshoe vortex system and the mixing layer are present actively in the Reynolds stress results.

The importance of the horseshoe vortex becomes less noticeable for sloped groynes than for vertical wall groynes due to the geometry of the structure. Still, in model A, the horseshoe vortex system is observed. The other large turbulent structures are resolved in the mixing layer and are mostly dominant in the horizontal and vertical planes. These large eddy formations lead to the enormous Reynolds shear stresses in $\overline{u'v'}$ and on a smaller scale $\overline{u'w'}$. Hence, the models show that an increase in the porosity decreases the amount of developing large eddies in the mixing layer. The decrease of $\overline{u'v'}$ is approximately 10%, while the reduction in slope 1:1 to 1:3, the decrease is approximately 5%. In addition to the intensity decrease, downstream shifting of the enormous turbulence is recognised for the porous structure. The downstream shifting of the $\overline{u'v'}$ is also observed for the porous weir in the validation material shown in Leu et al. (2008).

The $\overline{u'w'}$ are much smaller than the $\overline{u'v'}$, yet these are important for the total turbulent structures. Model C shows some outlying results in terms of negative values in the mixing layer. In the other models, these negative values are not present. A relation between the negative downstream values, at approximately $9\ x/L$ for steep-sloped groynes, and the significant negative values in model C at $5\ x/L$ is possible. The increase of these stresses could be affected by the decrease of the slope. So the importance of the vertical and transverse fluctuated velocities affected by the slope change could be an interesting aspect for further studies.

Bed Shear stresses

The bed shear stresses are directly related to the Reynolds shear stresses, hence, the locations of the maximum values are of great importance. The most obvious relations between the models is observed in the mixing layer, while model A has some influence from the horseshoe vortex system upstream of the groyne and thus, bed shear stresses are present upstream. It is observed in Koken & Constantinescu (2014) that the maximum bed shear stresses for a sloped groyne, by indicating the bed friction, are observed near the head of the groyne within the mixing layer. Large bed shear stresses near the head of the groyne are observed in model A. However, maximum bed shear stresses are present more downstream, approximately 6 x/L. More gentle sloped groynes, such as model C, show maximum bed shear stresses closer to the groyne. Therefore, the model is expected to show the maximum bed shear stresses more downstream than as observed in the literature or in experimental studies.

The increase of the porosity has minor effects, at which the increase of the porosity to $60\ \%$ decreases the maximum values by roughly $5\ \%$. This is mostly observed in comparing model C with D, which is shown to be approximately $10\ \%$. However, it is clearly shown that the area of intensities for the maximum bed shear stress are reduced for increasing porosity. The shape size of the area in which the significant bed shear stresses are observed has been reduced for the porous groynes. From the literature, it is shown that an increase of porosity decreases the large turbulent structures and shifts the maximum values for the large turbulent structures downstream (Leu et al., 2008). Therefore, as shown within the model, porous structures can be conducted to reduce the amount of the bed shear, and therefore reducing the development of scour holes in the mixing layer downstream of the groyne. Mainly, it is shown that porosity shifts the bed shear stresses downstream.

Comparison flexible groyne with conventional groyne

Model C presents the conventional groyne structure, whereas model B presents the flexible groyne. Both presentations of the streamwise velocities show that the main channel maximum velocities do not differ very much. The streamwise velocity in the main channel is an essential characteristic of using groynes. Hence, the increasing velocity in the main channel must not be decreased. Otherwise, it reduces sedimentation problems in the main channel. Besides, the extension of the recirculation zone is remarkable for the flexible groyne, compared with the conventional groyne. The lateral and vertical velocities vary mainly at the head of the groyne, wherein the flexible groyne has some sort of horseshoe vortex system recognized. This turbulent structure is not visible at the conventional groyne.

Most interesting is the Reynolds shear stresses downstream of the groyne. The flexible groyne appears to have less intensity $\overline{u'v'}$ values and is located further downstream than the conventional groyne. $\overline{u'w'}$ shows some similarities, though the intensities are less for the flexible groyne. The same can be said for the bed shear stresses. It appears that the flexible groyne decreases the amount of turbulent flow and therefore reduces the bed shear stresses downstream with roughly $5\ \%$. This is somewhat similar to previous studies, which stated that the amount of accelerating flow is decreased by the porosity and steepness. Therefore, the intensity of the vortex in the mixing layer is decreasing Kang et al. (2011b).

Application multiple groynes

The differences between the impermeable and permeable groynes series are significant. It is observed that the macro-turbulent fluctuations and consequently the bed shear stresses are roughly similar for the peak values. However, it is observed that the location of the peak values varies significantly. The bed shear stresses for the impermeable, gentle groyne are observed close to the groyne, whereas the bed shear stresses for the flexible groynes are observed downstream in the mixing layer. This is somewhat similar to the results shown in Zhang & Nakagawa (2008) in which scour for permeable pile groynes were compared with impermeable groynes. The locations of the maximum scour were primarily observed in the mixing layer for the series of permeable groynes. The impermeable groynes showed maximum bed shear stresses more closely to the groyne. Additionally, when comparing these series of groynes with the single groynes, it shows that the intensity of the re-circulating zone is increased for both models. Hence, the groyne field increases the intensity of the re-circulation zone, which is also observed in previous studies Uijttewaal et al. (2001), Yossef & de Vriend (2011).

8 Conclusion and recommendations

The first section of this chapter presents the answers to the research question and gives a general conclusion of the results. Recommendations for further investigation are given in the second section.

8.1 Conclusion

The research question is:

- ”What are the effects of permeability and head steepness of groynes on flow characteristics?”

Five sub research questions have been considered.

What are the required capabilities of the software package, and what software package satisfies these requirements?
The software program is chosen in combination with the governing processes. The most critical capabilities of the software package are to process the non-hydrostatic pressure, porosity effects and development of large turbulent structures. In addition, it is proficient to include free surface flow, flexibility in the mesh to create various shapes of the groyne and implementations of a wall function. Fluent and OpenFOAM were shown to be sufficient for the required implementations for modelling flow dynamics around permeable groynes. From a practical perspective, Fluent is used for further modelling.

How capable is the chosen numerical model to represent flow around and through a porous groyne?
The validation of the numerical model is executed by using data sets of three different experimental studies. The validation of the first experimental study is used to identify the best numerical model due to the expectation of the most turbulent flow dynamics around the groyne. Various model settings are evaluated for optimization. The DES turbulence model with the RANS sub-model $k - \omega$ Shear Stress Transport (SST) is chosen for solving the large turbulent structures over the standard RANS $k - \omega$ (SST) due to the isotropic behaviour of the flow around groynes and improved capture of the mean flow velocities near the groyne shown from the sensitivity analysis. In addition, the PISO algorithm is favoured over the SIMPLE algorithm for the pressure-velocity solving method by comparing the mean flow velocities near the groyne using a sensitivity analysis. Finally, this model has been validated for the flow characteristics and the turbulent quantities with sufficient accuracy compared to the experimental data set.

Characteristics of the flexible groyne are steepness and porosity. Hence, both characteristics have been validated in the second and third models of the validation. The same implementations as the first model are used, and both experiments have been modelled and simulated with sufficient accuracy. All models have captured the mean streamwise velocity within 20 % accuracy for RMSE and PBIAS. The most critical flow properties are validated within an RMSE of 30 % and a PBIAS of 25 %. In addition, most peak values are shown to be captured roughly in the same location as observed in the contour plots. In summary, the numerical models generally tend to underestimate the mean flow velocities, overestimate the intensity of the Reynolds shear stresses, and shift the peak areas further downstream. The model can represent open channel flow with a porous structure and capture the most critical aspects of the flow characteristics.

How do permeability and head steepness of groynes affect macro turbulent structures?
Four configurations are identified for simulating flow around a porous, sloped groyne head. Simulating porous groynes shows a reduction in the development of large eddies in the mixing layer compared to impermeable groynes. The eddies near the head of the groyne, vortex shedding, is also observed slightly less than the impermeable groynes. The horseshoe vortex system and the mixing layer are properly shown in both models with a steep slope (model A and B), which is slightly less in the porous groyne. Whereas both models C and D show only the mixing layer. Reynolds shear stresses are mostly observed in the mixing layer, in which the $\overline{u'v'}$ decreases 5 % while reducing the slope from 1:1 to 1:3. Increasing the porosity to 60 % of the groyne, $\overline{u'v'}$ decreases approximately 10 %. The same is shown in the $\overline{u'w'}$, though to a lesser extent. In addition, the peak values of the Reynolds shear stresses are shifted downstream for porous groynes. The downstream shift is because of the appearance of the momentum exchange between the free flow region and the porous structure and the outflow of the porous structure. These processes reduce the mean flow velocity and the velocity gradients close to the groyne. The decrease of the head steepness of the groyne shows a shift for the peak values of Reynolds shear stresses towards the groyne. This is most likely due to the flow that smoothly follows the groyne's geometry.

What are the effects of permeability and head steepness of groynes on bed shear stresses?
The bed shear stresses are directly related to the Reynolds shear stresses, and therefore most maximum values are observed in the mixing layer. The porosity of groynes affects the bed shear stresses significantly. Accordingly, for a porosity of 60 %, a reduction of 5 % for the peak values of the bed shear stresses is observed. For these specific porosity parameters, it is concluded that this affects the bed shear stresses. Decreasing the steepness of the slope from 1:1 to 1:3 without porosity decreases the bed shear stresses minimally. Even when combining both characteristics, a gentle slope and a porous groyne, it is shown that the bed shear stresses are decreased with 10 % compared to steep impermeable groynes. Mainly, the shape size of the bed shear stress area is reduced significantly for both parameters. Eventually, both permeability and head steepness indicate reducing the intensity of the bed shear stresses.

How does the flexible groyne improve flow characteristics compared to a conventional groyne?
The flexible groyne has proven to be of interest for both the mean flow velocities and the turbulent properties in open-channel flow. Compared to the conventional groyne, the flexible groyne reduced the turbulent flow around the groyne, mainly induced by the weakened deflection of the flow, as shown in the re-circulation zone. Consequently, the bed shear stresses are significantly reduced near the groyne. The maximum values of the bed shear stresses are almost similar. However, these maximum values are shifted downstream, especially for the multiple groynes. The results show that both combined characteristics, steep head slope and permeability, affect the flow properties and improve the flow dynamics around groynes regarding the issues with developing scour holes close to the groyne. Hence, the possibility of deformation due to stability failure is less expected.

What are the effects of permeability and head steepness of groynes on flow characteristics?
The numerical model tends to overestimate the Reynolds shear stresses and slightly shifts the areas of the peak values downstream. However, the model is validated for the mean flow velocities and turbulent properties within an acceptable range. The numerical model is used for determining the effects of permeability and head steepness of groynes on flow characteristics.

Beforehand, it was expected that the flow velocities and turbulent properties around groynes should be reduced due to porosity. In addition, it is expected that a decreasing slope reduces the bed shear stresses around the groyne. This research confirms the hypothesises about porous groynes and the steepness of groynes in which an increase of the porosity, or a more gentle slope, reduces the turbulence and mean flow velocities significantly around the groyne. Moreover, an increase in the permeability of the groynes shifts the maximum values for the turbulence and bed shear stresses further downstream than impermeable groynes. Instead, the turbulence and bed shear stresses lead to a slight shift towards the groyne for more gentle slopes.

8.2 Recommendations

Limitations and simplifications of the model

This research is seen as a first approach for modelling a porous, sloped groyne. Hence, limitations are present within the scope of this study. There is always an ongoing debate about the possibilities of a numerical model and which turbulence model is best for the model. Therefore, it is essential to analyze the different possibilities and verify this within the research boundaries. This model is set up by using the manual of Fluent and is based on previous literature. Some improvements are analyzed, however, there are still many possibilities to improve or analyze this numerical model. Hence, the crucial limitations and simplifications are stated, which are recommended to increase the adequacy of the model.

- Comparing more turbulent models for optimizing turbulence modelling
- Further improvement of the model by approaching the simplifications within the numerical model. Such as the approach of the free-surface flow by using the volume of fluid method (VOF), the control parameters and the higher order solution methods
- Increasing the amount of mesh cells and changing the mesh type to increase the accuracy of the solutions

Real case scenarios

Experimental studies are most important for validating the numerical models. The absence of an extensive experimental study is compensated by using multiple data sets from experimental models. However, it is worthwhile to investigate the mean flow properties and turbulent properties around a flexible groyne for validation purposes. In addition, more insight is obtained for both the hydrodynamics and morphology by using an experimental study. Using experimental studies is also essential for conducting the porosity of the structure. Variations in the width of the flexible groyne lead to changing porosities. Therefore, conducting the various porosities from experimental studies is crucial to increase the coherence of approaching the model.

Model simplifications allow for assessing specific aspects of the problem in more detail. However, some details may have an impact on the actual representation of the real case scenarios. One of these aspects is the friction due to the bottom, the wall and the groyne structure. In the model of this thesis, no friction is used, and therefore smooth walls are assumed. In addition, this model applies the standard wall function. Therefore, it is recommended for further studies to specify friction related to river studies and groyne materials, which is shown to affect the flow downstream (Möws & Koll, 2019).

Another interesting aspect is the variation in bed levels over the cross- and length sections. Typically in rivers, the width and depth vary over a particular reach. The model should represent an actual river, and therefore the length scales for the depth and width should be considered. In addition, most rivers have bends along the way downstream, which leads to secondary flow. For strong river bends, this has to be considered in the model.

One of the motives of this research is to prevent sedimentation in the main channel of the river. Normally, groynes reduce the amount of sedimentation in the river. Still, scour holes will occur around the groyne and stability problems or, consequently, additional flow dynamics may occur. Erosion or deposition causes the development of other macro-turbulent structures in the flow dynamics. Hence, different additional flow features may occur around the groyne. A model with both solving the flow dynamics in the open-channel flow and morphology could advance this research in two ways: verifying the locations of the bed shear stresses and improving the research by using a movable bed.

Further research recommendations

Four configurations have been used for varying steepness and porosity of groynes. However, more simulations must be made to gain more insight into the relations between these groyne features and the flow characteristics. Hence, further recommendations are suggested to obtain these relations and understand the flow dynamics around these types of groynes. For gaining information on steepness, it is advised to investigate models for varying steepness from 1:1 to 1:3. To obtain more insight into the flow dynamics for porous groynes, one should aim to model different porosity of groynes between 0 % and 60 %. An important aspect, in this case, is to implement the varying porosity by using some empirical formula, such as considered by Stephenson (1979). Another method is to use experimental models to determine the input settings of the porosity.

At last, spacing within multiple groynes is an intriguing aspect for modelling flow around groynes. The results of this study show that the flow dynamics and bed shear stresses are slightly different for multiple groynes compared with a single groyne simulation. Further studies should show the flow effects of spacing around multiple series of flexible groynes and conventional groynes.

References

Ambagts, L. (2019). *Flow over and around submerged groynes*. Master's thesis, Delft University of Technology.

ANSYS (2019). *ANSYS Fluent User's Guide, 2019R1*. Ansys, Inc.

Ariëns, E. (1993). *Relatie tussen ontgrondingen en steenstabiliteit van de toplaag*. Master's thesis, Delft University of Technology.

Baba, Y., Camenen, B., Peltier, Y., Thollet, F., & Zhang, H. (2010). Flows and bedload dynamics around spur dyke in a compound channel. *11th International Symposium on River Sedimentation (ISRS)*.

Bahrami Yarahmadi, M., Pagliara, S., Yabarehpour, E., & Najafi, N. (2020). Study of Scour and Flow Patterns around Triangular-Shaped Spur Dikes. *KSCE Journal of Civil Engineering*, *24*.

Banerjee, A., Pasupuleti, S., Pradeep Kumar, G. N., & Chandra Dutta, S. (2018). A Three-Dimensional CFD Simulation for the Nonlinear Parallel Flow Phenomena Through Coarse Granular Porous Media. In M. Singh, B. Kushvah, G. Seth, & J. Prakash (Eds.) *Applications of Fluid Dynamics*, (pp. 469–480). Springer Singapore.

Biron, P. M., Robson, C., Lapointe, M. F., & Gaskin, S. J. (2004). Comparing different methods of bed shear stress estimates in simple and complex flow fields. *Earth Surface Processes and Landforms*, *29*(11), 1403–1415.

Bradbury, A. P., Crossman, M. P., Allsop, N. W. H., Segura-Dominguez, S., & Simm, J. D. (2003). Economical rock groynes - reducing lifecycle costs. In *Coastal Structures 2003*, (pp. 975–987).

Chang, C.-K., Lu, J.-Y., Lu, S.-Y., Wang, Z.-X., & Shih, D.-S. (2020). Experimental and numerical investigations of turbulent open channel flow over a rough scour hole downstream of a groundsill. *Water*, *12*, 1488.

Choufu, L., Abbasi, S., Pourshahbaz, H., Taghvaei, P., & Tfwala, S. (2019). Investigation of Flow, Erosion, and Sedimentation Pattern around Varied Groynes under Different Hydraulic and Geometric Conditions: A Numerical Study. *Water*, *11*(2).

Chrisohoides, A., Sotiropoulos, F., & Sturm, T. W. (2003). Coherent Structures in Flat-Bed Abutment Flow: Computational Fluid Dynamics Simulations and Experiments. *Journal of Hydraulic Engineering*, *129*(3), 177–186.

de Vriend, H., Havinga, H., van Prooijen, B., Visser, P., & Wang, Z. (2011). River Engineering. TU Delft, Department Hydraulic Engineering.

Delft3D (2021). *Delft3D Flexible Mesh Suite*. Deltares.
URL `https://www.deltares.nl/en/software/delft3d-flexible-mesh-suite/`

Dombroski, D. E., & Crimaldi, J. P. (2007). The accuracy of acoustic Doppler velocimetry measurements in turbulent boundary layer flows over a smooth bed. *Limnology and Oceanography: Methods*, *5*(1), 23–33.
URL https://aslopubs.onlinelibrary.wiley.com/doi/abs/10.4319/lom.2007.5.23

Dong, Y., Yan, Y., & Liu, C. (2016). New visualization method for vortex structure in turbulence by lambda2 and vortex filaments. *Applied Mathematical Modelling*, *40*(1), 500–509.

Duan, J. G. (2009). Mean flow and turbulence around a laboratory spur dike. *Journal of Hydraulic Engineering*, *135*(10), 803–811.

Ettema, R., & Muste, M. (2004). Scale Effects in Flume Experiments on Flow around a Spur Dike in Flatbed Channel. *Journal of Hydraulic Engineering*, *130*(7), 635–646.

Finel (2012). *Finel3D*. Svasek Hydraulics.
URL https://www.svasek.nl/en/model-research/finel/

Flow Science, I. (2019). *FLOW-3D, Version 12.0*. Santa Fe, NM.
URL https://www.flow3d.com/

Ghaldarbandi, R., Keshavarz, M. K., & Hakimzadeh, H. (2013). Investigation of the Bed and Structural Slopes on Bed Shear Stress and Flow Characteristics around an Impermeable Groyne. *Journal of Hydraulic Structures*, *1*(1), 11–23.

Giri, S., Shimizu, Y., & Surajate, B. (2004). Laboratory measurement and numerical simulation of flow and turbulence in a meandering-like flume with spurs. *Flow Measurement and Instrumentation*, *15*(5), 301–309.

Han, X., & Lin, P. (2013). Permeability effects of single groin on flow characteristics. *Journal of Hydraulic Research*, *51*(1), 102–102.

Havinga, H. (2020). Towards Sustainable River Management of the Dutch Rhine River. *Water*, *12*(6).

Herrera-Granados, O. (2018). Turbulence Flow Modeling of One-Sharp-Groyne Field. In M. B. Kalinowska, M. M. Mrokowska, & P. M. Rowiński (Eds.) *Free Surface Flows and Transport Processes*, (pp. 207–218). Cham: Springer International Publishing.

Higham, J., Brevis, W., Keylock, C., & Safarzadeh, A. (2017). Using modal decompositions to explain the sudden expansion of the mixing layer in the wake of a groyne in a shallow flow. *Advances in Water Resources*, *107*, 451–459.

Ho, J., Yeo, H., Coonrod, J., & Ahn, W.-S. (2007). Numerical modeling study for flow pattern changes induced by single groyne. Has not been published.

Hoffmans, G., & Verheij, H. (1997). *Scour Manual*. A.A. Balkema.

Holtz, K. (1991). Numerical simulation of recirculating flow at groynes. *Computer Methods in Water Resources*, *2*(2), 463–477.

Iqbal, S., Pasha, G. A., Ghani, U., Ullah, M. K., & Ahmed, A. (2021). Flow Dynamics Around Permeable Spur Dike in a Rectangular Channel. *Arabian Journal for Science and Engineering*.

Jagers, H., & Schijndel, S. (2000). 3D rekenen rondom constructies: Rapportage 2000. *Hydraulic Engineering Reports*.

Jansen, P. P., van Bendegom, L., van den Berg, J., de Vries, M., & Zanen, A. (1979). *Principles of river engineering: The non-tidal alluvial river (republished by VSSD Delft, 1994)*. Delftse Uitgevers Maatschappij.

Jeon, J., Lee, J. Y., & Kang, S. (2018). Experimental Investigation of Three-Dimensional Flow Structure and Turbulent Flow Mechanisms Around a Nonsubmerged Spur Dike With a Low Length-to-Depth Ratio. *Water Resources Research*, *54*(5), 3530–3556.

Jin, Y., & Kuznetsov, A. V. (2017). Turbulence modeling for flows in wall bounded porous media: An analysis based on direct numerical simulations. *Physics of Fluids*, *29*(4), 045102.

Kandasamy, J., & Melville, B. (1998). Maximum local scour depth at bridge piers and abutments. *Journal of Hydraulic Research*, *36*(2), 183–198.

Kang, J., Yeo, H., Kim, S., & Ji, U. (2011a). Experimental investigation on the local scour characteristics around groynes using a hydraulic model. *Water and Environment Journal*, *25*(2), 181–191.

Kang, J., Yeo, H., Kim, S., & Ji, U. (2011b). Permeability effects of single groin on flow characteristics. *Journal of Hydraulic Research*, *49*(6), 728–735.

Kang, S., Khosronejad, A., & Yang, X. (2021). Turbulent flow characteristics around a non-submerged rectangular obstacle on the side of an open channel. *Physics of Fluids*, *33*(4), 045106.

Kang, S., & Sotiropoulos, F. (2012). Assessing the predictive capabilities of isotropic, eddy viscosity Reynolds-averaged turbulence models in a natural-like meandering channel. *Water Resources Research*, *48*(6).
URL https://agupubs.onlinelibrary.wiley.com/doi/abs/10.1029/2011WR011375

Katopodes, N. D. (2019). Free-Surface Flow: Shallow Water Dynamics. In N. D. Katopodes (Ed.) *Free-Surface Flow:*. Butterworth-Heinemann.

Khosronejad, A., Arabi, M. G., Angelidis, D., Bagherizadeh, E., Flora, K., & Farhadzadeh, A. (2019). Comparative Hydrodynamic Study of Rigid-Lid and Level-Set Methods for LES of Open-Channel Flow. *Journal of Hydraulic Engineering*, *145*(1), 04018077.

Koken, M., & Constantinescu, G. (2008). An investigation of the flow and scour mechanisms around isolated spur dikes in a shallow open channel: 1. Conditions corresponding to the initiation of the erosion and deposition process. *Water Resources Research - WATER RESOUR RES*, *44*.

Koken, M., & Constantinescu, G. (2009). An investigation of the dynamics of coherent structures in a turbulent channel flow with a vertical sidewall obstruction. *Physics of Fluids*, *21*(8), 085104.

Koken, M., & Constantinescu, G. (2011). Flow and turbulence structure around a spur dike in a channel with a large scour hole. *Water Resources Research*, *47*(12).

Koken, M., & Constantinescu, G. (2014). Flow and Turbulence Structure around Abutments with Sloped Sidewalls. *Journal of Hydraulic Engineering*, *140*(7), 04014031.

Kumar, M., & Malik, A. (2016). 3D Simulation of Flow around Different Types of Groyne Using ANSYS Fluent. *Imperial journal of interdisciplinary research*, *2*.

Leu, J., Chan, H., & Chu, M. (2008). Comparison of turbulent flow over solid and porous structures mounted on the bottom of a rectangular channel. *Flow Measurement and Instrumentation*, *19*(6), 331–337.

Mansoori, A. R. (2014). *Study on Flow and Sediment Transport around Series of Spur Dikes with Different Head Shape*. Ph.D. thesis, Kyoto University.

McCoy, A., Constantinescu, G., & Weber, L. J. (2008). Numerical Investigation of Flow Hydrodynamics in a Channel with a Series of Groynes. *Journal of Hydraulic Engineering*, *134*(2), 157–172.

Mehraein, M., Ghodsian, M., mashizi, m., & Vaghefi, M. (2017). Experimental Study on Flow Pattern and Scour Hole Dimensions Around a T-Shaped Spur Dike in a Channel Bend Under Emerged and Submerged Conditions. *International Journal of Civil Engineering*, *15*.

Melville, B. W. (1992). Local Scour at Bridge Abutments. *Journal of Hydraulic Engineering*, *118*(4), 615–631.

Mike3 (2017). *Mike 3*. DHI.
URL `https://manuals.mikepoweredbydhi.help/2017/MIKE_3.htm`

Mioduszewski, T., & Maeno, S. (2005). Three dimensional analysis of flow around a porous spur dike. *Journal of applied mechanics*, *8*, 793–801.

Mohammadpour, R., Ab. Ghani, A., & Azamathulla, H. (2013). Numerical modeling of 3-D flow on porous broad crested weirs. *Applied Mathematical Modelling*, *37*(22), 9324–9337.

Muneta, N., & Shmizu, Y. (1993). Study of flows around spur-dikes. *International Conference on Environmentally sound water resources utilization*, *8*.

Muraoka, H., Fushimi, T., Kadota, A., & Suzuki, K. (2009). Experimental Study on Changes of Bed Configuration Caused by a Permeable Groyne of Stone Gabion. In *Advances in Water Resources and Hydraulic Engineering*, (pp. 1072–1077). Berlin, Heidelberg: Springer Berlin Heidelberg.

Möws, R., & Koll, K. (2019). Roughness effect of submerged groyne fields with varying length, groyne distance, and groyne types. *Water*, *11*, 1253.

Nakagawa, H., Zhang, H., Ishigaki, T., & Muto, Y. (2004). Prediction of 3D flow field with non-linear k-ε model based on unstructured mesh. *Journal of applied mechanics*, *7*, 1077–1088.

OpenFOAM (2021). *OpenFOAM Technical Documentation*. The OpenFOAM Foundation Ltd.
URL `https://openfoam.org/`

Ouillon, S., & Denis, D. (1997). Three-Dimensional Computation of Flow around Groyne. *Journal of Hydraulic Engineering*, *123*, 962–970.

Paik, J., Bombardelli, F., & Lee, N. J. (2014). Numerical Simulation of Turbulent Free Surface Flow Around a Circular Cylinder. In *ICHE 2014. 11th International Conference on Hydroscience & Engineering*, vol. ICHE 2014 - 11th International Conference on Hydroscience & Engineering.

Paik, J., & Sotiropoulos, F. (2005). Coherent structure dynamics upstream of a long rectangular block at the side of a large aspect ratio channel. *Physics of Fluids*, *17*(11), 115104.

Perry, A. E., & Chong, M. S. (1982). On the mechanism of wall turbulence. *Journal of Fluid Mechanics*, *119*, 173–217.

Prinos, P., Sofialidis, D., & Keramaris, E. (2003). Turbulent Flow Over and Within a Porous Bed. *Journal of Hydraulic Engineering*, *129*(9), 720–733.

Przedwojski, B., Błażejewski, R., & Pilarczyk, K. (1995). *River training techniques: fundamentals, design and applications.*. A.A. Balkema.

Rajaratnam, N., & Nwachukwu, B. A. (1983). Flow Near Groin-Like Structures. *Journal of Hydraulic Engineering*, *109*(3), 463–480.

Raudkivi, A. J. (1996). Permeable Pile Groins . *Journal of Waterway, Port, Coastal, and Ocean Engineering*, *122*(6), 267–272.

Rodi, W. (1997). Comparison of les and rans calculations of the flow around bluff bodies. *Journal of Wind Engineering and Industrial Aerodynamics*, *69-71*, 55–75. Proceedings of the 3rd International Colloqium on Bluff Body Aerodynamics and Applications.
URL https://www.sciencedirect.com/science/article/pii/S0167610597001475

Rodi, W. (2017). Turbulence Modeling and Simulation in Hydraulics: A Historical Review. *Journal of Hydraulic Engineering*, *143*(5), 03117001.

Roulund, A., Sumer, B. M., FredsØe, J., & Michelsen, J. (2005). Numerical and experimental investigation of flow and scour around a circular pile, volume=534. *Journal of Fluid Mechanics*.

Saberi, O., & Galoie, M. (2017). Numerical Modeling of Flow Around Groynes with Different Shapes Using TELEMAC-3D Software. *American Journal of Water Science and Engineering*, *2*, 43–52.

Schlichting, H., & Gersten, K. (2017). *Boundary-Layer Theory*. Springer, 9th ed.

Shamloo, H., & Pirzadeh, B. (2014). Numerical Simulation of the Angle of Groyne. *Journal of River Engineering*, *2*.

Shampa, Hasegawa, Y., Nakagawa, H., Takebayashi, H., & Kawaike, K. (2020). Three-Dimensional Flow Characteristics in Slit-Type Permeable Spur Dike Fields: Efficacy in Riverbank Protection. *Water*, *12*(4).

Spalart, P. (2000). Strategies for turbulence modelling and simulations. *International Journal of Heat and Fluid Flow*, *21*(3), 252–263.

SSRS (2020). Self supporting river system. https://www.ssrs.info/over-ssrs/. Accessed: 2020-12-02.

Stephenson, D. (1979). Chapter 2 - flow through rockfill. In *Rockfill in Hydraulic Engineering*, vol. 27 of *Developments in Geotechnical Engineering*, (pp. 19–37). Elsevier.

Talstra, H. (2011). *Large-scale turbulence structures in shallow separating flows*. Ph.D. thesis, Delft University of Technology.

Telemac-3D (2020). *Telemac-3D, Version v8p2*. Laboratoire National d'Hydraulique et Environment.
URL http://www.opentelemac.org/

Trampenau, T., Oumeraci, H., & Dette, H. H. (2004). Hydraulic Functioning of Permeable Pile Groins. *Journal of Coastal Research*, (pp. 160–187).

Tritthart, M., Liedermann, M., & Habersack, H. (2009). Modelling spatio-temporal flow characteristics in groyne fields. *River Research and Applications*, *25*(1), 62–81.

Uijttewaal, W. (2005). Effects of Groyne Layout on the Flow in Groyne Fields: Laboratory Experiments. *Journal of Hydraulic Engineering*, *131*(9), 782–791.

Uijttewaal, W., Lehmann, D., & van Mazijk, A. (2001). Exchange processes between a river and its groyne fields: Model experiments. *Journal of Hydraulic Engineering*, *127*(11), 928–936.

Uijttewaal, W., & Tukker, J. (1998). Development of quasi two-dimensional structures in a shallow free-surface mixing layer. *Experiments in Fluids*, *24*(3), 192–200.

van der Wal M. (2020). Bank Protection Structures along the Brahmaputra-Jamuna River, a Study of Flow Slides. *Water*, *20*.

Weitbrecht, V., & Jirka, G. (2001). Flow patterns in dead zones of rivers and their effect on exchange processes. In *2001 International Symposium on Environmental Hydraulics*.

Weitbrecht, V., Socolofsky, S. A., & Jirka, G. H. (2008). Experiments on Mass Exchange between Groin Fields and Main Stream in Rivers. *Journal of Hydraulic Engineering*, *134*(2), 173–183.

Wetser, A. (2016). Flexibele krib - technisch rapport. Tech. rep., Delft University of Technology and BAM Infraconsult.

Wilcox, D. (2006). *Turbulence Modeling for CFD*. No. v. 1 in Turbulence Modeling for CFD. DCW Industries.

Yazdi, J., Sarkardeh, H., Azamathulla, H. M., & Ghani, A. A. (2010). 3D simulation of flow around a single spur dike with free-surface flow. *International Journal of River Basin Management*, *8*(1), 55–62.

Yeo, H., Kang, J., & Kim, S. (2005). An experimental study on tip velocity and downstream recirculation zone of single groynes of permeability change. *Ksce Journal of Civil Engineering - KSCE J CIV ENG*, *9*, 29–38.

Yossef, M. F. M. (2002). The Effect of Groynes on Rivers: Literature review. Delft Cluster.

Yossef, M. F. M., & de Vriend, H. J. (2011). Flow Details near River Groynes: Experimental Investigation. *Journal of Hydraulic Engineering*, *137*(5), 504–516.

Yousefi, A., & Hosseini, S. (2019). Development and Comparison of Two New Methods for Quantifying Uncertainty in Analysis of Flow Through Rockfill Structures. *Iranian Journal of Science and Technology - Transactions of Civil Engineering*, *43*, 277–288.

Zhang, H., & Nakagawa, H. (2008). Scour around Spur Dyke: Recent Advances and Future Researches. *Ann Disaster Prevent Res Inst Kyoto Univ*, *51*.

Zhang, H., Nakagawa, H., Ishigaki, T., & Muto, Y. (2005). Prediction of 3D flow field and local scouring around spur dykes. *Proceedings of Hydraulic Engineering*, *49*, 1003–1008.

Zhang, R. (2020). *Hydraulic functioning of permeable pile groins*. Ph.D. thesis, Delft University of Technology.

A Input numerical model

A.1 Solving methods

Discretization of the Momentum Equation

The momentum equation solves the velocity quantity using the finite-volume method prior to knowing the pressure field and mass fluxes. However, the pressure field and mass fluxes are not known and therefore part of obtaining the solution. ANSYS Fluent uses a co-located scheme where both velocities as pressures are stored in the centre of the cell. Nevertheless, the discretization of the momentum equation requires the pressure quantity at the face of the cell. Hence, an interpolation scheme is used for defining the pressure at the face of a cell.

Various schemes can be used for the interpolation scheme in a pressure-based solver. By default, the second-order approach is used. However, when simulating mixtures or volume of fluid multi-phases (VOF), the **PRESTO!** is the default option, and **Body Force Weighted** is the second option. The **PRESTO!** gives normally more accurate results for high swirling flow, but will computationally cost significantly compared to the **Body Force Weighted**. In this model, the **PRESTO!** is preferred due to the accuracy.

Discretization of the Continuity Equation

The continuity equation solves the mass flux quantity using the finite-volume method prior to knowing the pressure field and velocities. The discretization of the continuity equation uses face values of the mass flux, and therefore, the velocity has to be defined at the face. The stored velocity values in the centre have to be interpolated to the face of the cell using weighting factors, which can be changed in the controls menu. The flux density has to be defined and uses a density interpolation scheme for solving this issue. For multi-phase VOF models, default approach is the arithmetic averaging for in-compressible phases.

Pressure-Velocity Coupling

When solving the discretizations of the momentum and continuity equations, the pressures and velocities are updated. The pressure-based solver uses a pressure-velocity coupling scheme for controlling the manner of updating the pressure and velocity. The pressure-velocity coupling scheme can either be executed by using a segregated system or a coupled system. By default, the **SIMPLE** algorithm is applied and usually is used when executing resolved eddy simulations for the turbulence closure models. **PISO** is another option, which in most scenarios, is a great possibility to use. However, compared to the **SIMPLE** algorithm, the **PISO** algorithm is much more expensive in the computational aspect. Most numerical modelling for flow around groynes uses the **SIMPLE** algorithm and has found great accuracy compared with the experimental studies.

Still, the various solver method options have been considered to increase the solution. Therefore, a sensitivity analysis is used to determine the proper solver method. In specifics, simplified models are made for the SIMPLE algorithm and PISO algorithm to verify which model simulates the model more accurate.

Time-Advancement Algorithm

The pressure-based solver uses for the temporal discretization a transient derivative and an implicit discretization of the transport equation. The amount of accuracy of the solution is dependant on the chosen scheme. Accordingly, second-order schemes are used for accuracy purposes of the solution. When deriving transient flow, any independent variable will be discretized, such as the volume fraction, turbulent kinetic energy and dissipation rate.

So in summary, the solver methods and variables used in the models are defined as shown in figure Fig. A.1

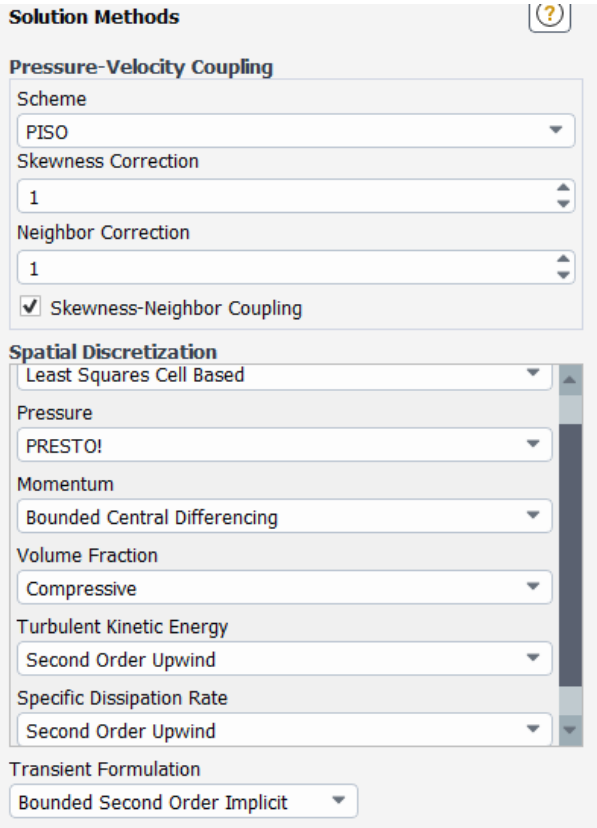

Figure A.1: Summary of the input settings for the solver method in ANSYS Fluent

A.2 Set-up of initial model

A.2.1 Initializing

Multiple options are possible for initializing the model. The default initializing results in velocities at the boundaries, although the model has no initial conditions through the domain. Therefore, using the default initializing, the water level and velocities through the domain must be defined. By using the hybrid initializing, the whole domain is automatically initialized. This option is preferable in which errors are possible avoided and the spin-up time is decreased to a minimum. Furthermore, the amount of water in the system has to be patched up to and including the water level.

A.2.2 Calculation set-up

For the calculation set-up, the system's stability is managed, which depends on the schemes and the meshing properties. In the calculation set-up, settings are adjusted to increase the stability of the system and, therefore, a smooth simulation of the model. This model mainly focuses on the time step and iterations. Total simulation time and data sampling can be specified, though this is dependant on the preferable results for the specific model.

The time step is dependant on the Courant number and, accordingly, dependant on the mesh quality. As stated before in Section 4.1.1, in the domain of the model, greater values of 20 for the Courant number is not preferable for a stable system. The Courant number can be verified by calculating the Courant numbers manually by using equation Eq. (4.1) or solving the solution for some time steps and showing the results in the whole domain. However, there is an option available in which the Courant number is adjusted to one specific value. In this way, the model adjusts the time step to the specified Courant number. This time step method is used in every numerical model with a initial Courant number of 10.

For the implicit formulation of solving the time-dependent equations, iterations must converge the solution for each time step. Iterations around 5 - 10 per time step are preferable in ANSYS Fluent for an implicit formulation. Therefore, a maximum iterations per time step is set as 20 to create enough space to converge to the solution without drawbacks from iterating.

B Calculating approaches for flow properties

B.1 Reynolds stresses

As stated before in Section 2.3.2 and Section 3.2.2, the Navier-Stokes equation describes the motion of a fluid. By using time-averaging, the turbulent quantities become more measurable and adaptable for calculating the equations. This method is also called Reynolds decomposition, in which the velocity property is split between a fluctuation quantity and time-averaged quantity. However, due to this process, an appearance of the correlation between the time-averaged quantity and fluctuation quantity occurs. These correlations are known as the Reynolds stresses, a time-averaged rate of the momentum transfer by the turbulence. This Reynolds stress can be split into two components, each in x,y and z directions, also known as the normal Reynolds stresses and shear Reynolds stresses. So in order to compute the mean-flow properties of the turbulent flow, a prescription is required of these stresses. The complexity of computing the Reynolds stresses is a fundamental problem within the turbulent flow Wilcox (2006).

A first approach for the Reynolds stresses is by investigating the fluctuations of the time-averaged quantities and define these stresses. However, this method is complicated due to the extensive measurements of the flow. For numerical studies, this method requires enormous computational resources to observe every fluctuation.

Another approach is the use of the Boussinesq approach, in which the Reynolds stresses are assumed to be a value directly calculated from the flow characteristics and properties. In other words, the Boussinesq assumption follows that the turbulent stresses are related to the mean velocity gradients, whereas the viscous stresses are related to the complete velocity gradients. Therefore, this assumption is based on neglecting the variation of the density of the flow with exception of the buoyancy term. This approach is suitable when density variations are due to thermal rather than pressure changes. Hence, water is a great example for using this approach.

B.2 Bed shear stresses

Shear stress is a measure of the force from a fluid acting on a mass body or obstacle. In open channel flow, a direct relation is found between the erosion on the bank or bed and the water's shear stresses. Bed shear stresses greater than the gravitational force of the distinct bed sediment exhibits the movement of the sediment. Shear velocity is commonly used to estimate these shear stresses. Hence, bed shear stresses and shear velocities are fundamental variables in river studies to quantify the sediment transport.

The general approach to calculate the average bed shear stress is as follows:

$$\tau_0 = \rho g R S_f \tag{B.1}$$

where ρ is the density of the fluid, g is the gravitational acceleration R is the hydraulic radius and S_f is the energy slope or water level slope. This method is not appropriate to use for small-scale estimations of the bed shear stress, in which small variations due to local velocity variations are not taken into account. Therefore, a more fitted function is used which follows the velocity distribution close to the wall, also known as the logarithmic law distribution (Schlichting & Gersten, 2017):

$$\frac{u}{u_*} = \frac{1}{k} ln(\frac{z_a}{z_0}) \tag{B.2}$$

where u is the velocity, u_* is the friction velocity ($= \sqrt{\frac{\tau_0}{\rho}}$), z_a is the height above the bed, k is von Karman's constant, and z_0 is a statistical roughness length. With complex flow near the wall, the velocity profile may not be logarithmic and thus this equation is not appropriate. Therefore, when turbulence measurements are available, bed shear stresses can be calculated using the velocity fluctuations in the form of Reynolds stresses:

$$\tau_0 = -\rho\overline{u'v'} \tag{B.3}$$

where ρ is noted as the density and u' v' are the velocity fluctuations in the streamwise and transverse direction. The $\overline{\ }$ denotes an average component.

C Validation approach

Sensitivity analysis for the square groyne

Remaining results of the sensitivity analysis for the square groyne:

Comparison between turbulence models

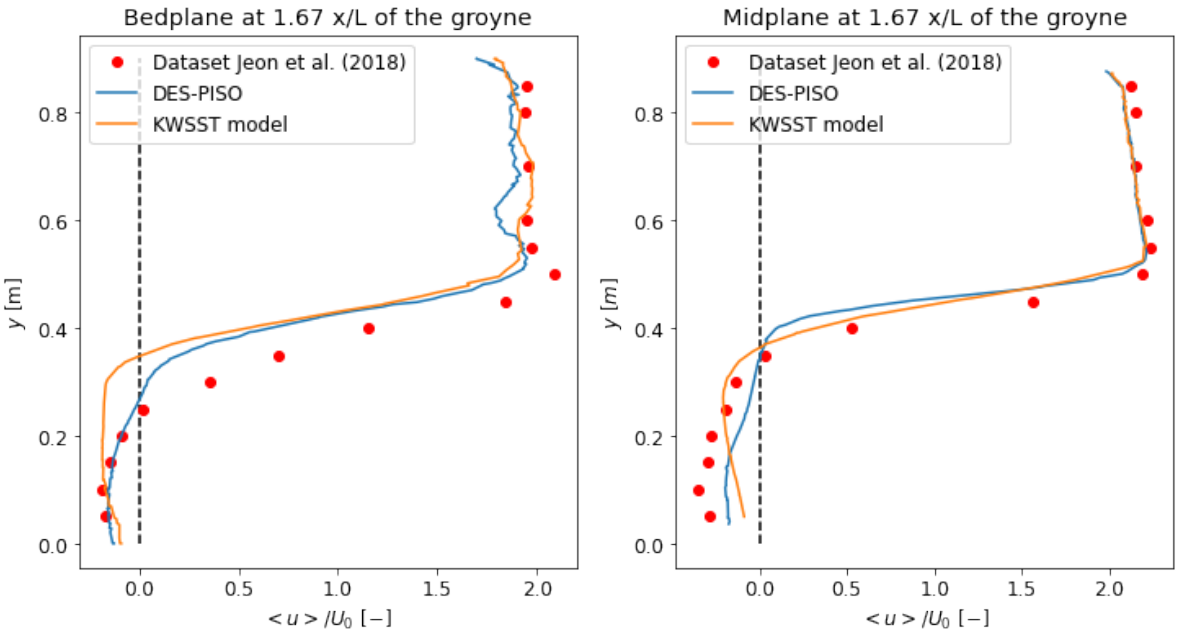

Figure C.1: Comparison DES model with the KW-SST model for the x-velocity

Comparison between curvature correction options

Solver algorithm

Grid dependency for the triangular groyne

Grid dependency test

Remaining results of the grid dependency test for the triangular groyne:

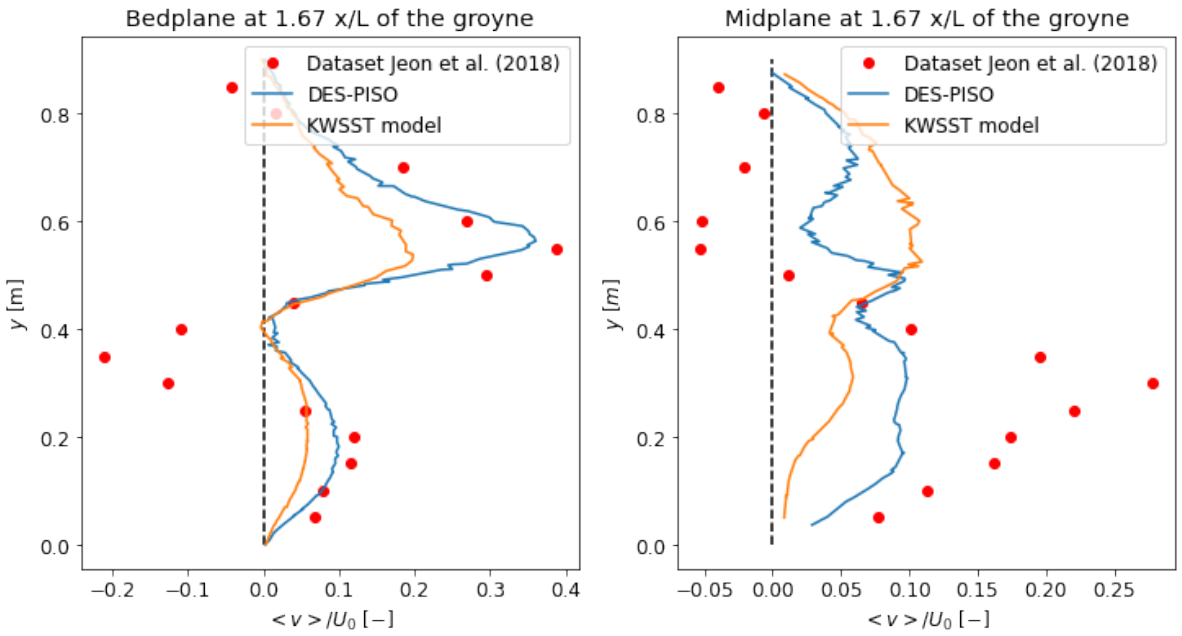

Figure C.2: Comparison DES model with the KW-SST model for the y-velocity

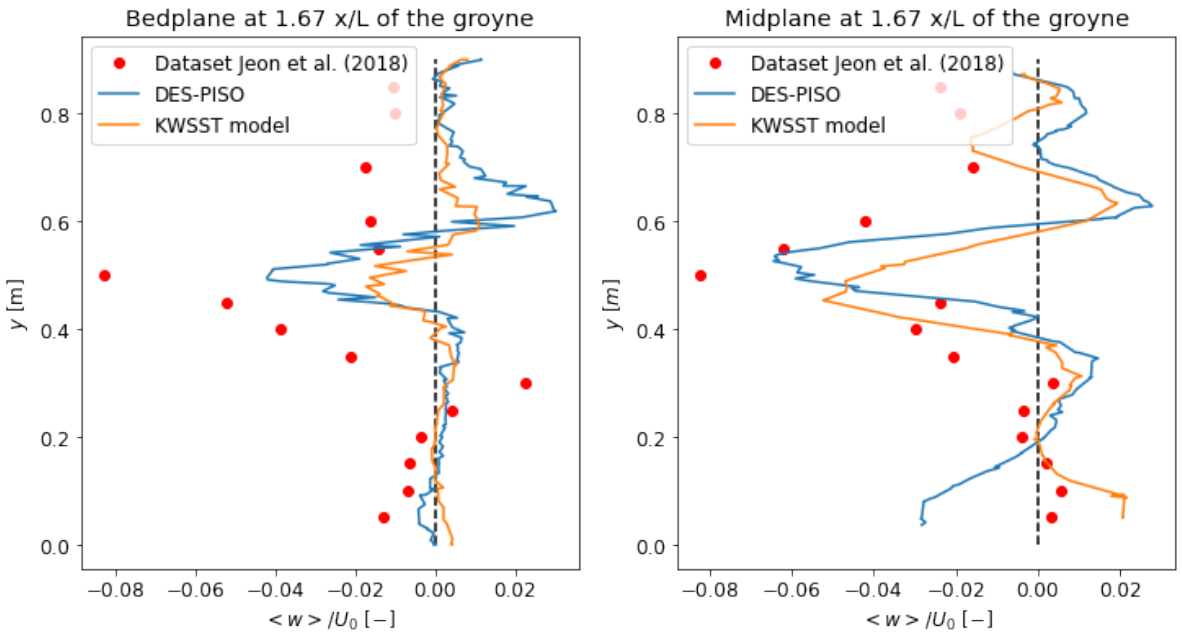

Figure C.3: Comparison DES model with the KW-SST model for the z-velocity

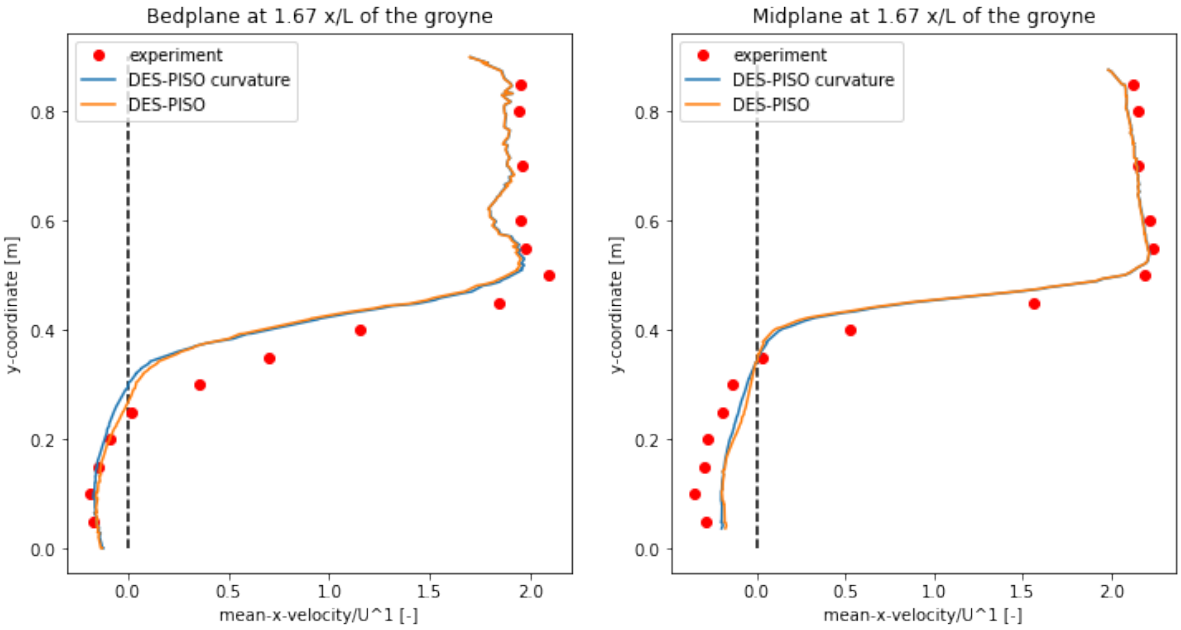

Figure C.4: Comparison DES model with and without curvature correction for the x-velocity

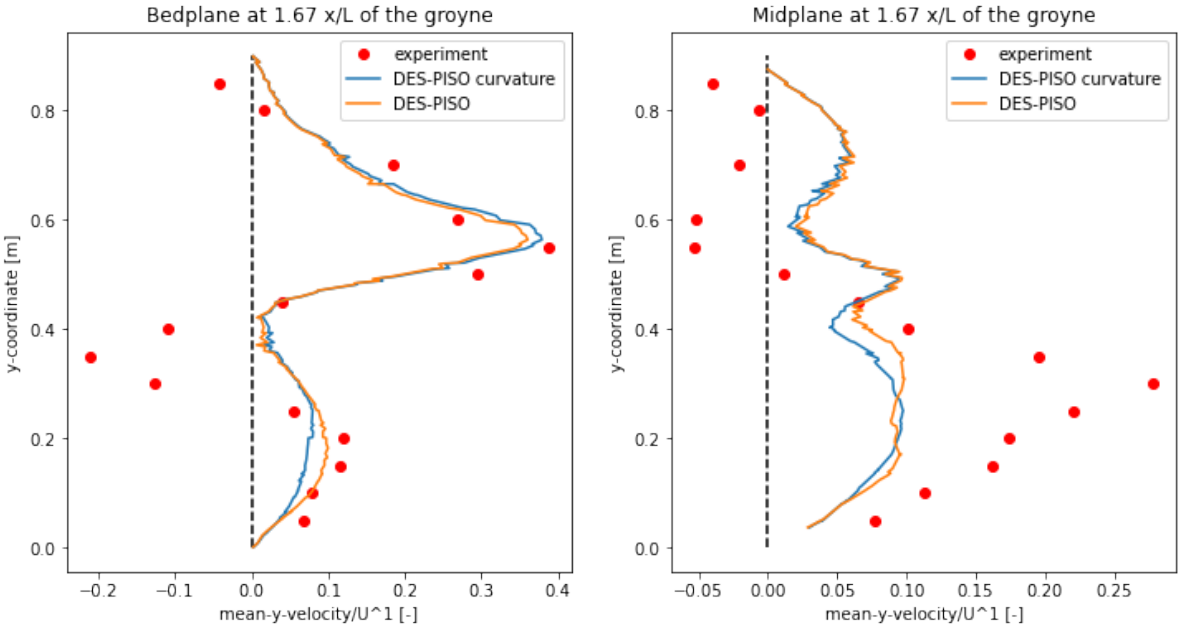

Figure C.5: Comparison DES model with and without curvature correction for the y-velocity

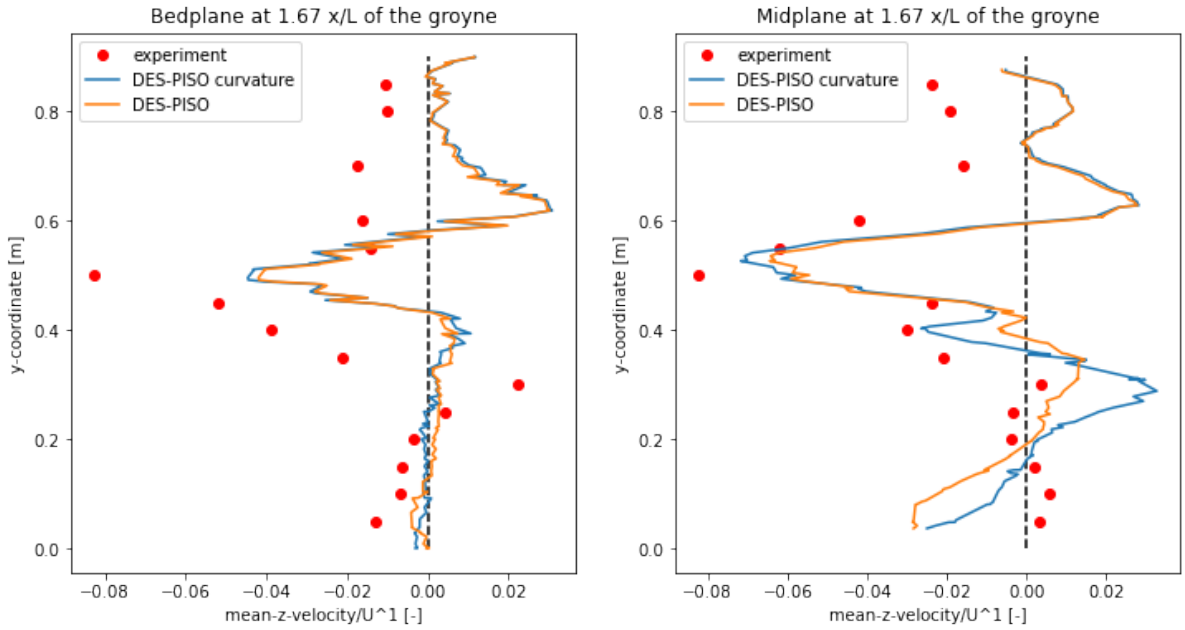

Figure C.6: Comparison DES model with and without curvature correction for the z-velocity

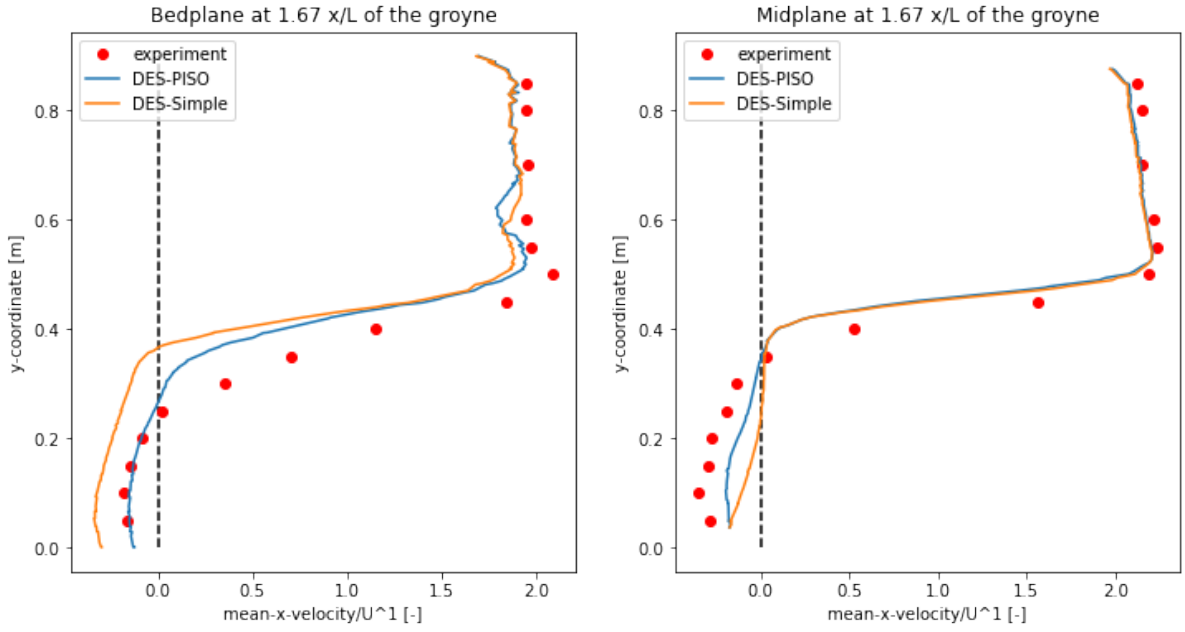

Figure C.7: Comparison solver method PISO algorithm and SIMPLE algorithm for the x-velocity

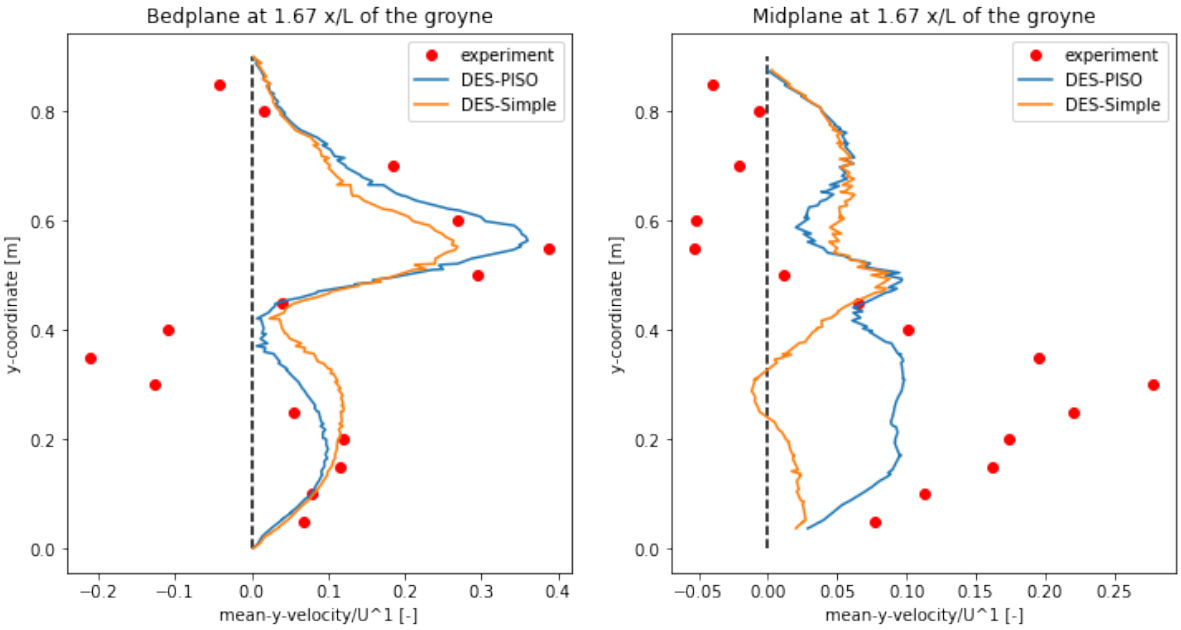

Figure C.8: Comparison solver method PISO algorithm and SIMPLE algorithm for the y-velocity

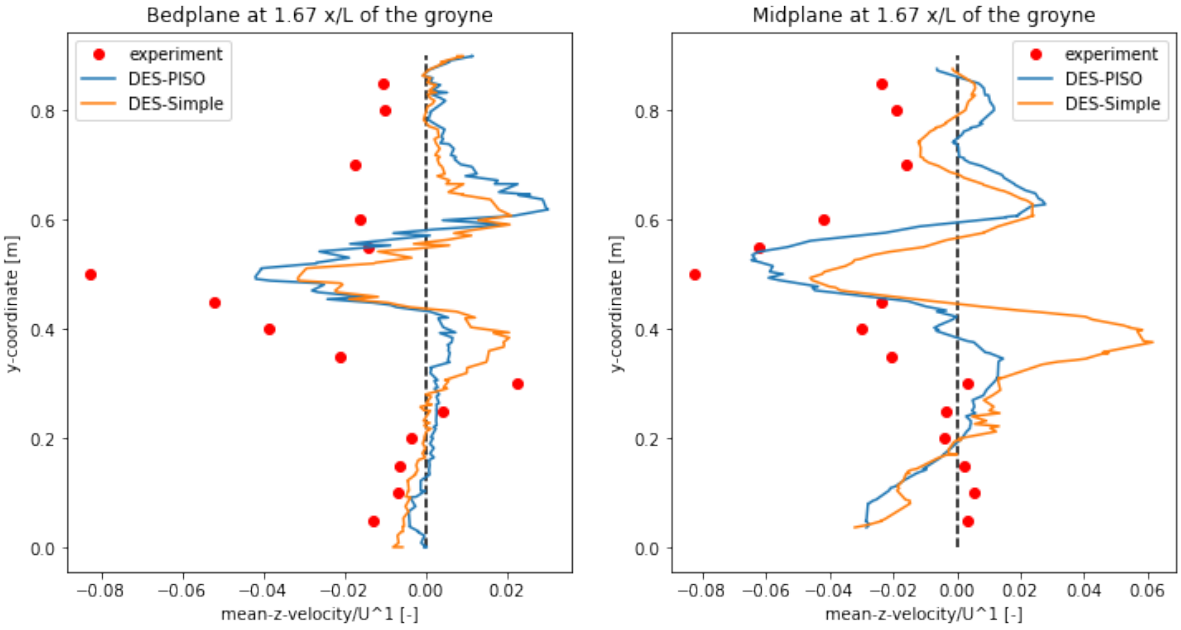

Figure C.9: Comparison solver method PISO algorithm and SIMPLE algorithm for the z-velocity

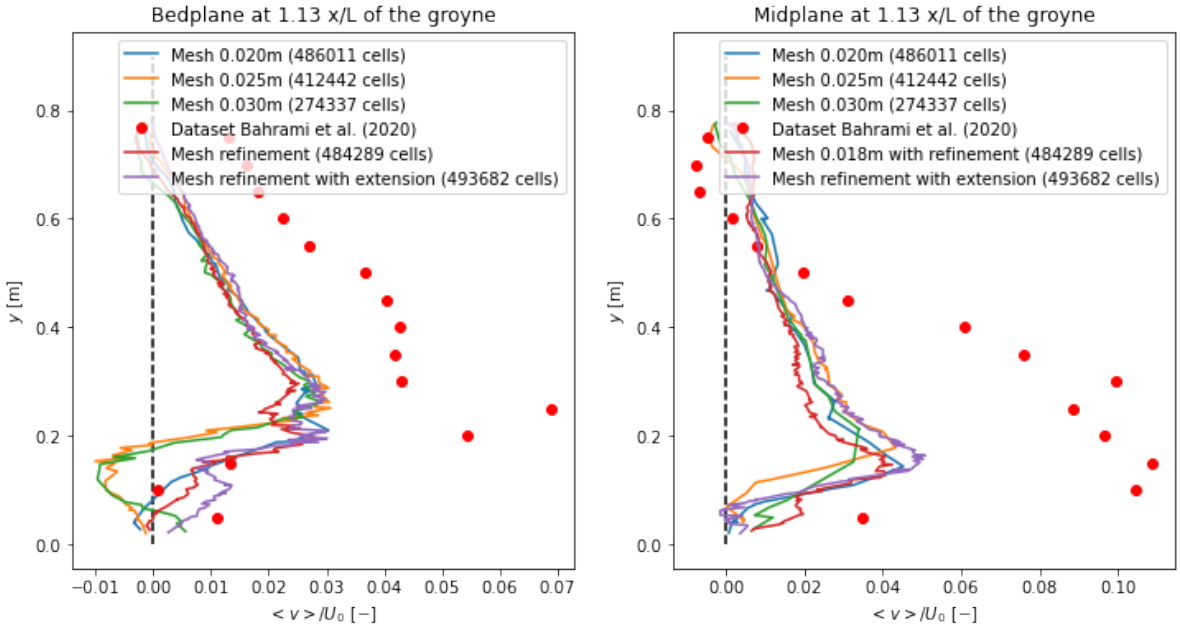

Figure C.10: Grid dependency test for the mean-y-velocity for a time simulation of 60 s at 113 x/L

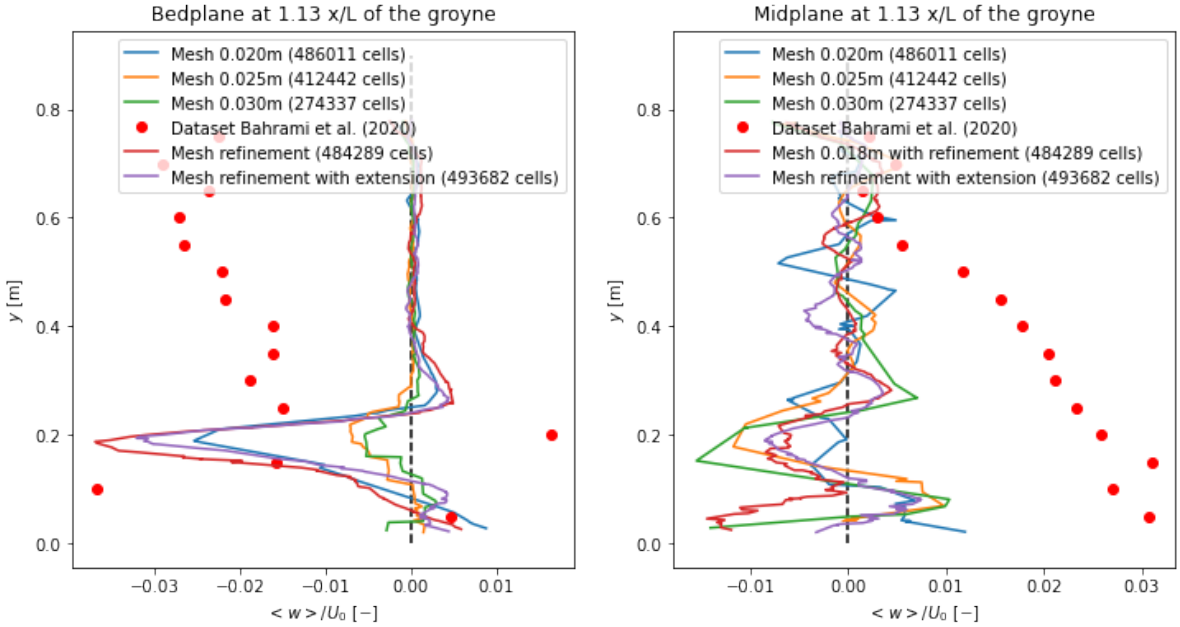

Figure C.11: Grid dependency test for the mean-z-velocity for a time simulation of 60 s at 113 x/L

D Validation results

D.1 Square groyne

Remaining results from the numerical model of the squared groyne are shown in this section.

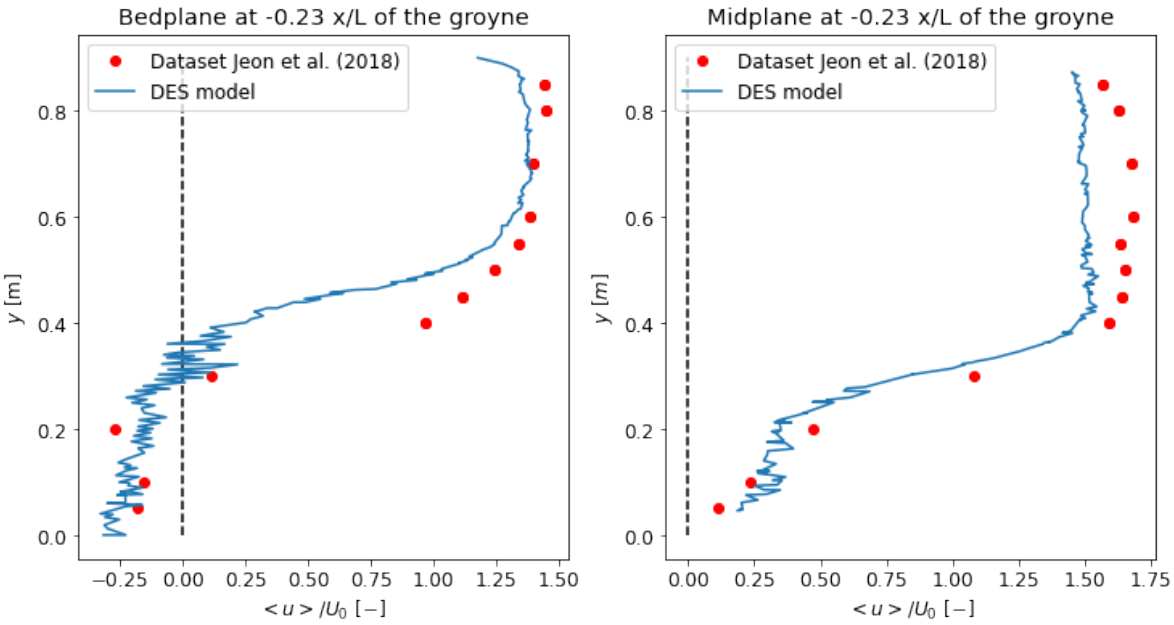

Figure D.1: mean-x-velocity for $-0.23\ x/L$, upstream of the groyne

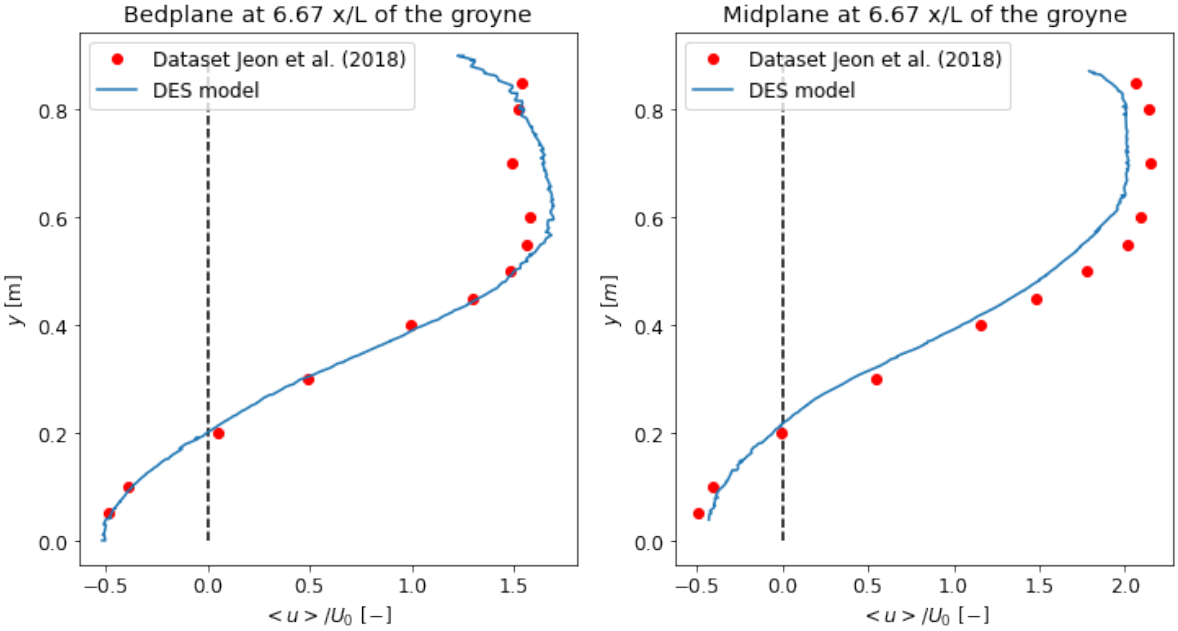

Figure D.2: mean-x-velocity for $6.67\ x/L$, downstream of the groyne

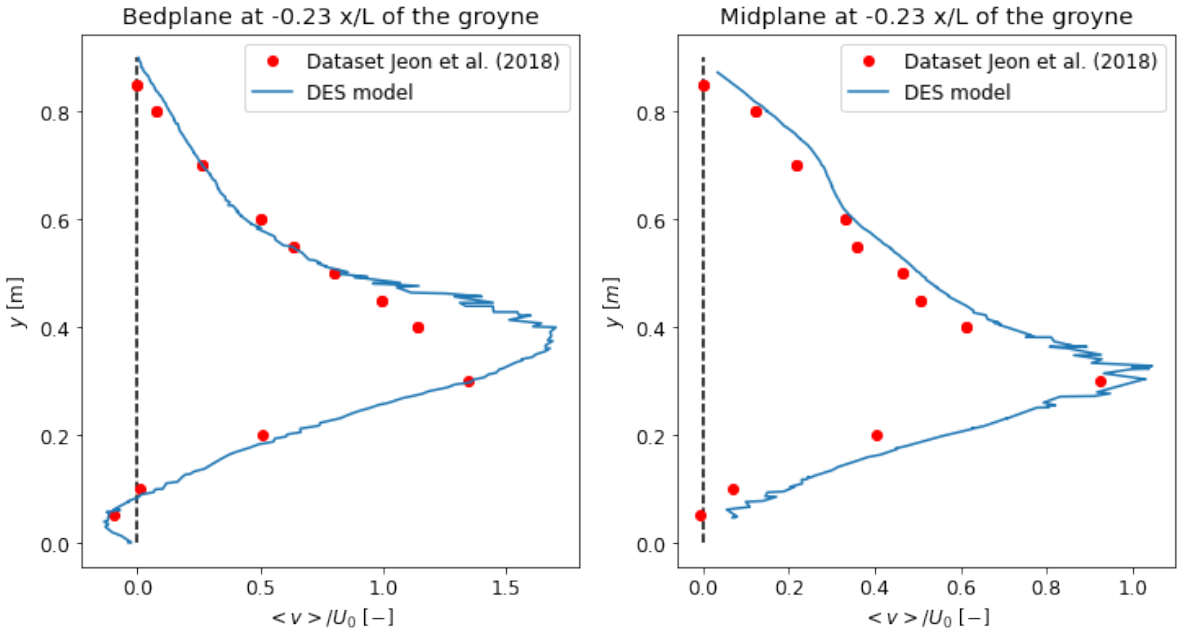

Figure D.3: mean-y-velocity for $-0.23\ x/L$, upstream of the groyne

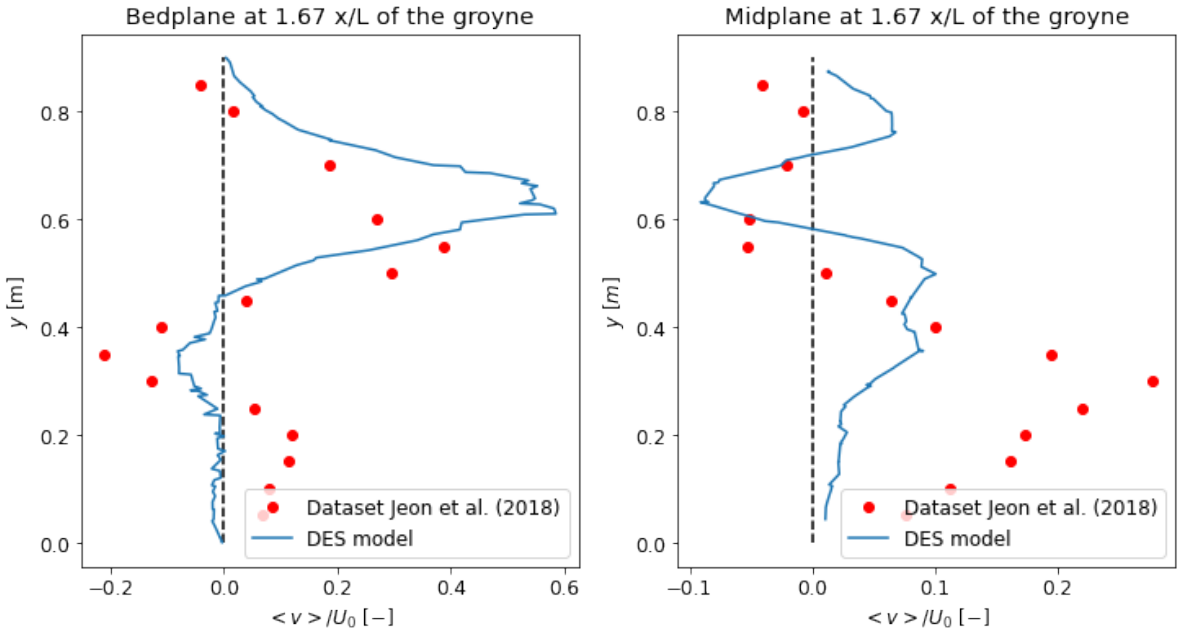

Figure D.4: mean-y-velocity for $1.67\ x/L$, downstream of the groyne

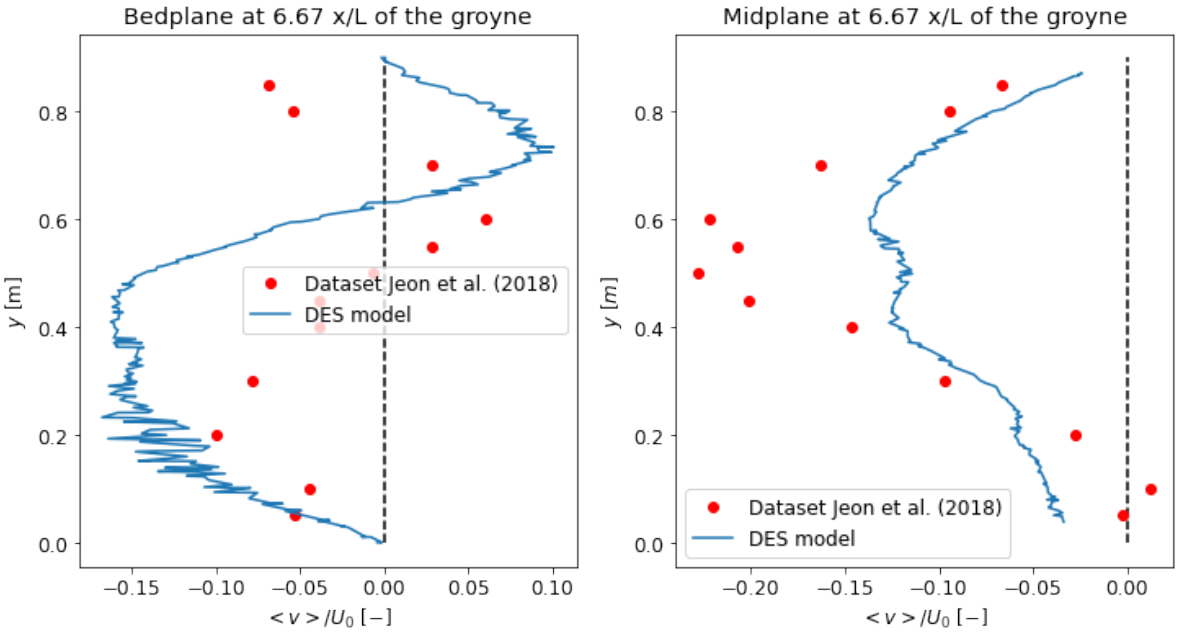

Figure D.5: mean-y-velocity for $6.67\ x/L$, downstream of the groyne

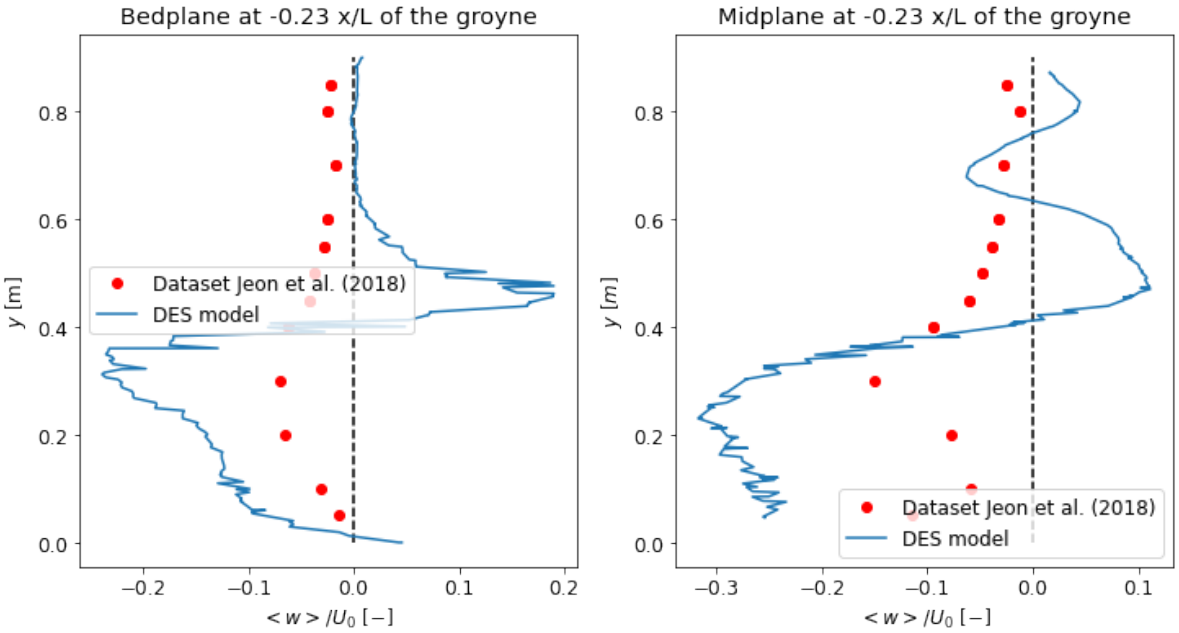

Figure D.6: mean-z-velocity for $-0.23\ x/L$, upstream of the groyne

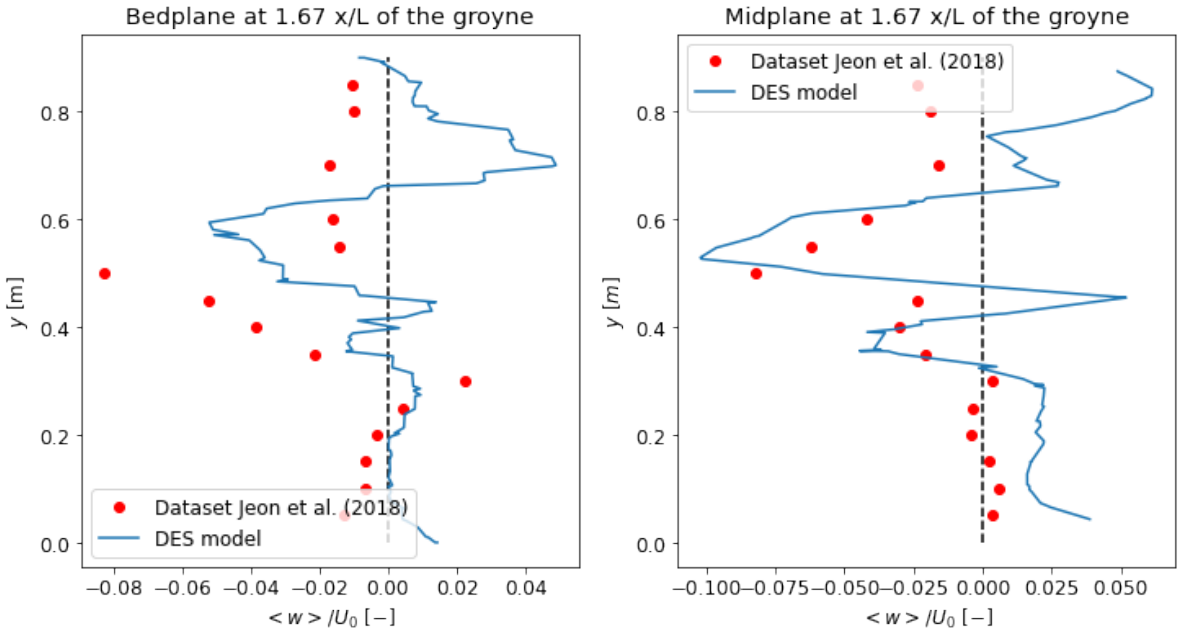

Figure D.7: mean-z-velocity for 1.67 x/L, downstream of the groyne

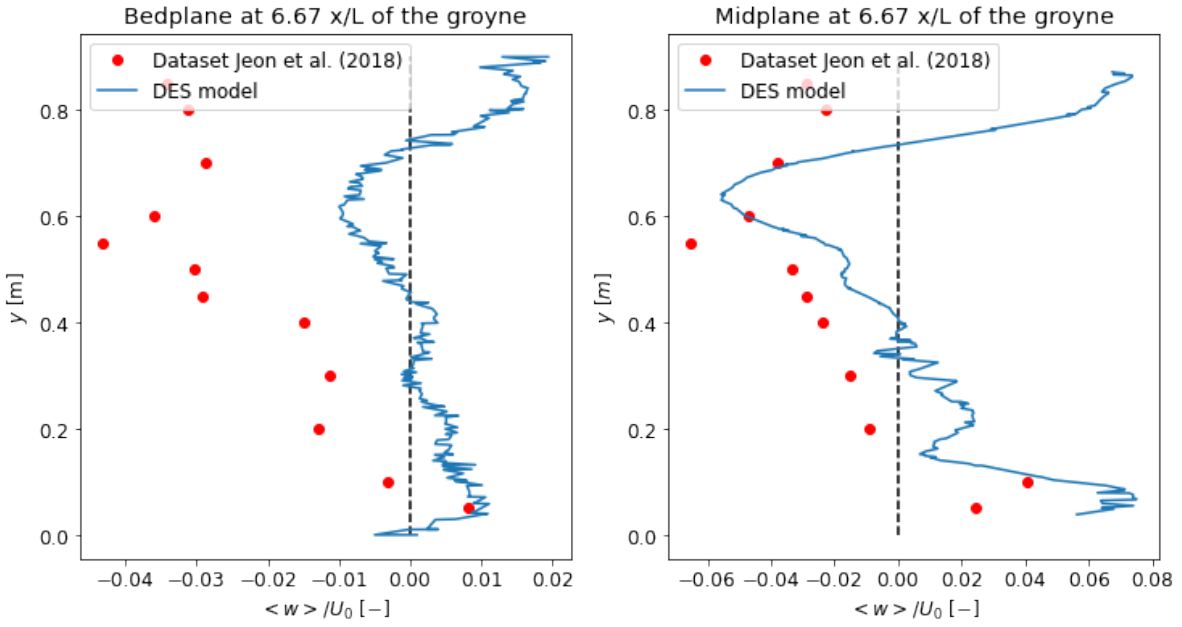

Figure D.8: mean-z-velocity for 6.67 x/L, downstream of the groyne

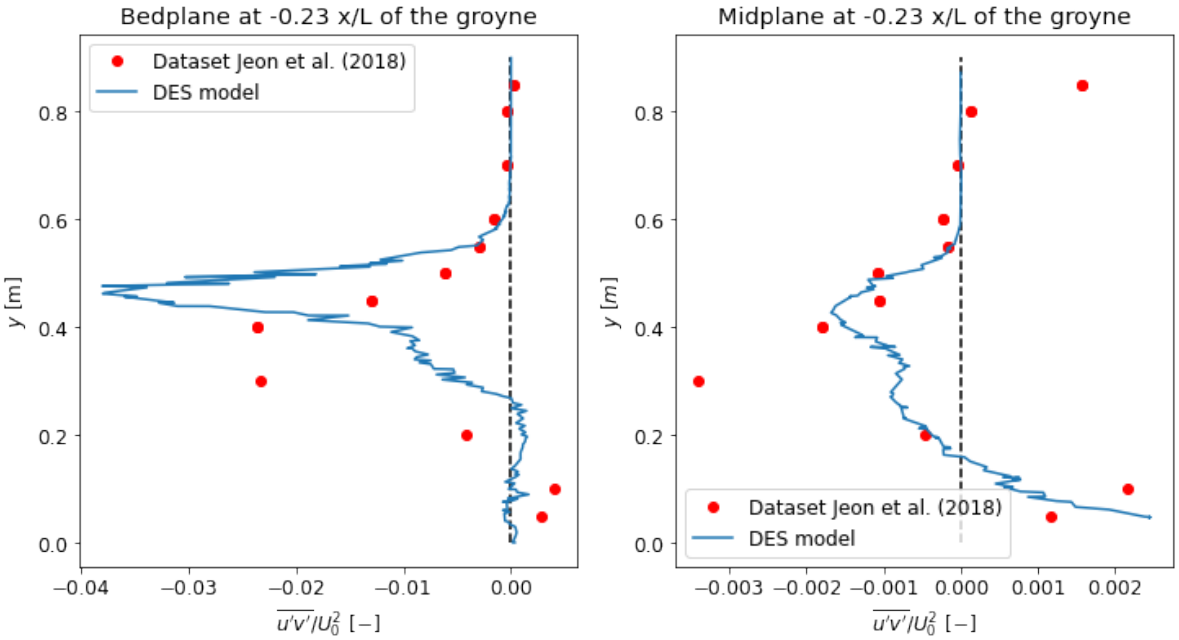

Figure D.9: $\overline{u'v'}$ stress for $-0.23\ x/L$, upstream of the groyne

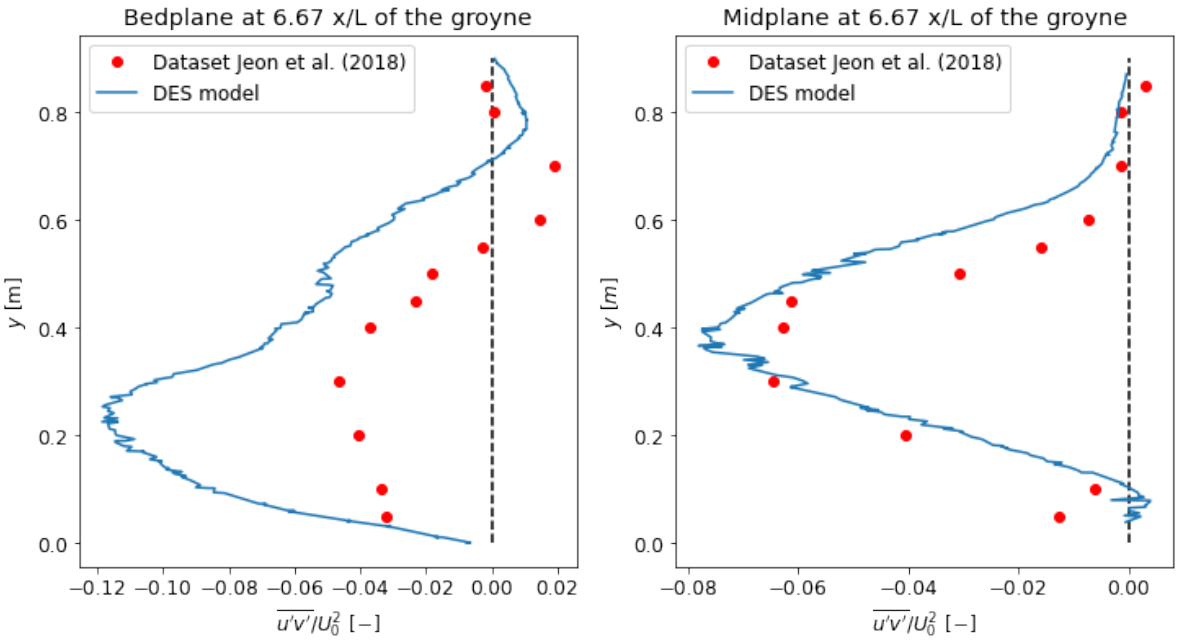

Figure D.10: $\overline{u'v'}$ for $6.67\ x/L$, downstream of the groyne

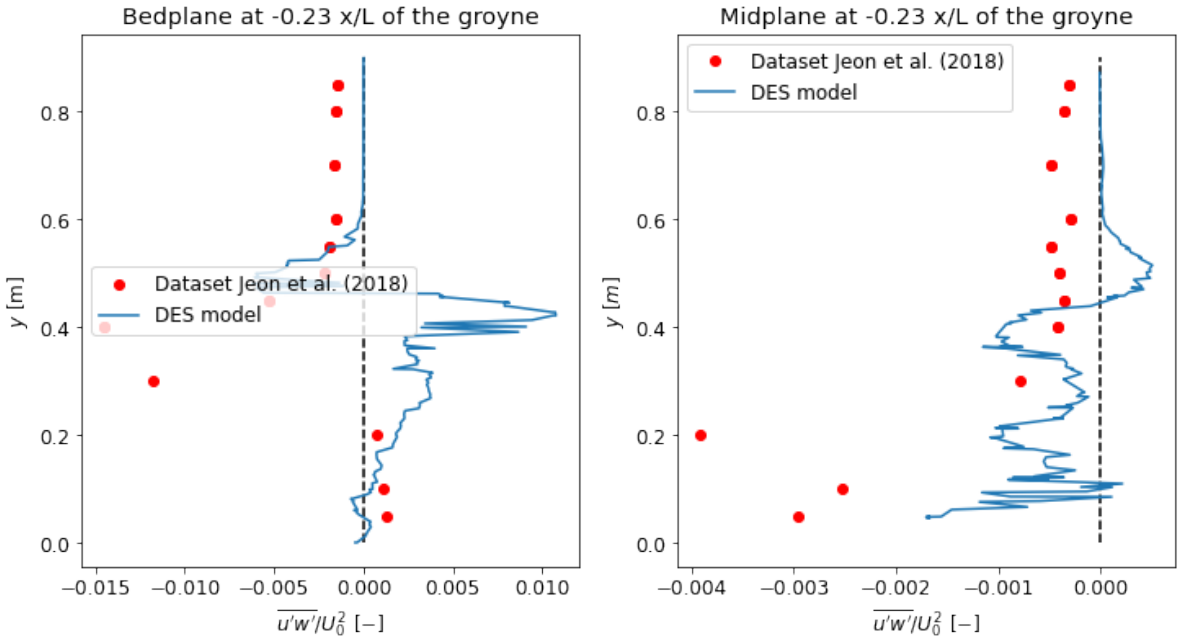

Figure D.11: $\overline{u'w'}$ for $-0.23\ x/L$, upstream of the groyne

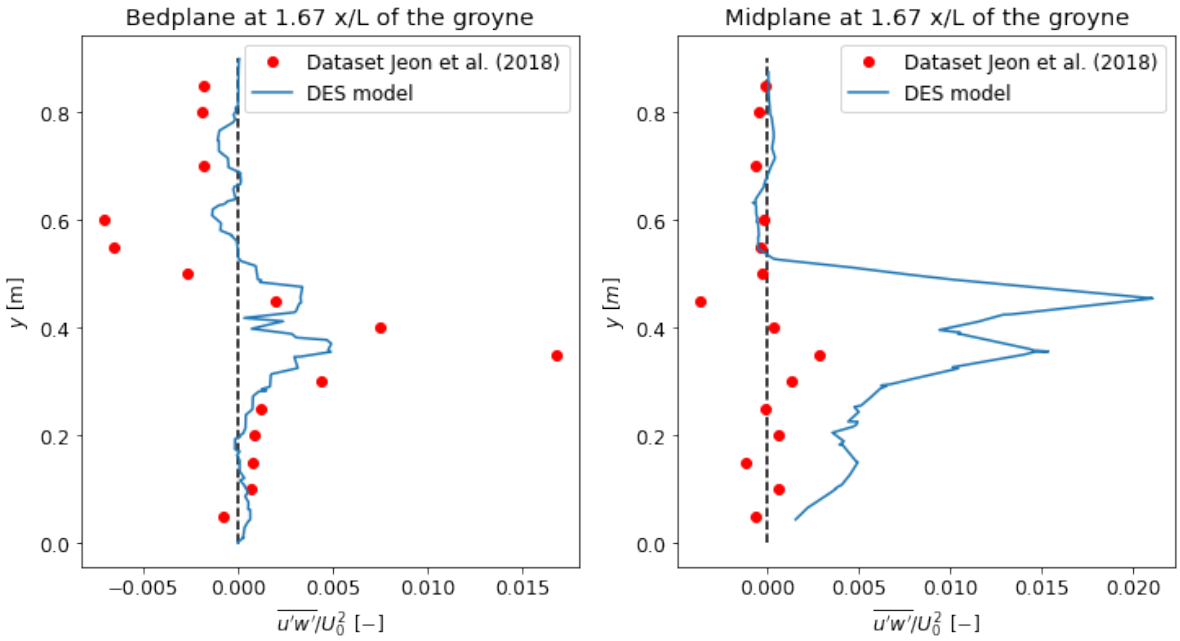

Figure D.12: $\overline{u'w'}$ for $1.67\ x/L$, downstream of the groyne

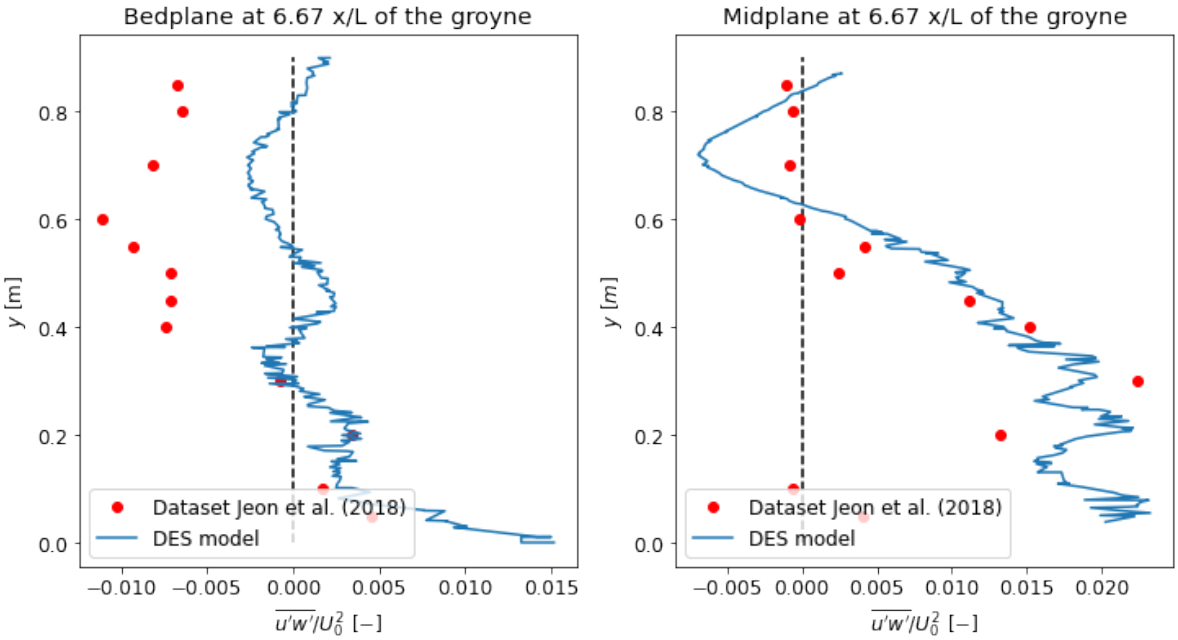

Figure D.13: $\overline{u'w'}$ for $6.67\ x/L$, downstream of the groyne

D.2 Porous weir

Remaining results from the numerical model of the porous weir are shown in this section.

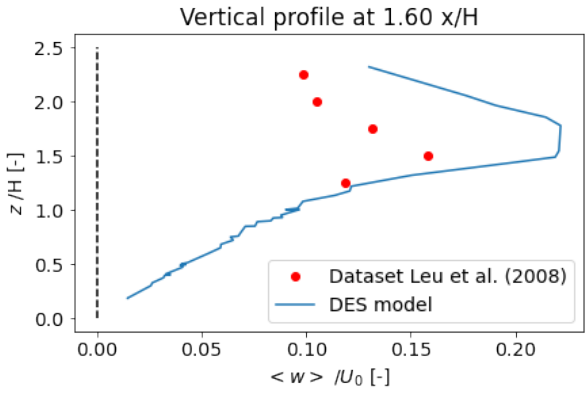

(a) 1.6 x/L, on the porous structure

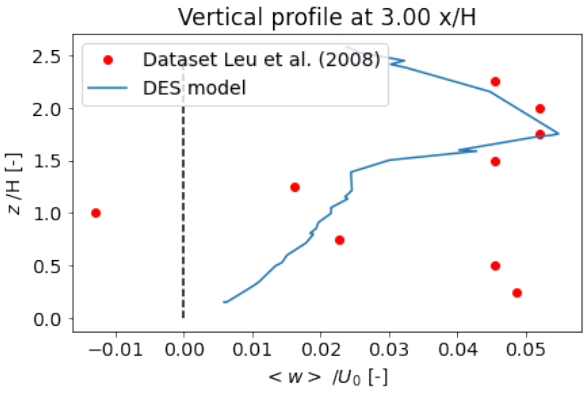

(b) 3.0 x/L downstream of the groyne

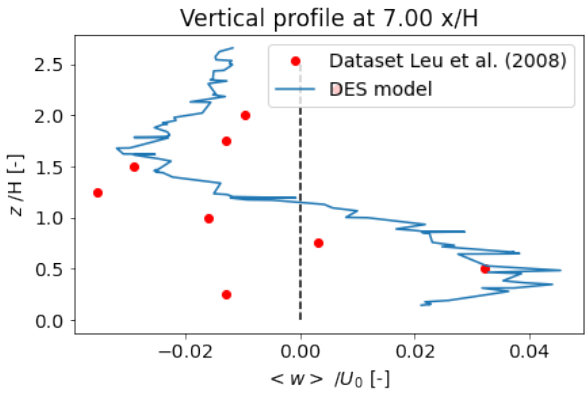

(c) 7 x/L downstream of the groyne

Figure D.14: The z mean velocity for specified vertical profiles in the numerical model

D.3 Sloped groyne

Remaining results from the numerical model of the sloped groyne are shown in this section.

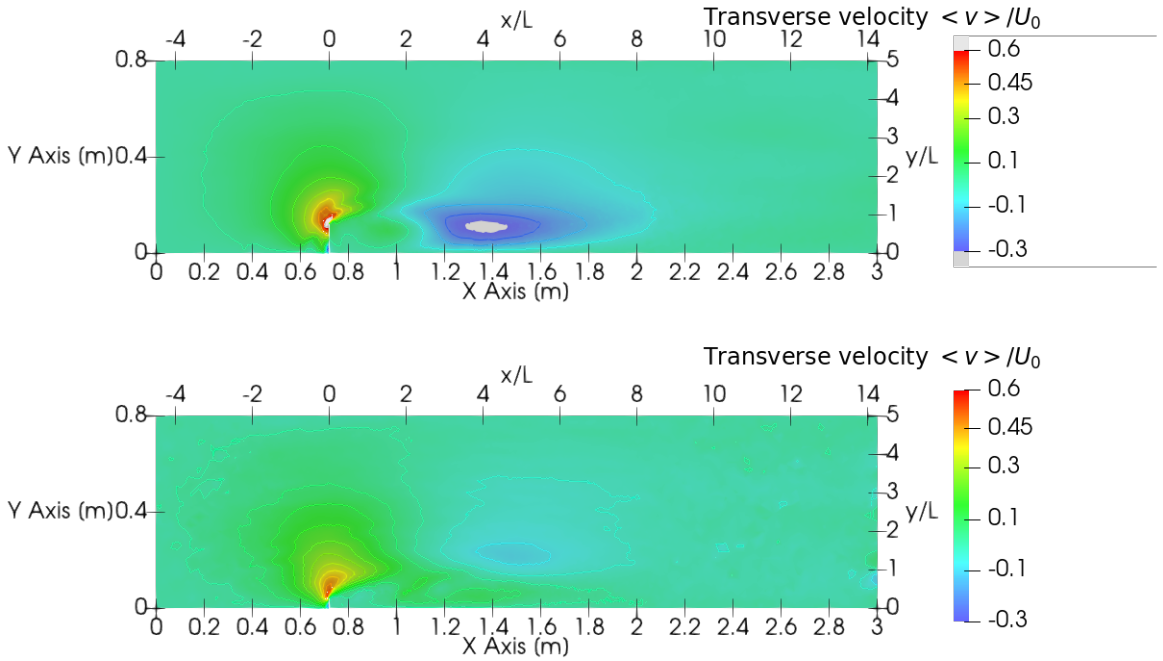

Figure D.15: Mean y velocity over the whole domain near the bed plane (0.03m) and mid plane (0.14m) from the numerical model

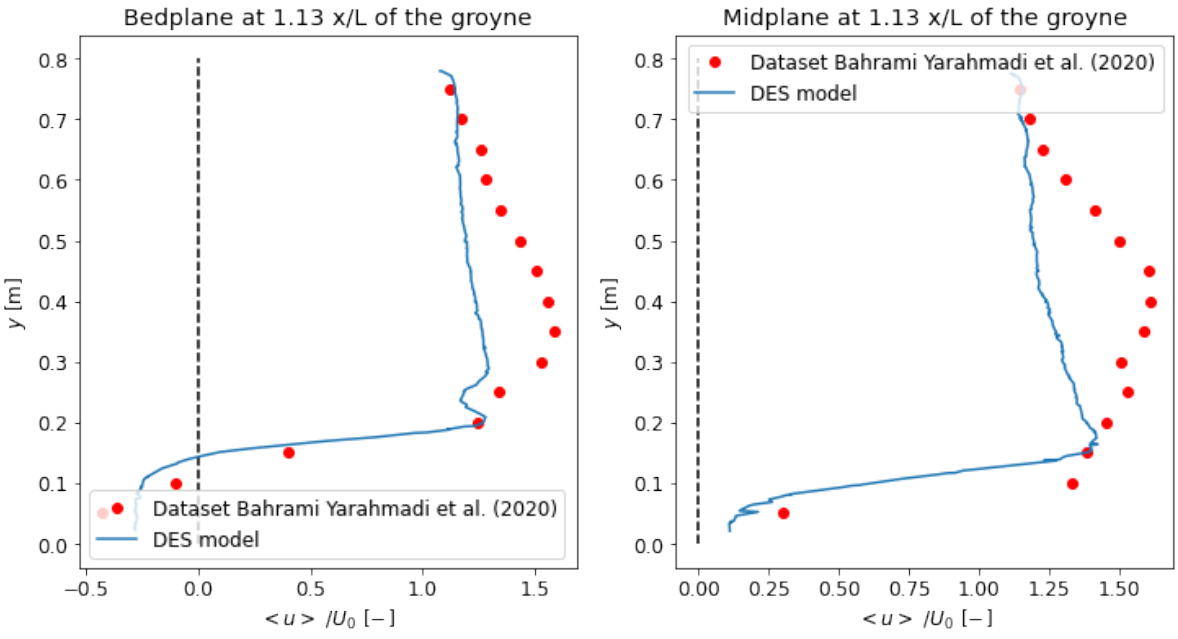

Figure D.16: x-velocity for $1.13\ x/L$, downstream of the sloped groyne

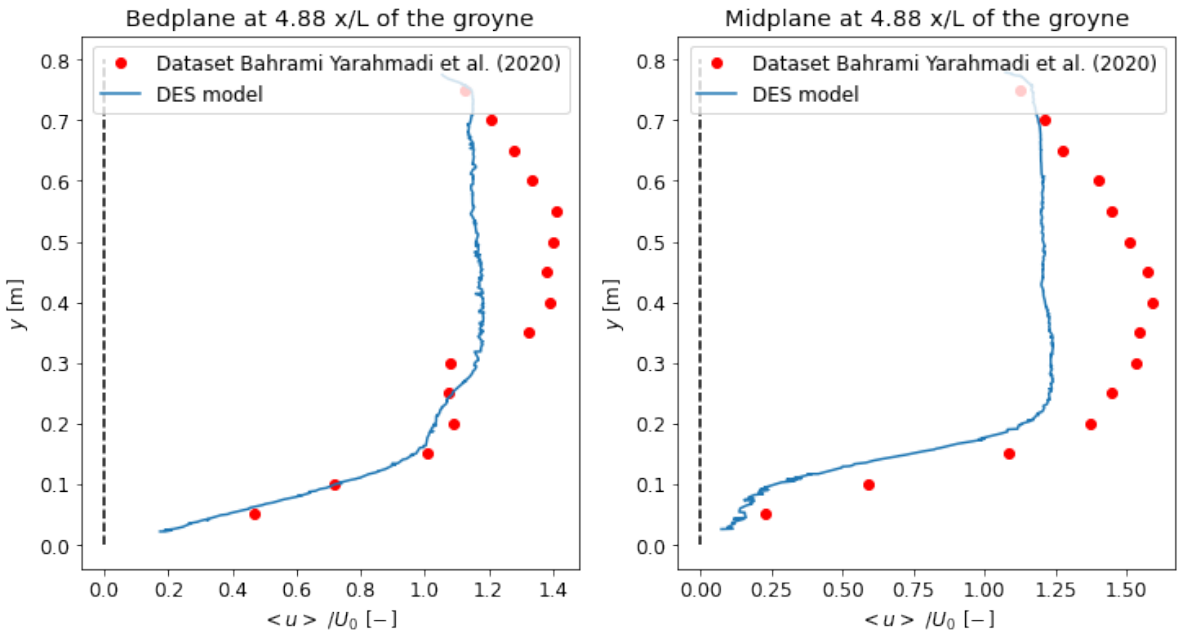

Figure D.17: x-velocity for $4.88\ x/L$, downstream of the sloped groyne

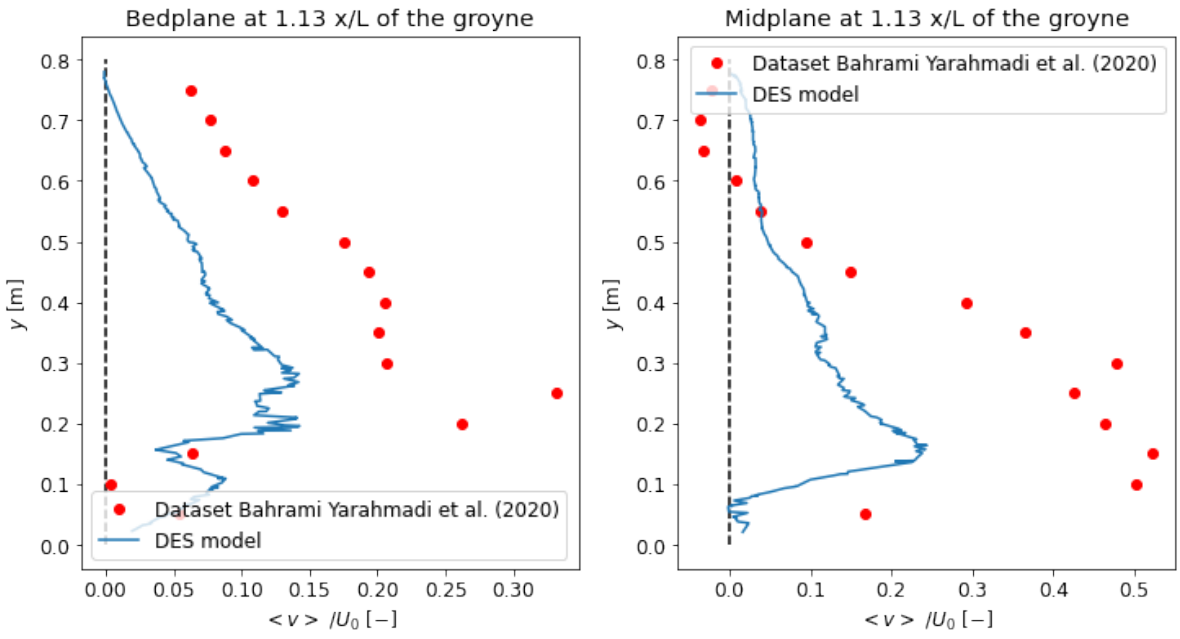

Figure D.18: y-velocity for $1.13\ x/L$, downstream of the sloped groyne

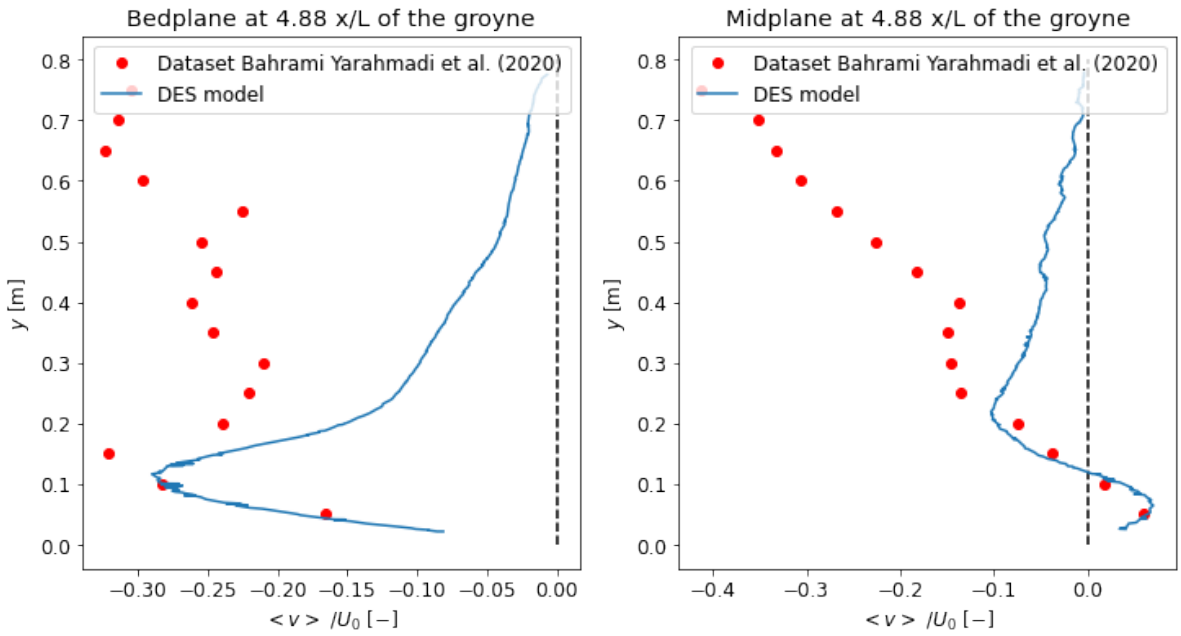

Figure D.19: y-velocity for $4.88\ x/L$, downstream of the sloped groyne

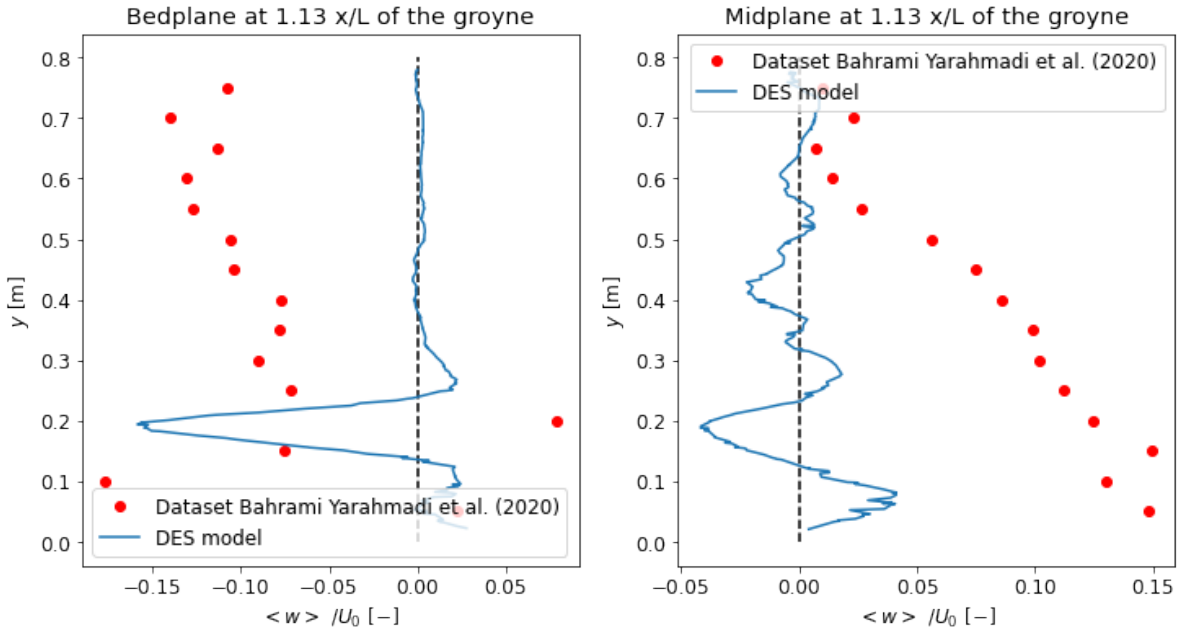

Figure D.20: z-velocity for $1.13\ x/L$, downstream of the sloped groyne

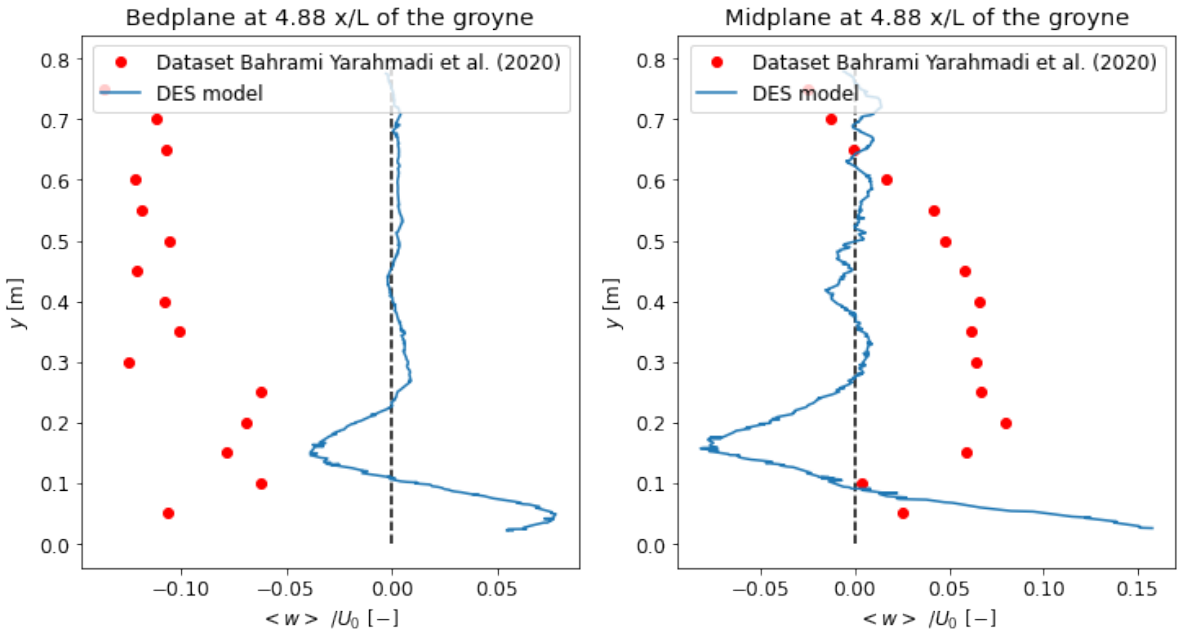

Figure D.21: z-velocity for $4.88\ x/L$, downstream of the sloped groyne

E Approach to configuration simulations

Approach to configuration

Additional information for the set-up of the numerical model is configured as shown in Figure E.1, Figure E.2 and Figure E.3.

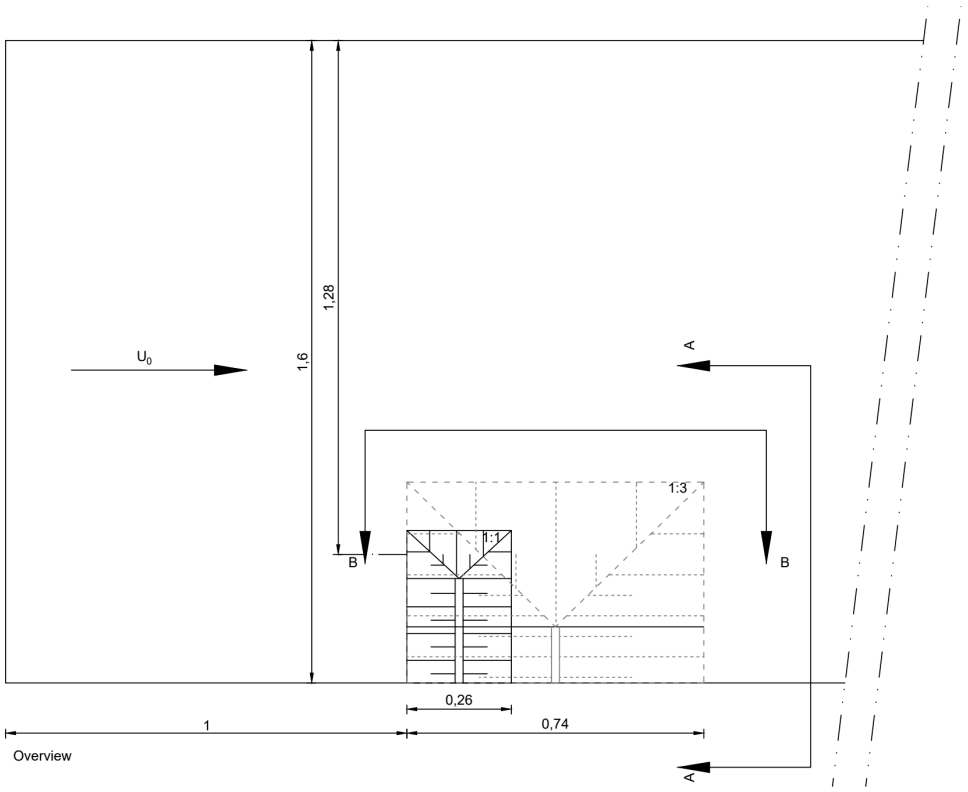

Figure E.1: Overview of the numerical model for a groyne with a slope of 1:1 VH and a slope of 1:3 VH

As stated in the literature, groynes have a length between 1/3 til 1/6 of the width of the domain. Therefore, the various slopes are calculated from the axis of the slope at 1/5 of the total width of the domain, which is comparable with the conditions of the IJssel.

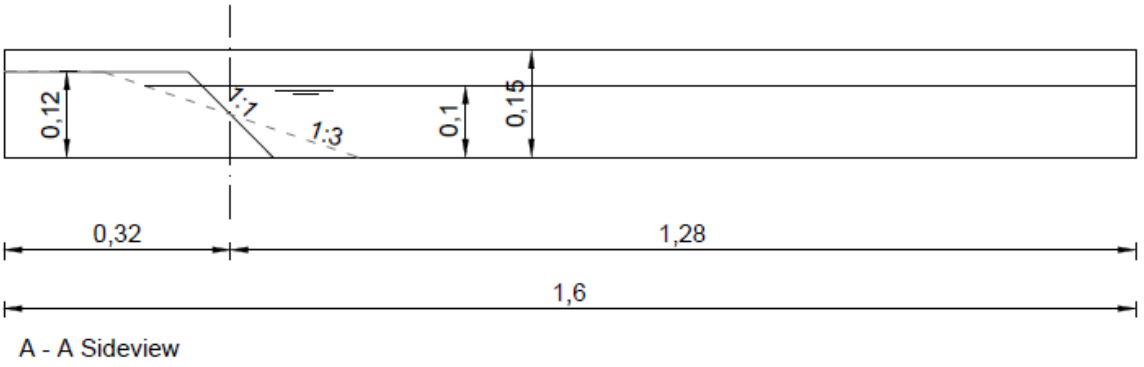

Figure E.2: Sideview of the numerical model for a groyne with a slope of 1:1 VH and a slope of 1:3 VH

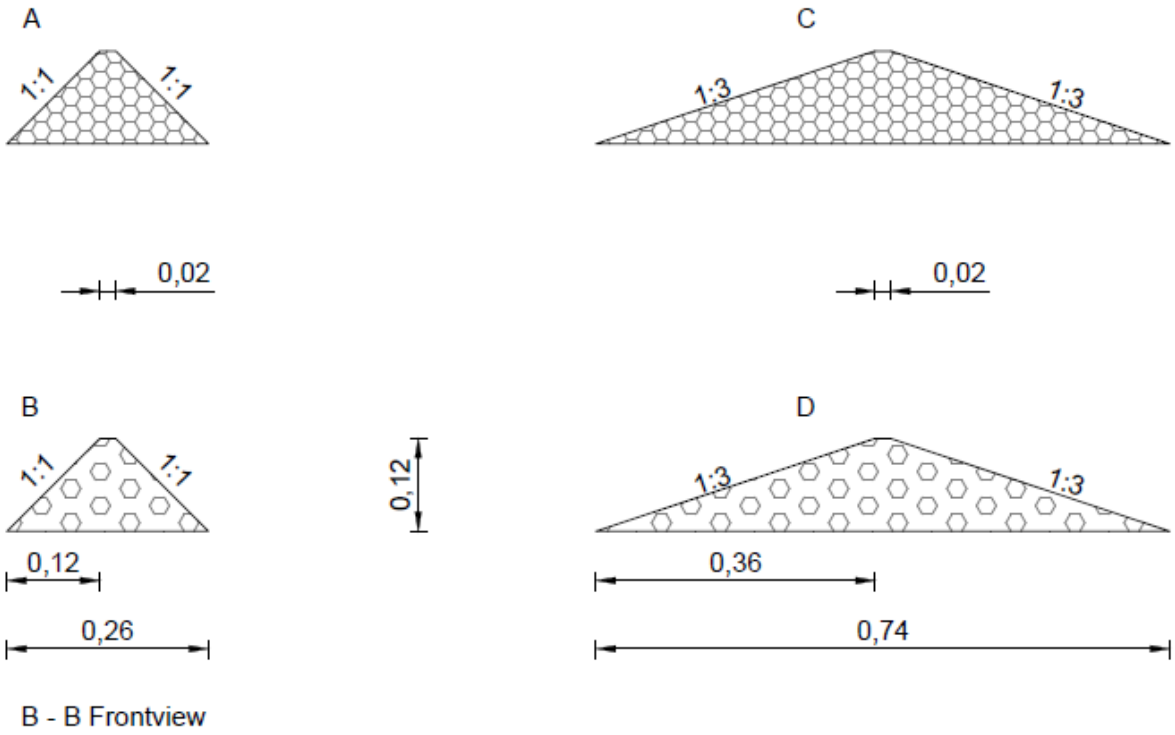

Figure E.3: Frontview of the four simulations. A) Solid groyne with slope 1:1 B) Porous groyne 60 % with slope 1:1 C) Solid groyne with slope 1:3 D) Porous groyne 60 % with slope 1:3

Grid dependency test

Remaining results for the grid dependency test:

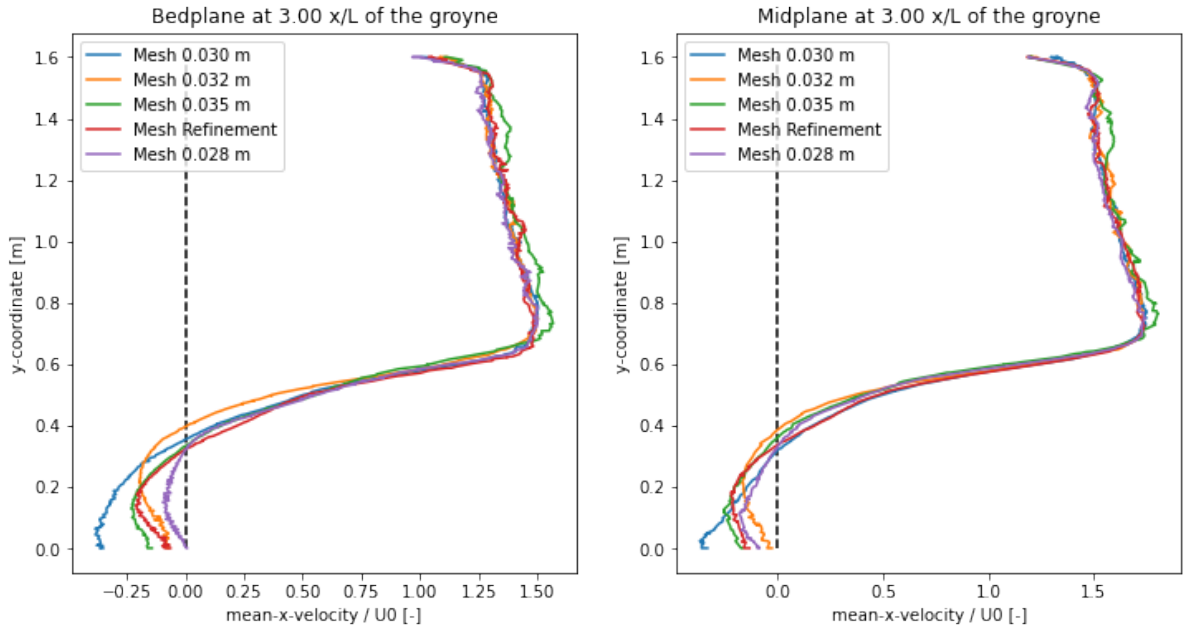

Figure E.4: Grid dependency test for the mean-x-velocity for a time simulation of 120 s

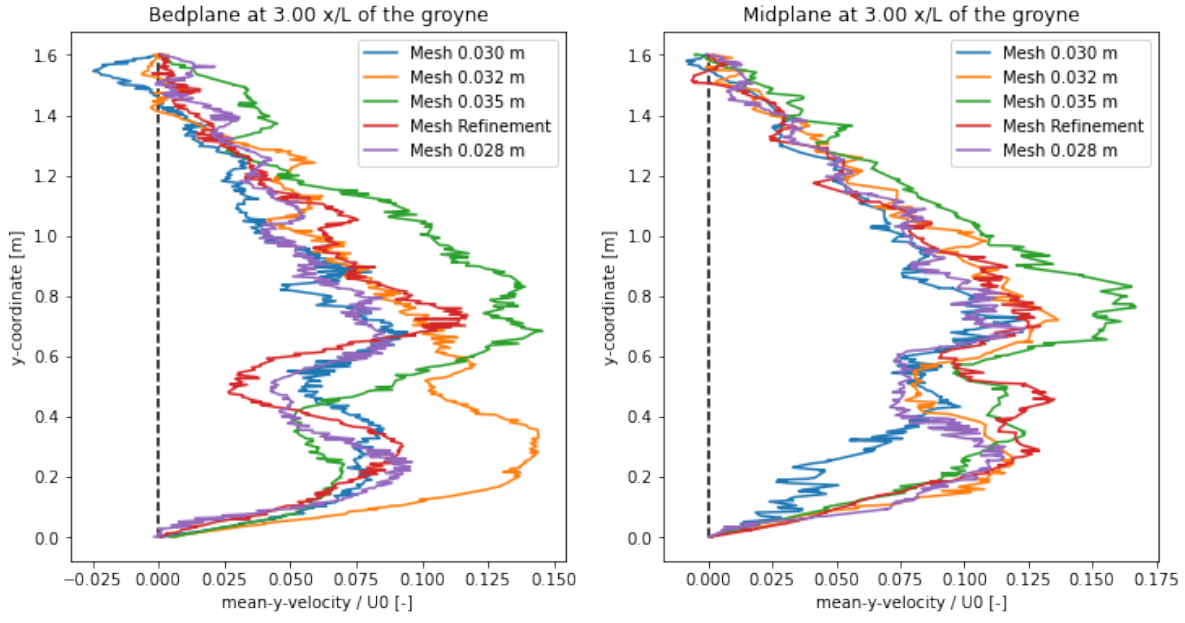

Figure E.5: Grid dependency test for the mean-y-velocity for a time simulation of 120 s

F Results from configuration simulations

Results from configuration

Remaining results of the various configurations for models A till D.

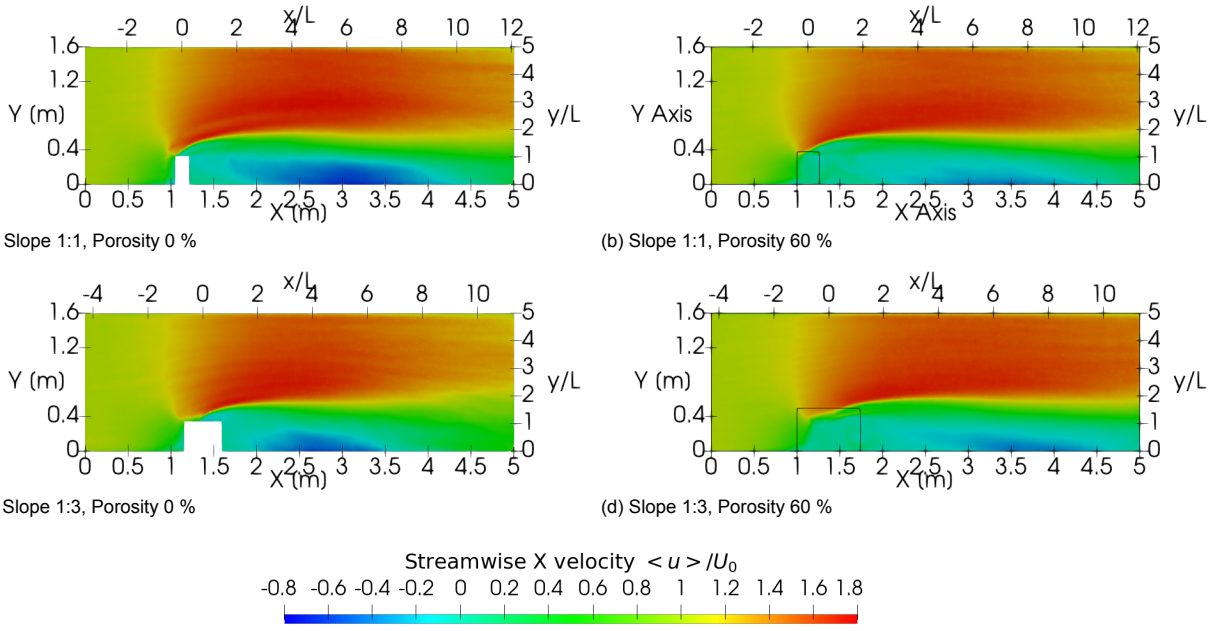

(a) Slope 1:1, Porosity 0 %

(b) Slope 1:1, Porosity 60 %

(c) Slope 1:3, Porosity 0 %

(d) Slope 1:3, Porosity 60 %

Figure F.1: Mean X velocities in the midplane for the numerical model in non-dimensional units

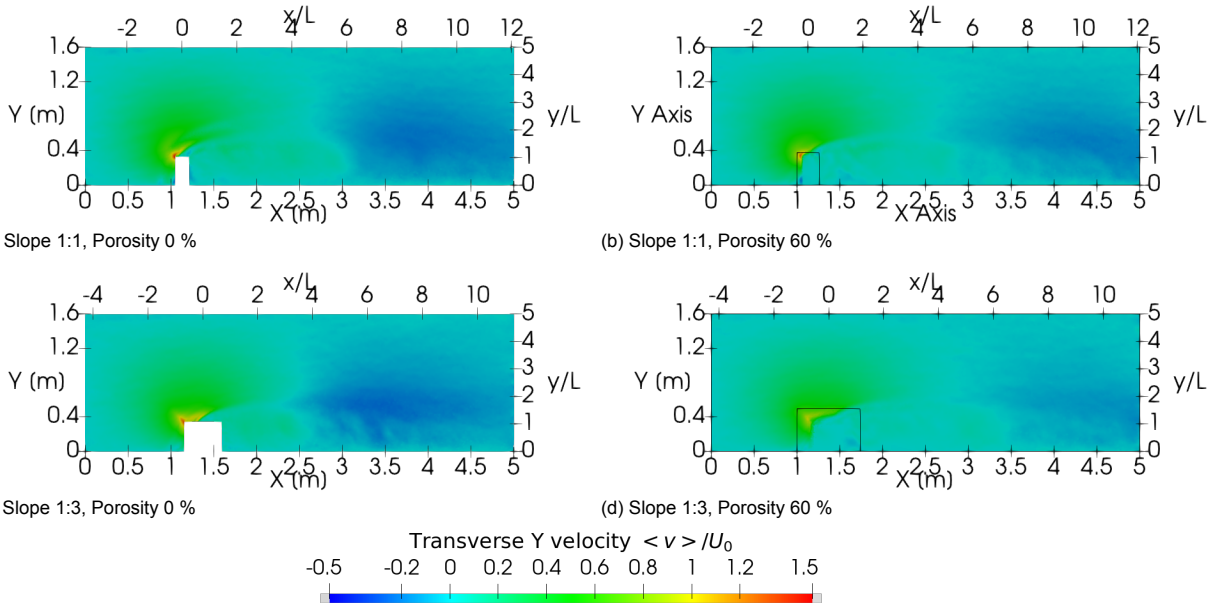

(a) Slope 1:1, Porosity 0 %

(b) Slope 1:1, Porosity 60 %

(c) Slope 1:3, Porosity 0 %

(d) Slope 1:3, Porosity 60 %

Figure F.2: Mean Y velocities in the midplane for the numerical model in non-dimensional units

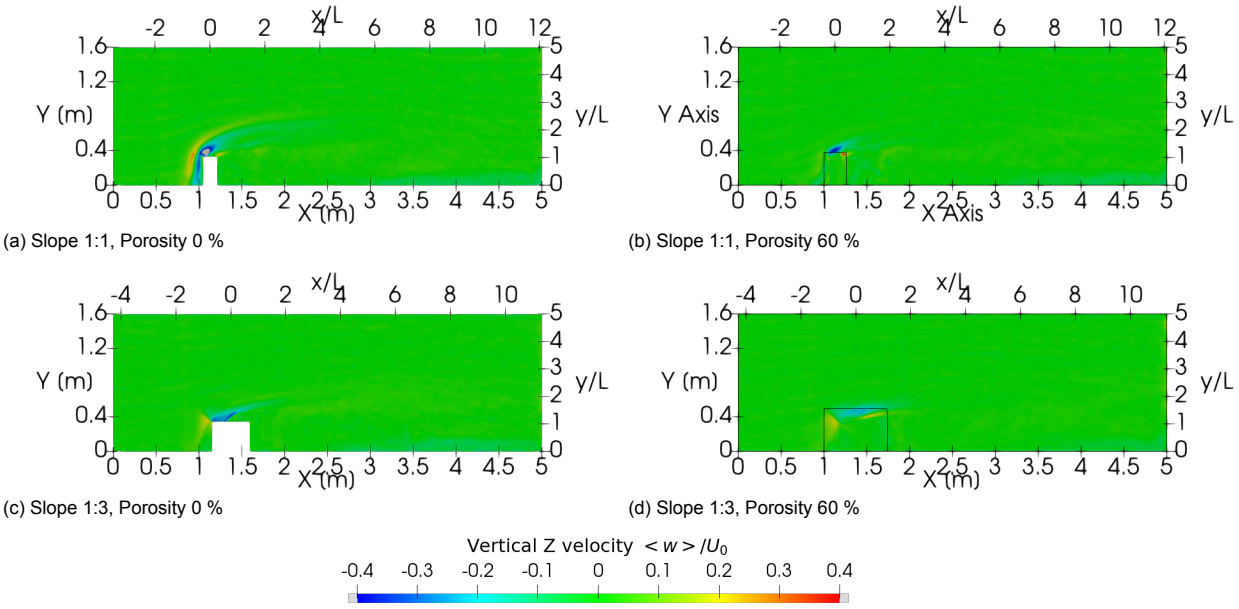

(a) Slope 1:1, Porosity 0 %

(b) Slope 1:1, Porosity 60 %

(c) Slope 1:3, Porosity 0 %

(d) Slope 1:3, Porosity 60 %

Figure F.3: Mean Z velocities in the midplane for the numerical model in non-dimensional units

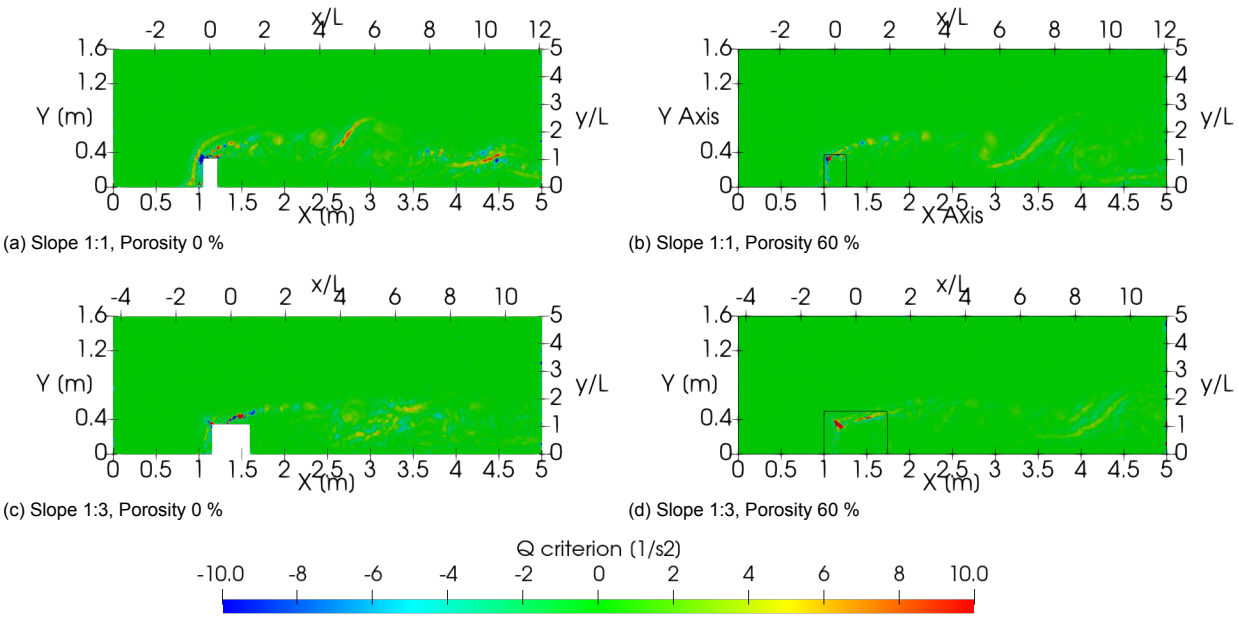

(a) Slope 1:1, Porosity 0 %

(b) Slope 1:1, Porosity 60 %

(c) Slope 1:3, Porosity 0 %

(d) Slope 1:3, Porosity 60 %

Figure F.4: Vortical structures in the midplane by using the Q criterion

G Summary of studies for flow dynamics around groynes

Table G.1: Experimental researches on flow dynamics for groynes in rivers

Year	Researcher(s)	Type groyne/specifications	Focus research	Results
1983	Rajaratnam & Nwachukwu	• Straight thin plate • Semi cylindrical • Smooth-rough beds • Single groyne	Studying the disturbance of the flow and the boundary layer	• Velocity vectors (Prandtl tube) • Bed shear stress (Preston tube) • Water level (Detector)
1991	Holtz	• Rectangular groyne • Sharpe-edge groyne • Single groyne	Flow around groynes	• Isolines water dephts • Isolines velocity
1993	Ariëns	• Constriction • Rectangular plate	Roughness and turbulence around a constriction	• Turbulent values (RMS) • Max. Velocity (EVM) • Roughness • Stability factor (K-factor)
2000	Jagers & Schijndel	• Groyne with slopes • Series of groynes • Shallow groyne field	Summary of calculating flow around groynes and in groyne fields	• Velocity vectors (Tracer) • Turbulent fluctuations
2001	Uijttewaal et al.	• Rectangular groyne • Groyne with slope • Series of groynes	Exchange of processes between river and groyne fields	• Position of gyres (PIV) • Mean flow velocity (PIV) • Exchange coefficients (Dye) • Water depths
2001	Weitbrecht & Jirka	• Rectangular groyne • Series of groynes • Shallow groyne field • Multiple angles	Flow patterns in dead zones and the influence of the inclination angle of groynes	• Mean flow velocity (PIV) • Exchange parameter
2003	Chrisohoides et al.	• Rectangular groyne • Circular-edge groyne, • Single groyne • Fixed, flat bed	Investigating 3D large-scale turbulent flow structures for groynes on a flat bed	• Mean flow velocity (exp.) • Turbulent structures (exp.) • Bed Elevation
2004	Ettema & Muste	• Rectangular groyne • Single groyne • Flat-bed	Determining scale effects of flow around a single groyne	• Velocity vectors (LSPIV) • Path of max. water depth • Seperation line
2004	Giri et al.	• Rectangular groyne • Series of groynes • Smooth rigid bed • Bending case	Near-bed flow and turbulence induced by groynes in a meandering-like experiment	• Velocity vectors (ADV) • Reynold stresses • Turbulent properties • Visualisations of eddies
2005	Uijttewaal	• Various groyne slopes • Series of groynes • Permeable groynes • Emerged and submerged	Finding efficient alternative designs for standard groynes	• Velocity vectors (PT • Turbulent properties • Power density spectra
2005	Zhang et al.	• Rectangular groyne • Series of groynes • Equilibrium state • Initial riverbed of sand	Numerical investigation of the 3D flow and sediment transport around a series of groynes	• Velocity vectors (PIV) • Bed shear stresses • Scour hole

2005	Yeo et al.	• Rectangular groyne • Series of groynes • Pile rows for permeability	Evaluating the influence of the interval of groynes and recirculation zone with variable permeability's	• Velocity vectors (LSPIV) • Incidence angle • Tip velocity (ADV)
2005	Paik & Sotiropoulos	• Rectangular groyne • Single groyne • Special Experimental visualization tecnique	Visualize the rich dynamics of the flow in the upstream recirculating zone for groynes	• Vertical vorticity • 3D Turbulent structures • Isolines water depths • Velocity vectors • Reynold stresses
2008	Koken & Constantinescu	• Rectangular groyne • Single groyne • Relatively low RE number	Investigating the flow physics in the development of scour holes around a vertical spur dike	• Velocity vectors (LSPIV) • Bed shear stresses • Turbulent properties • Vorticity
2008	Weitbrecht et al.	• Rectangular groyne • Half cylinder at the end • Series of groynes • Shallow groyne field • Multiple angles, spacing and length	Studying the mass exchange of dissolved tracer between the main stream and the groyne field	• Water depths • Exchange coefficients (dye) • Velocity vectors (LDV, PIV) • Voriticity
2009	Duan	• Rectangular groyne • Single groyne • Fixed-bed	3D turbulent flow field around a spur dike	• Mean velocity (ADV) • Turbulent properties (micro-ADV) • Reynold stresses • Bed shear stresses
2009	Tritthart et al.	• Rectangular groyne • Series of groynes • River bed • Various flow stages	Deriving a numerical particle-tracing method to model flow characteristics for groyne fields	• Velocity vectors (ADV) • Turbulent properties (ADV) • River morphology (LiDAR) • Flow patterns
2010	Baba et al.	• Rectangular groyne • Single groyne • With flood plains • Pile rows for permeability • Impermeable and permeable groyne	Flows and bedload dynamics around a groyne on a floodplain	• Velocity vectors (EVM, LSPIV) • Length recirculation zone • Scour depths • Bed load transport
2009 and 2011	Koken & Constantinescu	• Rectangular groyne • Single groyne • Flat-bed with sediment • Fully developed flow	Investigating flow and large turbulence structure around a spur dike and with a large scour hole	• Velocity vectors (LSPIV) • Bed shear stresses • Scour depths • Turbulent properties • Vorticity
2011	Yossef & de Vriend	• Groyne with slopes • Series of groynes • Emerged and submerged • Fixed-bed • Various flow stages	Study the 2D dynamics of the flow near groynes for a schematized straight river	• Velocity vectors (PTV) • Turbulent structure (EMF) • Turbulent intensities • Energy density spectra
2011	Kang et al.	• Rectangular groyne • Single groyne • Pile rows for permeability • Various permeability and triangular shapes	Flow characteristics of a single groyne for various geometries and permeability's	• Velocity vectors (LSPIV) • Tip velocity (ADV) • Flow separation angle • Recirculation zone scale
2011	Kang et al.	• Rectangular groyne • Single groyne • Pile rows for permeability • Various permeability and angles	Flow characteristics and scours of a single groyne for various angles and permeability's	• Velocity vectors (LSPIV) • Tip velocity (ADV) • Flow separation angle • Scour holes

2014	Koken & Constantinescu	• Groyne with slopes • Single groyne • Use of bed protection • Fully developed flow • Equilibirum state	Flow and turbulent structures around a sloped groyne for an equilibrium state of the bathymetry	• Velocity vectors (ADV) • Turbulent properties • Turbulent structures • Vorticity
2014	Mansoori	• Rectangular groyne • Single and series • Fixed-bed with sediment • Various head shapes • Movable bed case	flow field and sediment transport of a spur dike with different head shape	• Velocity vectors (LSPIV) • Flow depth • Exchange coefficient • Bed features
2017	Higham et al.	• Straight thin plate • Single groyne • Shallow water depth • Large downstream section of groyne	Using modal decompositions to explain the sudden expansion of the mixing layer downstream	• Velocity vectors (PIV) • Vorticity • Reynold stresses • Turbulent properties • Modal decompositions
2017	Mehraein et al.	• T-shaped groyne • Single groyne • Emerged and submerged • Bending case	The flow field and the scour hole dimensions around a T-shaped spur dike in a 90° bend	• Mean velocity (ADV) • Scour holes • Turbulent properties • Flow patterns
2018	Jeon et al.	• Rectangular groyne • Single groyne • Fixed-bed • Shallow water depth • Large downstream section of groyne	Investigating the 3D flow structure and turbulent flow mechanisms around a groyne	• Velocity vectors (ADV) • Turbulent structure • Reynold stresses • Turbulen properties • Free surface elevation
2020	van der Wal M.	• Rectangular groyne • Groynes with slopes • Series of groynes • Pile rows for permeability • Use of bed protection	Focus on reducing local scour holes near groynes in the Brahmaputra-Jamuna River	• Surface velocity • Flow depth • Scour depths • Bed features
2020	Shampa et al.	• Series of groynes • Pile rows for permeability • Staggered installation • Multiple angles	Finding efficient solutions for the design of highly permeable pile spur dike field	• Surface velocity (PIV) • Flow depth
2020	Bahrami Yarahmadi et al.	• Rectangular groynes • Series of groynes • Triangular groynes • Flat-bed with sediment	Scour, deposition patterns and 3D velocity components around triangular and straight spur dikes	• Velocity vectors (EVM) • Flow depth • Scour depths • Bed features

Table G.2: Numerical researches on flow dynamics for groynes in rivers

Year	Researcher(s)	Type groyne/specifications	Focus research	Results
1991	Holtz	• Rectangular groyne • Sharpe-edge groyne • Single groyne	Flow around groynes	• Isolines water dephts • Isolines velocity
1993	Ouillon & Denis	• Rectangular groyne • Sharpe-edge groyne • Single groyne • Steady flow simulation • RANS $k-\varepsilon$ model	3D flow around groynes, the reattachment length and free surface	• Velocity vectors • Bed-shear stress • Dynamic Pressures • Reattachment lengths
1993	Muneta & Shmizu	• Rectangular groyne • Single groyne • Simplified, averaged numerical model	Flow patterns behind groynes, in particular the transverse flow velocities downstream	• Downward flow velocity • Transverse flow velocity
2000	Jagers & Schijndel	• Groyne with slopes • Series of groynes • HLES with a SGS model • Various grids • Various cut-off numbers	Summary of calculating flow around groynes and in groyne fields	• Velocity vectors • Turbulent fluctuations
2003	Chrisohoides et al.	• Rectangular groyne • Circular-edge groyne, • Single groyne • Fixed, flat bed • RANS $k-\omega$ model	Investigating 3D large-scale turbulent flow structures for groynes on a flat bed	• Velocity vectors • Turbulent structures
2004	Giri et al.	• Rectangular groyne • Series of groynes • Smooth rigid bed • Bending case • 2D State-of-the-art model	Near-bed flow and turbulence induced by groynes in a meandering-like experiment	• Velocity vectors • Reynold stresses • Turbulent properties • Visualisations of eddies
2005	Zhang et al.	• Rectangular groyne • Series of groynes • RANS $k-\varepsilon$model • Steady state simulation • Hexahedral mesh	Numerical investigation of the 3D flow and sediment transport around a series of groynes	• Velocity vectors • Bed shear stress • Scour hole
2005	Paik & Sotiropoulos	• Rectangular groyne • Single groyne • Flat, rigid-lid assumption • DES with Spalart-Allmaras model	Visualize the rich dynamics of the flow in the upstream recirculating zone for groynes	• Vertical vorticity • 3D Turbulent structures • Isolines water depths • Velocity vectors • Reynold stresses
2007	Ho et al.	• Rectangular groyne • Series of groynes • Permeable groyne • RANS $k-\varepsilon$ model • FAVOR method for permeability	Evaluating the influence of the interval of groynes and recirculation zone with variable permeabilities	• Velocity vectors • Incidence angle • Tip velocity
2008	Koken & Constantinescu	• Rectangular groyne • Single groyne • Relatively low RE number • Hexahedral mesh • LES with Smagorinsky model	Investigating the flow physics in the development of scour holes around a vertical spur dike	• Velocity vectors • Bed shear stress • Turbulent properties • Vorticity

2009	Tritthart et al.	• Rectangular groyne • Series of groynes • River bed • Various flow stages • RANS $k-\varepsilon$ model	Deriving a numerical particle-tracing method to model flow characteristics for groyne fields	• Velocity vectors • Turbulent properties • River morphology • Flow patterns
2010	Yazdi et al.	• Rectangular groyne • Single groyne • Multiple angles • Various discharges • RANS $k-\omega$ model	Deriving the flow patterns and 3D turbulence around a groyne with a free-surface flow model	• Velocity vectors • Length recirculation zone • Turbulent structures • Bed shear stresses
2009 and 2011	Koken & Constantinescu	• Rectangular groyne • Single groyne • Flat-bed with sediment • Fully developed flow • DES with Spalart-Allmaras model	Investigating flow and large turbulence structure around a spur dike and with a large scour hole	• Velocity vectors • Bed shear stresses • Scour depths • Turbulent properties • Vorticity
2013	Ghaldarbandi et al.	• Groyne with slopes • Single groyne • Complex mesh • RANS $k-\varepsilon$ RNG model • Various bed slopes in groyne field and various groyne-walls	Investigating the influence of the cross-shore and wall slopes on flow parameters for groynes	• Velocity vector • Bed shear stresses • Reattachment length • Water elevation
2014	Koken & Constantinescu	• Groyne with slopes • Single groyne • Flat-bed with sediment • Fully developed flow • DES with Spalart-Allmaras model	Flow and turbulent structures around a sloped groyne for an equilibrium state of the bathymetry	• Velocity vectors • Turbulent properties • Turbulent structures • Vorticity
2014	Shamloo & Pirzadeh	• Rectangular groyne • Single groyne • Flat-bed with sediment • Subcritical flow • Multiple angles • RSM model	Insight in the angle of groyne installation on the separation zone length	• Velocity vector • Reattachment length
2014	Mansoori	• Rectangular groyne • Single and series • Fixed-bed with sediment • Various head shapes • RANS $k-\varepsilon$ model	flow field and sediment transport of a spur dike with different head shape	• Velocity vectors • Flow depth • Exchange coefficient • Bed features
2016	Kumar & Malik	• Rectangular groyne • Single groyne • Various head shapes • RANS $k-\varepsilon$ model • Coupling morphology model implemented	Modeling flow around groynes with different shapes	• Surface velocity • Flow depth • Bedshear stresses • Reattachment length
2017	Saberi & Galoie	• Rectangular groyne • Single groyne • Various head shapes • RANS $k-\varepsilon$ model • Coupling morphology model implemented	Modeling flow around groynes with different shapes	• Surface velocity • Flow depth • Bedshear stresses • Reattachment length
2019	Choufu et al.	• Rectangular groyne • Series of groynes • Non-equal lengths • Mutliple angles • RANS $k-\varepsilon$ RNG model	The effects of altering groyne orientation and spatial setup on flow patterns, bed erosion, and sedimentation	• Velocity vectors • Bed features • Scour depths

2020	Shampa et al.	• Series of groynes • Pile rows for permeability • Staggered installation • Multiple angles • RANS $k-\omega$ SST model • Van-Rijn formula for sediment transport	Finding efficient solutions for the design of highly permeable pile spur dike field	• Velocity vector • Flow depth • Turbulent structures • Bed shear stresses • Exchange coefficients